National Library
of Canada

Acquisitions and
Bibliographic Services Branch

395 Wellington Street
Ottawa, Ontario
K1A 0N4

Bibliothèque nationale
du Canada

Direction des acquisitions et
des services bibliographiques

395, rue Wellington
Ottawa (Ontario)
K1A 0N4

Your file Votre référence

Our file Notre référence

NOTICE

The quality of this microform is heavily dependent upon the quality of the original thesis submitted for microfilming. Every effort has been made to ensure the highest quality of reproduction possible.

If pages are missing, contact the university which granted the degree.

Some pages may have indistinct print especially if the original pages were typed with a poor typewriter ribbon or if the university sent us an inferior photocopy.

Reproduction in full or in part of this microform is governed by the Canadian Copyright Act, R.S.C. 1970, c. C-30, and subsequent amendments.

AVIS

La qualité de cette microforme dépend grandement de la qualité de la thèse soumise au microfilmage. Nous avons tout fait pour assurer une qualité supérieure de reproduction.

S'il manque des pages, veuillez communiquer avec l'université qui a conféré le grade.

La qualité d'impression de certaines pages peut laisser à désirer, surtout si les pages originales ont été dactylographiées à l'aide d'un ruban usé ou si l'université nous a fait parvenir une photocopie de qualité inférieure.

La reproduction, même partielle, de cette microforme est soumise à la Loi canadienne sur le droit d'auteur, SRC 1970, c. C-30, et ses amendements subséquents.

Canada

UNIVERSITY OF ALBERTA

RADIO FREQUENCY HEATING OF SOIL

by

Robert Armstrong ©

A thesis submitted to the Faculty of Graduate Studies and Research in partial fulfillment of the requirements for the degree of MASTER OF SCIENCE

IN

GEOTECHNICAL ENGINEERING

DEPARTMENT OF CIVIL ENGINEERING

EDMONTON, ALBERTA
FALL 1993

National Library
of Canada

Acquisitions and
Bibliographic Services Branch

395 Wellington Street
Ottawa, Ontario
K1A 0N4

Bibliothèque nationale
du Canada

Direction des acquisitions et
des services bibliographiques

395, rue Wellington
Ottawa (Ontario)
K1A 0N4

Your file Votre référence

Our file Notre référence

The author has granted an irrevocable non-exclusive licence allowing the National Library of Canada to reproduce, loan, distribute or sell copies of his/her thesis by any means and in any form or format, making this thesis available to interested persons.

L'auteur a accordé une licence irrévocable et non exclusive permettant à la Bibliothèque nationale du Canada de reproduire, prêter, distribuer ou vendre des copies de sa thèse de quelque manière et sous quelque forme que ce soit pour mettre des exemplaires de cette thèse à la disposition des personnes intéressées.

The author retains ownership of the copyright in his/her thesis. Neither the thesis nor substantial extracts from it may be printed or otherwise reproduced without his/her permission.

L'auteur conserve la propriété du droit d'auteur qui protège sa thèse. Ni la thèse ni des extraits substantiels de celle-ci ne doivent être imprimés ou autrement reproduits sans son autorisation.

ISBN 0-315-88137-2

Canada

UNIVERSITY OF ALBERTA

RELEASE FORM

NAME OF AUTHOR	Robert Charles Armstrong
TITLE OF THESIS	RADIO FREQUENCY HEATING OF SOIL
DEGREE FOR WHICH THESIS WAS PRESENTED	MASTER OF SCIENCE
YEAR THIS DEGREE GRANTED	FALL 1993

Permission is hereby granted to the University of Alberta Library to reproduce single copies of this thesis and to lend or sell copies for private, scholarly or scientific research purposes only.

The author reserves all other publication and other rights in association with the copyright in the thesis, and except as hereinbefore provided neither the thesis nor any substantial portion thereof may be printed or otherwise reproduced in any material form whatever without the author's prior written permission.

Robert Armstrong

PERMANENT ADDRESS:
4 Maki Pl.
Nepean, Ontario
K2H 9B5

Aug. 6/93 1993

THE UNIVERSITY OF ALBERTA

FACULTY OF GRADUATE STUDIES AND RESEARCH

The undersigned certify that they have read, and recommend to the Faculty of Graduate Studies and Research, for acceptance, a thesis entitled RADIO FREQUENCY HEATING OF SOIL submitted by Robert ARMSTRONG in partial fulfillment of the requirements for the degree of Master of Science.

Dr. N.R. Morgenstern..............................
Dr. F.E. Vermeulen.......F.E. Vermeulen.......
Dr. F.S. Chute.........F Chute..................

Supervisors

Dr. C. Mendoza.......Carl Mendoza..........

Date.....July 21/93.......

ABSTRACT

Treatment of ground containing hazardous waste typically involves excavation of the contaminated soil for possible processing and disposal. A possible less expensive alternative is *in-situ* remediation using radio frequency (RF) energy. By applying RF energy to the soil, volatiles and organic wastes in the ground are vaporized and can thus be steam-stripped from the ground and collected at the surface. An additional possible application of RF heating is ground stabilization through high temperature vitrification of soil into glass-like anchors.

This experimental program addresses a number of issues involved in heating large volumes of soil to 100-300°C using RF energy. A series of small scale RF heating tests assess the reaction of four soils in a coaxial RF electric field. A larger scale laboratory test assesses the potential of an electrode array to create a uniform electric field to produce uniform RF heating. A numerical model is used to study the effects of heating along an electrode, which addresses the issue of uniform heating to a significant depth.

Athabasca clay, Devon silt, bentonite and kaolinite were all heated and dried using RF energy. All of the samples behaved electrically in a similar manner. Vitrification of Athabasca clay, Devon silt and bentonite into a hard glass-like substance has been accomplished on a small scale. During the large scale heating tests there was considerable migration of water within the sample. This circulation of water diffused the heating pattern and retarded the formation of a dried region near the electrodes. A dielectric coating of dry material along an electrode will promote uniform heating along the electrode.

ACKNOWLEDGMENTS

I would like to thank Dr. Morgenstern, Dr. Vermeulen, Dr. Chute, Dr. Peter Stroemich and Jim Fern for their help and enthusiastic support.

The financial assistance provided by the University of Alberta, the National Research Council of Canada and LUSCAR Ltd. is gratefully acknowledged.

Special thanks are extended to my two good friends John Shimeld and Frank Seglenieks, for without their humor, wit and wisdom, I could never have completed this work.

Lastly I wish to offer that the path to wisdom begins with the statement, I do not know, and in that light quotes from two books I have read, but did not really understand:

"The study of the art of motorcycle maintenance is really a miniature study of the art of rationality itself. Working on a motorcycle, working well, caring, is to become part of a process, to achieve an inner peace of mind. The motorcycle is primarily a mental phenomenon."

-Robert M. Pirsig

Zen and the Art of Motorcycle Maintenance

"...the question of why it is that we and the universe exist. If we find the answer to that, it would be the ultimate triumph of human reason-for then we would know the mind of God."

-Stephen W. Hawking

A Brief History of Time

TABLE OF CONTENTS

ABSTRACT

ACKNOWLEDGMENTS

TABLE OF CONTENTS

LIST OF TABLES

LIST OF FIGURES

LIST OF PLATES

1.0 INTRODUCTION TO RADIO FREQUENCY HEATING 1

2.0 LITERATURE REVIEW 5

- 2.1 Electrical Heating of Tar Sand Deposits 5
- 2.2 Simple Soil Decontamination Heating Experiments 8
- 2.3 Electrical Soil Decontamination Heating Experiments 10
- 2.4 Radio Frequency In-situ Heating Soil Decontamination Field Test 11
- 2.5 Modeling Uniform Heating along a Waveguide 13
  - 2.5.1 Transverse and Axial Electric Fields in a Non-Homogeneous Medium 13
  - 2.5.2 Promoting Axial Uniform Radio Frequency Heating 13
  - 2.5.3 Modeling Radio Frequency Heating of Moist Porous Material in a Coaxial Geometry 14
- 2.6 Cost Estimate of Remediation using In-situ Electrical Heating 16
- 2.7 Environmental Remediation using Vitrification 16

3.0 SCOPE OF THE EXPERIMENTAL PROGRAM 18

4.0 SIMPLE COAXIAL RADIO FREQUENCY HEATING OF SOIL 20

- 4.1 Experimental Design 20

4.1.1 Apparatus 20
    4.1.1.1 Electrical Parameter Measurements 20
    4.1.1.2 Sample Holder 21
    4.1.1.3 Electrical Components 22
    4.1.1.4 Monitoring Instrumentation and Procedure 23
4.1.2 Sample Preparation 25
4.1.3 Geotechnical Properties of Soils 25
4.2 Experimental Results and Discussion 27
4.2.1 Electrical Properties of Soils 27
4.2.2 Drying Experiments 29
4.2.3 Vitrification Experiments 34
4.3 Summary 37
5.0 ENGINEERING SCALE RADIO FREQUENCY HEATING OF CLAY 39
5.1 Experimental Design 39
5.1.1 Apparatus 39
    5.1.1.1 Sample Holder 39
    5.1.1.2 Electrical Components 41
    5.1.1.3 Monitoring Instrumentation 41
5.1.2 Clay and Sample Preparation 43
    5.1.2.1 Mixing 43
    5.1.2.2 Preparation and Compaction 43
5.2 Experimental Results and Discussion 44
5.2.1 Experiment 1 44
    5.2.1.1 Trial 1 44
    5.2.1.2 Trial 2 45
5.2.2 Experiment 2 47

5.3 Summary 49

6.0 MODELING AXIAL UNIFORM HEATING OF PARALLEL PLATE CONDUCTORS 51

6.1 Modeling Technique 51

6.2 Results and Discussion 55

6.3 Summary 55

7.0 CONCLUSIONS 56

7.1 Electrical Parameters of Soil and their Effect on RF Heating 56

7.1.1 Electrical Conductivity and Dielectric Constant 56

7.1.2 Drying Experiments 56

7.1.3 Vitrification Experiments 57

7.2 Electrode Array Geometry 57

7.3 Axial Uniform Heating along an Electrode 58

8.0 RECOMMENDATIONS 60

FIGURES 61

PLATES 137

REFERENCES 145

LIST OF TABLES

Table 2.1: Contaminant removal for RF heating field experiment (adapted from Dev *et al* 1988) 12

Table 4.1: Geotechnical parameters of the tested soils 27

Table 4.2: Dielectric constant of dry soils, 10-100 MHz. 28

Table 4.3: Devon silt (DS3)-energy efficiency during the heating test 31

Table 4.4: Pre-test geotechnical parameters for the drying experiments 32

Table 4.5: Post-test geotechnical parameters for the drying experiments 33

Table 4.6: Water removal calculated for the drying experiments 34

Table 4.7: Pre-test geotechnical parameters for the vitrification experiments 36

Table 4.8: Post-test geotechnical parameters for the vitrification experiments 37

LIST OF FIGURES

Figure 1.1: RF *in-situ* treatment module (adapted from Dev *et al* 1987). 62

Figure 2.1: A tri-plate electrode array (adapted from Dev *et al* 1988). 63

Figure 2.2: Parallel plate waveguide configuration with a low conductivity dielectric layer (adapted from Maslowski *et al* 1992). 64

Figure 2.3: Axial variation of the transverse electric field magnitude in a transversely homogeneous medium (adapted from Maslowski *et al* 1992). 65

Figure 2.4: Axial variations of the transverse and axial electric field magnitudes after introduction of a low conductivity layer (adapted from Maslowski *et al* 1992). 66

Figure 2.5: Variation of transverse and axial electric field (adapted from Nachai *et al* 1992), (a) time=0, no axial field, (b) time=18 min., growing axial field. 67

Figure 2.5: Variation of transverse and axial electric field (adapted from Nachai *et al* 1992), (c) time=110 min., full inter-leafing of nodes and anti-nodes, (d) time=240 min., the material has dried out, axial field is negligible. 68

Figure 4.1: Coaxial capacitor used as a sample holder in RF drying experiments. 69

Figure 4.2: Coaxial capacitor used as a sample holder in RF vitrification experiments. 70

Figure 4.3: Schematic diagram of the electrical configuration for the drying experiments. 71

Figure 4.4: Athabasca clay, wc=24.3%, (a) dielectric constant, (b) electrical conductivity. 72

Figure 4.5: Devon silt, wc=22.8%, (a) dielectric constant, (b) electrical conductivity. 73

Figure 4.6: Kaolinite, wc=38.5%, (a) dielectric constant, (b) electrical conductivity. 74

Figure 4.7: Bentonite, wc=213%, (a) dielectric constant, (b) electrical conductivity. 75

Figure 4.8: Athabasca clay, experiment AC2, impedance, (a) magnitude, (b) phase. 76

Figure 4.9: Devon silt, experiment DS2, impedance, (a) magnitude, (b) phase. 77

Figure 4.10: Devon silt, experiment DS3, impedance, (a) magnitude, (b) phase. 78

Figure 4.11: Kaolinite, experiment K1, impedance, (a) magnitude, (b) phase. 79

Figure 4.12: Bentonite, experiment B2, impedance, (a) magnitude, (b) phase. 80

Figure 4.13: Impedance phase of a sample as it decouples. 81

Figure 4.14: Equivalent circuit for RF drying and vitrification tests. 82

Figure 4.15: Impedance magnitude of a sample as it decouples. 83

Figure 4.16: Athabasca clay, experiment AC2, temperature at the inner electrode. 84

Figure 4.17: Devon silt, experiment DS2, temperature at the inner electrode. 85

Figure 4.18: Devon silt, experiment DS3, temperature at the inner electrode. 86

Figure 4.19: Kaolinite, experiment K1, temperature at the inner electrode. 87

Figure 4.20: Bentonite, experiment B2, temperature at the inner electrode. 88

Figure 4.21 (a): Athabasca clay (AC2), water content distribution at 2:00 hours @1500 W. 89

Figure 4.21 (b): Athabasca clay (AC2), water content distribution at 4:30 hours @1500 W. 90

Figure 4.22 (a): Devon silt (DS2), water content distribution at 1:20 hours @1500 W. 91

Figure 4.22 (b): Devon silt (DS2), water content distribution at 2:50 hours @1500 W. 92

Figure 4.22 (c): Devon silt (DS2), water content distribution at 3:50 hours @1500 W. 93

Figure 4.23 (a): Devon silt (DS3), water content distribution at 1:20 hours @1500 W. 94

Figure 4.23 (b): Devon silt (DS3), water content distribution at 2:40 hours @1500 W. 95

Figure 4.23 (c): Devon silt (DS3), water content distribution at 4:20 hours @1500 W. 96

Figure 4.24 (a): kaolinite (K1), water content distribution at 2:30 hours @1500 W. 97

Figure 4.24 (b): kaolinite (K1), water content distribution at 4:15 hours @1500 W. 98

Figure 4.25 (a): bentonite (B2), water content distribution at 5:00 hours @1500 W. 99

Figure 4.25 (b): bentonite (B2), water content distribution at 11:05 hours @1500 W. 100

Figure 5.1: Electrode array, plan view with outline of engineering scale laboratory experiment. 101

Figure 5.2: Engineering scale laboratory experiment sample holder. 102

Figure 5.3: X, Y, Z co-ordinates of engineering scale test. 103

Figure 5.4: Plan view of the electric field during Stage 1. 104

Figure 5.5: Plan view of the electric field during Stage 2. 105

Figure 5.6: Temperature monitoring points for the engineering scale test. 106

Figure 5.7: Engineering scale test, impedance, experiment 1, trial 1, stage 1, (a) magnitude, (b) phase. 107

Figure 5.8: Engineering scale test, impedance, experiment 1, trial 2, stage 1, (a) magnitude, (b) phase. 108

Figure 5.9: Temperature in the plane y=0 cm after 5:09 hours @1500 W, experiment 1, trial 2, stage 1. 109

Figure 5.10: Temperature in the plane y=0 cm after 7:04 hours @1500 W, experiment 1, trial 2, stage 1. 110

Figure 5.11: Temperature in the plane z=27 cm after 11:42 hours @1500 W, experiment 1, trial 2, stage 1. 111

Figure 5.12: Temperature in the plane z=15 cm after 0 hours, experiment 1, trial 2, stage 2, day 3. 112

Figure 5.13: Temperature in the plane z=15 cm after 2:00 hours @1500 W, experiment 1, trial 2, stage 2, day 3. 113

Figure 5.14: Temperature in the plane z=15 cm after 4:01 hours @1500 W, experiment 1, trial 2, stage 2, day 3. 114

Figure 5.15: Temperature in the plane z=15 cm after 6:03 hours @1500 W, experiment 1, trial 2, stage 2, day 3. 115

Figure 5.16: Temperature in the plane z=15 cm after 8:07 hours @1500 W, experiment 1, trial 2, stage 2, day 3. 116

Figure 5.17: Water content in the plane z=25 cm after 8:07 hours @1500 W, experiment 1, trial 2, stage 2, day 3. 117

Figure 5.18: Engineering scale test, impedance, experiment 2, stage 1, (a) magnitude, (b) phase. 118

Figure 5.19: Temperature in the plane y=0 cm, 4:01 hours @1500 W, experiment 2, stage 1. 119

Figure 5.20: Temperature in the plane y=0 cm after 5:59 hours @1500 W, experiment 2, stage 1. 120

Figure 5.21: Temperature in the plane y=0 cm after 8:02 hours @1500 W, experiment 2, stage 1. 121

Figure 5.22: Temperature in the plane y=0 cm after 12:01 hours @1500 W, experiment 2, stage 1. 122

Figure 5.23: Temperature in the plane z=27 cm after 12:01 hours @1500 W, experiment 2, stage 1. 123

Figure 5.24: Temperature in the plane z=15 cm after 0 hours, experiment 2, stage 2. 124

Figure 5.25: Engineering scale test, impedance, experiment 2, stage 2, (a) magnitude (b) phase. 125

Figure 5.26: Temperature in the plane z=15 cm after 2:03 hours @1500 W, experiment 2, stage 2. 126

Figure 5.27: Temperature in the plane x=30 cm after 15:17 hours @1500 W, experiment 2, stage 2. 127

Figure 5.28: Temperature in the plane x=30 cm after 33:14 hours @1500 W, experiment 2, stage 2. 128

Figure 5.29: Temperature in the plane x=30 cm after 41:26 hours @1500 W, experiment 2, stage 2. 129

Figure 5:30: Water content in the plane z=15 cm after 41:26 hours @1500 W, experiment 2, stage 2. 130

Figure 6.1: Plan view of staggered single phase electrode array and computational cell (adapted from Nachai *et al* 1992). 131

Figure 6.2: (a) Cross-sectional view of the grid block structure in r-z space (b) three dimensional view of toroidal grid block i,j (adapted from Nachai *et al* 1992). 132

Figure 6.3: Water content at 10.8 hours, case with dielectric coating, residual electrical conductivity=1 x 10^{-5} S/m. 133

Figure 6.4: Water content at 24.2 hours, case with dielectric coating, residual electrical conductivity=1 x 10^{-5} S/m. 134

Figure 6.5: Water content at time 41.7 hours, case with dielectric coating, residual electrical conductivity=1 x 10^{-5} S/m. 135

Figure 6.6: Water content at time 41.7 hours, case with dielectric coating, residual electrical conductivity=1 x 10^{-3} S/m. 136

LIST OF PLATES

Plate 4.1: Athabasca clay (AC/Cuϕ7) vitrification experiment, cut section. The sample is 10 cm long by 7 cm wide. ... 138

Plate 4.2: Devon silt (DS/Cuϕ7) vitrification experiment, cut section. The sample is 6 cm long by 4 cm wide. Note the copper from the electrode on the edge of the solidified material. ... 139

Plate 4.3: Athabasca clay (AC/weld) vitrification experiment, cut section. The sample is 13 cm long by 10 cm wide. ... 140

Plate 4.4: Bentonite (B/steelϕ3) vitrification experiment. The product of vitrification is a fragile shell. The sample is 6 cm long by 5 cm wide. ... 141

Plate 5.1: Sample holder with the matching network in place. Power amplifier and signal generator are in the background. ... 142

Plate 5.2: Sample prior to a test with thermocouples and thermometers in place. ... 143

Plate 5.3: Sample after a test illustrating the shrinkage cracks. ... 144

1.0 INTRODUCTION TO RADIO FREQUENCY HEATING

The conventional treatment of ground contaminated with hazardous waste involves excavation, possible processing, and transport of contaminated soil to a suitable waste landfill facility. The expense of these operations has promoted the search for new effective technologies for *in-situ* remediation, which consists of treating the soil in place to remove the volatiles, thus reclaiming the land. One of the promising methods being explored is *in-situ* heating using radio frequency (RF) energy. The volatiles and organic wastes in the ground are heated using RF energy and vaporized and/or steam-stripped to be recovered at the surface (Figure 1.1). The challenge is to heat uniformly large volumes of soil to 100 to 300°C using RF energy.

In general RF is considered to range from 45 Hz to 10 GHz, but for most heating applications the range is considered to be 6.78 MHz to 2.45 GHz (Dev *et al* 1987). The broadcast frequency is in the industrial, scientific, and medical band. The frequency of energy is selected on the basis of the electromagnetic (EM) characteristics of the medium to be heated. Electrically, earth media, such as soil, are generally considered as lossy heterogeneous dielectrics. They consist of a low loss dielectric matrix or particle pack impregnated with a conducting aqueous solution.

The electrical properties of the soil, the dielectric constant and electrical conductivity, help determine the amount of RF energy that can be dissipated in the ground. The electrical properties are a function of the frequency of the applied electric field, soil temperature and the composition of the soil, primarily water content and density. Secondary effects of soil composition that affect the electrical properties are organic matter content, salinity, the number of layers of bound water molecules, which is dependent upon the particle size distribution and mineralogy (soils with large surface area will have a greater amount of water held at the surface), the porosity, the direction of propagation of the wave relative to any regular geometry of the components and the interaction between the saturating fluid and solid matrix (Santamarina and Wakim 1992). The electrical parameters determine the depth of penetration of the EM field for a given frequency. If the frequency is too high the earth medium is very lossy and the depth of penetration of energy is limited. Only a small volume of material close to the energy source will be heated. If the frequency chosen is too low, then very little energy absorption will take place in the earth medium and heating will be ineffective. The frequency of operation must therefore be matched to the electrical characteristics of the soil, resulting in an optimum range of frequencies for a given volume of material and its electrical parameters.

Appropriate electrical impedance matching methods must be used to ensure effective energy transmission from the source to the earth medium. Provisions must be made to maintain the impedance match as heating progresses and the electrical parameters of the soil change.

The principle of RF heating is that heat is generated largely as the result of a dielectric rather than an ohmic loss mechanism. Ohmic heating is the result of an ionic current that flows in a material in response to an electric field. The electrons pushed up into the conduction band and through the soil mass produce resistance heating. Dielectric heating is produced by the physical distortion of the atomic or molecular structure of polar materials in response to a time-varying electric field. The dipole moments of the molecules in a polar substance have random orientation. Application of an external electric field will cause the dipole moments to begin to align. Orientation is hindered by internal friction, molecules colliding with each other, preventing complete alignment. The physical distortion of molecules dissipates mechanical energy which is translated into thermal energy. Viscous drag, hydrogen bonding *etc.* resist molecular rotation creating a delay in the response to the electric field. The rate of change of the field must be faster than the rate of change of the molecules but not too fast or little molecular displacement will take place.

The difference in the polarization vector resulting from the sum of the dipole moments of the molecules and the electric field vector can be expressed by defining a complex dielectric constant, ε^*, where

$$\varepsilon^* = \varepsilon' - i\varepsilon''.$$

The imaginary component of the complex dielectric constant accounts for all dielectric loss processes. The ratio of the real and complex parts of the dielectric constant

$$\tan d = \varepsilon''/\varepsilon'$$

is called the loss tangent and d is the loss angle. A high loss tangent means that the polar molecules are having considerable difficulty aligning themselves with the electric field and thus effective RF heating is possible (Smith and Hinchee 1993). Earth materials have a high loss tangent when they are moist and a low loss tangent when they are dry. RF heating of an earth-type formation can be likened to the heating that would occur in a large scale microwave oven.

A higher level of intensity of electric heating would result in vitrification of the soil mass. By heating a volume of soil to 1100 to 1600°C the soil will melt and vitrify and upon cooling become a hard glass-like lump. Vitrification has been studied as an alternative for site remediation (Arienti *et al* 1988, Timmons *et al* 1990, Byers *et al* 1991 and Jacobs *et al* 1992). The product of the vitrification of soil is a solid glass material that would render all contaminants in the soil inert. An additional possible application of soil vitrification is slope stabilization. By creating a very intense localized electric field around an electrode it should be possible to vitrify soil into a glass anchor. A slope could be stabilized by placing an array of electrodes and vitrifying the soil around the electrodes creating an array of glass anchors.

2.0 LITERATURE REVIEW

The technology for RF heating of large volumes of earth material *in-situ* was first developed for enhancement of oil sand recovery. Since laboratory bench scale heating tests have illustrated the potential for heat to drive off organic compounds and other contaminants from soil there is hope that an *in-situ* environmental remediation application can be developed. There has been one pilot scale field test to assess the potential of RF heating as an environmental remediation method. Concurrent with experimentation is the development of algorithms and computer models to simulate RF heating of moist porous materials within a waveguide (electrode array).

2.1 Electrical Heating of Tar Sand Deposits

RF *in-situ* heating was first developed for the purpose of processing hydrocarbonaceous earth reservoirs to enhance bitumen recovery. The reservoir is first heated volumetrically to lower the viscosity of the bitumen. The bitumen is then recovered by conventional techniques such as fluid replacement or gravity drive. The principal difficulty of most other heating methods, because oil sand is a poor thermal conductor and is nearly impermeable, is the transfer of heat.

With the growing interest in electrical heating it is necessary to study the electrical parameters, dielectric constant and electrical conductivity, of oil sand. The feasibility of RF heating is dependent upon these factors. Chute *et al* (1979) generated data to clarify the dependence of the electrical properties of oil sand on density, water content and temperature with the intent to extend laboratory results to estimate the electrical properties of oil sand for given *in-situ* conditions. Such extrapolations are approximate given the variable nature of oil sand samples. The electrical parameters of two samples with identical water content and density can vary by as much as 20% due to pore water distribution. Laboratory tests can still provide a sufficiently accurate description of the electrical properties of oil sand *in-situ* to permit evaluation of the use of electrical energy to heat oil sand deposits.

Initial attempts at electrically heating large volumes of soil were made by placing simple electrical, 60 Hz, heating elements within the formation. This technique depends upon ambient water to provide electrical conductivity. Since the flow of electrical current is dependent on the presence of water, when the ground dries out around the electrode and the resistance becomes too high, current flow stops. The result is non-uniform heating, inefficient use of power due to the high temperatures reached near the electrodes, and relatively low temperatures elsewhere (Flock and Tharin 1975).

Later attempts at volumetric heating involved RF microwave dielectric heating (Albernathy 1974). By lowering antennas into boreholes relatively large volumes of ground could be heated, but still not uniformly. An energy delivery system was required that would create a uniform electric field and thus a uniform current density over a desired volume of the formation.

The Illinois Institute of Technology Research Institute has developed an efficient RF power deposition technology that can heat large volumes of oil sand to hasten and improve recovery of bitumen (Bridges *et al* 1979). Tubular electrodes are inserted into boreholes and energized by an RF power source. The electrode pattern, a tri-plate line configuration, is designed to minimize energy losses. A tri-plate line is a rectangular analog of a cylindrical coaxial cable where a row of electrodes simulates a high tension plate in the ground while two parallel rows of electrodes on either side are the ground electrodes (Figure 2.1). With appropriate spacing it is possible to contain almost all of the applied energy within the formation volume enclosed by the structure. The geometry of the tri-plate line is determined by the thickness of deposit and desired heating rate. Typically the spacing between adjacent rows is less than the length of the electrodes, and separation of the electrodes is less than the row spacing. Lower heating rates and temperatures allow the use of larger spacings. An expected spacing for production purposes might be a 10 m row separation, and a 4 m electrode spacing.

Stresty *et al* (1986) carried out a field experiment to test the potential for recovery of bitumen from tar sand deposits using RF energy. The volume of tar sand heated was 25 m^3. The electrodes were 6 m long and positioned vertically into the tar sand, 10 in the middle row and 14 on the outside rows. This number of electrodes implies a very close spacing, 1 m between rows and 20 cm between electrodes (Chute and Vermeulen 1989). The applied power was 40-75 kW. The frequency of operation was 2.2875 MHz while wet, and 13.56 MHz after drying. The average temperature attained during the first test, which had to be stopped due to inadequate roof support, was 120°C. During the second test the temperature peaked at 200°C, 14 days into the 20 day test. Electrically, initially the tar sand is a high loss material, but after moisture evaporation it becomes a low loss dielectric. Total bitumen production was 1.3 m^3, which represented about 35% recovery of the bitumen in place. Heating was uniform and energy loss was minimal. The formation was successfully uniformly heated.

2.2 Simple Soil Decontamination Heating Experiments

A series of laboratory tests were carried out by Dev *et al* (1987) to determine the potential for heat to drive off chlorinated organic compounds from sandy soil. Tetrachloroethylene, with a normal boiling point of 120.8°C, was selected as a representative contaminant to be used to spike soil samples taken from a waste site. A 500 ml flask was filled with approximately 1 kg of sand at 5-10% moisture content. The sand samples were spiked to concentrations of 9.28 and 957.3 ppm. The soil was heated by a heating mantle to the desired temperature and kept there for 4 hours. The distillate was collected and analyzed to directly determine the amount of the contaminant that was removed. The following results were obtained.

High concentration samples (957.3 ppm): Eight samples were heated to temperatures ranging from 89 to 131°C. The removal rates achieved were 94.2 to 99.8%. A sample at 21°C for 4 hours had a recovery of 0.4%. There was no significant variation in contaminant removal in the higher temperature range.

Low concentration samples (9.28 ppm): Five samples in the temperature range of 89 to 101°C had removal rates of 93.5 to 97.5%. A sample at 21°C for 4 hours had a removal rate of 0.3%.

The results are a positive indication of the potential to use heat to remove contaminants from soil.

Oma and Buelt (1988) also performed some simple heating experiments to measure contaminant recovery. Two sets of soil samples of sand, silty loam and bentonitic clay were prepared with 0.1 wt% of contaminant, one set with 2-chlorophenol, the other with hexachlorobenzene. These chemicals were chosen for their different boiling points, 175°C and 322°C, respectively. The samples were heated at a rate of 300°C/hour. They were removed at different temperatures to determine the relationship between removal efficiency, temperature, and boiling point of the chemical.

The removal efficiency was inversely proportional to the boiling point of the contaminant. The 2-chlorophenol achieved a removal efficiency in excess of 90% at a temperature just above its boiling point. Hexachlorobenzene required a temperature of 400°C, much in excess of its boiling point, to achieve a removal of 70%. When the 2-chlorophenol samples were heated to 330°C removal was 99.5%. It is expected that with sufficient heat 99.9% removal is possible. The results do not show a correlation between contaminant removal and soil type.

Simple application of heat can overcome sorption and remove contaminants with high boiling points at reasonable efficiencies. These tests suggest that temperatures must be 150°C above the boiling point to achieve greater than 99% removal. Results by Dev *et al* (1988) suggest that the opposite is true, and that significant removal of contaminants can occur at temperatures below the boiling point of the contaminant. Further study is required to ascertain the factors that determine the effectiveness of heat to remove contaminants from soil.

2.3 Electrical Soil Decontamination Heating Experiments

Oma and Buelt (1988) used a DC arcing technique to heat soil. Two tests were carried out using this technique on sand samples injected with 2-chlorophenol. When the power was first turned on there was simple resistive heating. As the sand dried out the resistance increased. As the resistance increased the applied voltage increased and repetitive arcing through the soil began. Electrical current follows the path of least resistance and therefore concentrates on areas of moisture.

Two samples were made up of 4.5 and 9.7 kg respectively. The samples were heated for 2.7 and 4.2 hours. The power levels were 125 and 115 W. The temperatures reached were 194 and 304°C. The removal efficiency of the contaminant was 60-70% and 95%.

The second test incorporated a vacuum recovery system and since the temperature of the contaminated sample was much higher, a much higher removal efficiency was possible. The 5% organics that were not recovered migrated away from the original injection point, and away from the heated zone. Tests by Dev *et al* (1988) suggest that migration would be towards the heated zone. If there is a net migration outward from the heated zone then this is a significant drawback to the process. In a field situation contaminants would not be removed and recovered but rather would simply be pushed outward into an adjacent area. The thermodynamics of a water-steam geothermal system are complex and thus it is an ongoing area of research (Freeze and Cherry 1979).

2.4 Radio Frequency *In-situ* Heating Soil Decontamination Field Test

Dev *et al* (1988) and Dev and Downey (1988) describe an RF heating environmental remediation field test at Camp Douglas National Guard Base in Wisconsin. The test area was an abandoned fire training pit used in simulated aircraft fire drills. It was estimated that 190 m^3 of unburned hydrocarbons had soaked into the ground over the lifetime of the pit. The boiling points of most of the contaminants are in the range of 80 to 300°C. Sample borings indicated that to the water table, approximately 3.66 m deep, the average concentration of hydrocarbons was approximately 4 000 mg/kg. Analysis of pre- and post-test samples were carried out to determine contaminant removal. A tracer was injected during the test to determine migration patterns.

A pilot test was performed prior to the field test. A stainless steel pipe 2.1 m long, 5 cm diameter was filled with soil mixed with jet fuel. The sample was heated to 150-160°C in 14 hours and kept there for 40 hours. Contaminant removal was 90 to 95%. Removal of pentadecane, which has a boiling point of 270.5°C, was 94%. This experiment indicated that contaminants could be removed at temperatures below their boiling point. For this experiment however a "steam sweep" was required i.e. injecting pre-heated water into the base of the column. It is felt that such a sweep occurs in the field naturally as cool water intrudes into the heated zone.

The soil at the site is homogeneous, medium grain sands to 4 m depth. The bedrock is fractured sandstone. To direct the RF energy into the ground 39 electrodes in a tri-plate configuration were inserted into the ground. The 3 rows of electrodes covered a 1.8 x 3.6 m area to a depth of 2.1 m. To monitor the temperature, thermocouples were located on the inner walls of the electrodes.

The frequency of RF energy was 6.78 MHz. The power input was 35 kW for the first 4 days to dry out the soil and 20 kW thereafter. The time to reach 100°C was 2 days. After 8 days the temperature was 150 to 160°C. Contaminants were removed from the ground in their vapor phase and were collected in a vapor barrier covering the surface, condensed, and collected in drums for disposal.

The test was shut down after 12.5 days and the test site was allowed to cool for 17 days before final sampling took place.

Table 2.1: Contaminant removal for RF heating field experiment

(adapted from Dev *et al* 1988)

Removal (%)	volatile	semi-volatile
aliphatics	99.3	94.3
aromatics	99.6	99.1

Significant removal, 83%, of higher boiling point, 287°C, hexadecane was also observed. This is almost certainly due to the steam sweep from boiling water and the long residence time at 150 to 160°C. Removal as a function of depth was fairly uniform. Soil samples that were taken below and outside the heated zone showed significant removal, approximately 70%. A tracer was injected 1.2 m from the electrodes at a depth of 1.8 m. In 107 minutes it was detected in the vented gases. All indications are that there was water migration into the heated zone.

2.5 Modeling Uniform Heating along a Waveguide

Considerable control can be exerted over the distribution of an electric field and the path of electrical current through a formation by using various electrode configurations. Therefore, temperature distribution in those configurations can be significantly controlled.

2.5.1 Transverse and Axial Electric Fields in a Non-Homogeneous Medium

To achieve uniform heating along the length of a waveguide, two parallel plate electrodes inserted into a formation, a low conductivity dielectric layer is introduced between the plates (Figure 2.2). This inhomogeneity changes the distribution of the initially transverse electric field by introducing an axial electric field component. The standing wave patterns created by the transverse and axial electric fields have inter-leafing nodes and antinodes. This inter-leafing of nodes leads to fairly uniform heating along the waveguide if the intensities of the transverse and axial electric fields are of the same order. The cause for the inter-leafing is that the transverse and axial electric field components of the traveling wave are reflected out of phase at the termination of the guiding wave structure. The mechanism is an example of guided propagation of an electromagnetic wave in a lossy non-homogeneous medium (Maslowski *et al* 1992).

2.5.2 Promoting Axial Uniform Radio Frequency Heating

An analytical example of the inter-leafing of transverse and axial electric fields can be obtained by solving Maxwell's equations for the electromagnetic field, subject to the boundary conditions imposed by the problem. Two closely spaced arrays of electrodes are approximated by two parallel plates, 15 m apart, 200 m long, and open circuited at the end removed from the power source. Electrical parameters typical of oil sand are used to represent the lossy homogeneous material filling the wave guide. The system is excited at a frequency of 200 kHz. For the electrical properties of oil sand the skin depth would be 36 m (Skin depth is the distance from the power source at which the amplitude of the EM wave falls to 37% of its initial amplitude. It diminishes as the frequency and electrical conductivity increase). The electric field is entirely transverse and rapidly decays with distance from the power source (Figure 2.3). The medium is lossy and results in very non-uniform heating along the length of the waveguide.

Now consider the same system except that, in addition to the oil sand, a dry, non-conducting layer is assumed to be present between the plates. The EM field between the plates is now affected so that there is an increase in wavelength. Also the attenuation of the EM field is greatly reduced, due to the fact that the oil sand is now electrically partially decoupled (reduction in current) from the guiding structure by the dielectric layer, and hence absorbs energy less effectively. The transverse discontinuity also causes the EM wave to acquire an axial field component. Interleafing of standing waves of the transverse and axial electric field appear and uniform heating results (Figure 2.4) (Maslowski *et al* 1992).

2.5.3 Modeling Radio Frequency Heating of Moist Porous Material in a Coaxial Geometry

The discussion so far has involved heating large blocks of soil using arrays of parallel electrodes. Nachai (1991a) developed the numerical model TMCOPTER to simulate RF heating of porous, lossy materials within a coaxial geometry. Temperature and water content are predicted as functions of time. An EM field solution is explicitly coupled with a heat conduction solver.

The numerical model was used to simulate RF heating of a fine grained sand, saturated with a brine solution. The frequency of the test was 50 MHz. The power was 500 W. Initially heating was very intense near the inner electrode. A dry zone formed almost instantly at the source end of the conductor. The dry coating reduces wave attenuation, allowing the wave to further penetrate and heat more of the load. At first the axial component is negligible (Figure 2.5a). As an axial uniform dry coating forms around the conductor the axial field becomes significant (Figure 2.5b). The thickness of the dry coating increases, creating concentric rings of varying water content. The coating also induces an axial current flow between the conductors. With both transverse and axial current flows quite uniform heating results. Figure 2.5c illustrates the full effect of the inter-leafing of nodes and antinodes. Finally, when the material has dried out the medium between the concentric conductors again approaches homogeneity, and the axial field again becomes negligible (Figure 2.5d).

There is no analytical solution for problems involving evolution of steam from a moist porous material subjected to RF heating. It is thus difficult to analytically verify a numerical model simulating RF heating. A physical verification of the numerical model was provided by a coaxial cell filled with a brine/sand mixture. Heating proceeded in the manner predicted by the model (Nachai *et al* 1992).

2.6 Cost Estimate of Remediation using *In-situ* Electrical Heating

There have been a number of estimates as to the cost of RF heating for environmental remediation. The cost would include a power delivery and a contaminant collection system.

The most detailed cost estimate was done by Dev *et al* (1987). Their calculations were based on the remediation of a 3 acre site heated in cells 30 x 30 m by 2.5 m deep. The average water content at the site was 12.1%. The desired soil temperature was 170°C. The project would take 1 year and the cost would approximately be \$100/m^3. The cost of remediation is dependent however upon the water content of the soil. The higher the water content the greater the energy that is required to dry the soil, and thus the greater the cost of remediation.

Other studies by Santamarina and Wakim (1992) and Oma and Buelt (1988) also estimated that the cost of similar operations would be \$100/m^3.

More standard remediation techniques of excavation and incineration typically cost \$400-500/m^3 (Dev and Downey 1988 and Dev *et al* 1988).

2.7 Environmental Remediation using Vitrification

Vitrification has also been tested as a treatment technology for contaminated soil. The intent is to heat the soil to such a high temperature as to form an inert glass product. The molten mass when cooled results in a glass monolith with chemical and physical characteristics similar to that of volcanic glass (Timmons *et al* 1990). The method is dependent on the conductivity of the molten mass. The depth to which soil could be heated is limited to perhaps 13 m. The volume reduction of the mass would be significant, 20 to 40%. Waste blocks would be expected to maintain their integrity for 10 000 years (Arienti *et al* 1988).

3.0 SCOPE OF THE EXPERIMENTAL PROGRAM

To develop RF *in-situ* heating for environmental remediation it is first necessary to be able to uniformly heat large volumes of soil to 100-300°C. There are three principal issues of RF heating that this program investigated: 1. measurement of electrical parameters of soil and their relationship to soil type and water content, 2. design of an electrode array for efficient energy delivery, 3. achievement of uniform heating along the length of an electrode. In addition, attempts were made to vitrify soil to assess its potential for ground stabilization.

Electrical conductivity and dielectric constant of four types of soil were measured over the frequency range from 10 to 100 MHz using an electric and magnetic probe. The same four soils were subjected to RF heating in a short coaxial cell to assess their general response in a high power RF environment. Each of the soils was also subjected to very intense electric fields in an attempt to achieve vitrification. By heating to very high temperatures soil will melt and when cooled will turn into a glass like mass. Such glass lumps, if consistent, could serve as ground anchors.

Heating a significant volume of soil will require an electrode array that will deposit energy efficiently into the ground. The efficiency of heating will depend upon the effectiveness of the power source to deliver energy to the formation, and the uniformity of the electric field that produces the heating. The electrode configuration must also minimize leakage by containing all of the energy. An engineering scale laboratory test will simulate a "piece of the field". That is, a two dimensional plan view section of an electrode array placed in a formation will be investigated. This will permit an examination of the heating that occurs in the plane transverse to the electrodes. The laboratory test will not allow study of heat deposition as a function of the third dimension, depth, that is distance measured along the length of the electrode.

An RF heating computer model TMCOPTER (Nachai 1991b), will be used to test the premise that a dielectric layer of dry soil introduced into a parallel plate waveguide adjacent to the wet soil will produce uniform heating along the length of the waveguide. The inhomogeneity of dry soil will run parallel along the inside of the electrodes on either side of the soil. Work by Nachai (1992) and Maslowski (1992) indicates that the dielectric coating will produce an axial electric field that is reflected out of phase with the transverse one at the far end of the electrode structure. This out of phase relationship causes the inter-leafing of nodes and antinodes of the transverse and axial electric fields and should result in uniform heating along the length of the electrode. The computer model will use as an initial condition the state of the formation in the transverse plane as produced in the "piece of the field" laboratory test, and then simulate the ensuing heating along the electrode to determine the extent to which the anticipated uniform drying materializes due to the inter-leafing effect.

4.0 SIMPLE COAXIAL RADIO FREQUENCY HEATING OF SOIL

4.1 Experimental Design

Two series of experiments were carried out to study the potential of RF energy for the purpose of environmental remediation and ground stabilization. Four soil types were heated within two different coaxial configurations. The principal goal of the first experiment was to dry soil. The second set of experiments attempted to vitrify the soil. Prior to running the RF heating tests measurements were made to determine the electrical conductivity and dielectric constant of the four soil types when dry and wet to determine how these parameters vary with frequency.

4.1.1 Apparatus

4.1.1.1 Electrical Parameter Measurements

The four soils, Athabasca clay, Devon silt, bentonite and kaolinite, were tested to measure electrical conductivity and dielectric constant of both wet and dry samples over a range of frequencies. The wet samples were mixed to approximately their optimum water content. The soils were tested over the frequency range 10 to 100 MHz using the measuring cell described by Chute *et al* (1978). The method was based on the measurement of electric and magnetic fields on the input of a coaxial transmission line filled with the tested material. The coaxial sample holder is fitted with electric and magnetic field probes. The voltage measured by the electric field probe is proportional to the electric field, and hence to the voltage in the coaxial cable at the sample-air interface. The induced probe voltages are related in a straight forward manner to the electrical properties of the sample. The probe was energized by an SP 3200B VHF Oscillator, the signal frequency was measured by an HP 5340A

Frequency Counter, and the magnitude and phase of voltage corresponding to the E and H fields were measured by an HP 8405A Vector Voltmeter. The cell permits the rapid and accurate evaluation of the electrical conductivity and dielectric constant of earth materials.

A MATLAB program called 'ehmeas' developed by Dr. P. Stroemich of the Department of Electrical Engineering University of Alberta was used to compute the electrical conductivity and dielectric constant of the tested soils based on the measured parameters.

4.1.1.2 Sample Holder

Both of the RF heating experiments used coaxial sample holders (Figure 4.1 and 4.2). In the drying tests more uniform heating was required than for the vitrification tests. Therefore the inner electrode for the drying tests was much thicker than the one used for the vitrification tests. This is because the electric field intensity around a conductive structure increases as its radius of curvature decreases; therefore, using thin inner conductors caused higher heating rates in the proximity of the conductor than using the thicker ones.

The drying experiments used a copper pipe 10.2 cm in diameter as the inner electrode. Its lateral surface was perforated with 0.5 mm diameter holes to facilitate the escape of steam from the sample.

In order to create a very high intensity field around the electrode the diameter of the inner conductor used in vitrification tests ranged from 3 to 7 mm . During the initial tests a 7 mm diameter copper pipe was used as the inner electrode. However, due to high temperatures and intensive arcing on the electrode surfaces, their continuity was usually destroyed before significant portions of the sample could be melted. In an attempt to correct this problem 3 mm diameter stainless steel rods were used as inner electrodes. Unfortunately, these electrodes were destroyed in the same manner described above. Plasmatic erosion proved destructive to 3 mm diameter tungsten electrodes (melting point greater than 3000°C). Eventually coated electrodes (coated welding rods) were used in order to prevent development of arcing between the center conductor and the sample. No damage to the electrode surface was noted and substantial fragments of the sample could be vitrified around the center part of the conductor.

4.1.1.3 Electrical Components

Figure 4.3 shows a schematic diagram of the electric circuitry for the drying experiments. A signal source was provided by an HP 8656A signal generator. The signal used was a continuous sinusoidal wave at 14 MHz. This signal was then amplified by an Amplifier Research 2000L RF amplifier. The upper power limit of the amplifier is 2000 W continuous wave, but during experiments no more than 1500 W were supplied to the sample. Past experience indicates that at this power level an unexpected surge in the reflected power due to sudden sample impedance changes was still safe for the power stage of the amplifier.

The amplified RF signal was then passed through a line section of characteristic impedance of 50 Ω and a matching network to the sample. An RF directional wattmeter coupled with the 50 Ω line section through two plug-in-directional couplers allowed monitoring of both the forward and reflected power flows.

The most important step in delivering energy into the sample was to establish the correct matching circuit. In order for energy to be absorbed by the load, the amplifier must "see" a resistance of 50 Ω, that matches its own output impedance. In the case of an impedance mismatch power is reflected back into the amplifier. This results in inefficiency in power delivery and can also be destructive to the amplifier itself. The matching network between the amplifier and the sample can be adjusted to "cancel" the reactive parameters (inductance or capacitance) and transform the resistance of the sample, and thus match the sample impedance with the output impedance of the amplifier. The matching network consists of a variable vacuum capacitor and variable inductor in a Γ configuration (the capacitor in parallel with the sample and inductor in series) (Figure 4.3). Additional, discrete capacitors can be connected in parallel with the variable capacitor, effectively extending the range of impedance that can be matched. Both variable elements of the matching network can be adjusted under full power conditions, therefore allowing the minimizing of reflected power levels on a continuous basis during a test. The components of the matching network were installed inside an aluminum box held at ground potential. This form of an EM screen was used to reduce RF radiation from network elements to levels defined as safe by national standards. The matching network box was installed directly on the sample holder via two banana plugs.

The EM radiation from all system components shown in Figure 4.3 was monitored for safety with a Narda electromagnetic radiation monitor model 8616 to ensure that power density levels were always well below 0.5 mW/cm^2.

4.1.1.4 Monitoring Instrumentation and Procedure

Sample temperature during the drying experiments was measured by three J-type thermocouples (TCs) and three alcohol thermometers. Heating was stopped for short periods of time to insert the TCs to measure the temperature near the inner electrode. Teflon tubes to hold the TCs were placed into the sample along the inner electrode prior to the test at 2.5, 8.5, and 14.5 cm from the bottom. Glass thermometers, which do not contain any metal parts, could remain in the sample while power was on to monitor the temperature in the central and outer regions of the sample (Figure 4.3). The glass thermometers maximum range of up to 110°C precluded their use close to the electrode where the temperature quickly exceeds that limit.

The impedance of the sample was also measured during these breaks in heating using a HP 4815A RF vector impedance meter. The impedance was measured to determine the increase in resistance of the sample as it dried out and to measure the corresponding decrease in phase angle. As the phase angle approached -90° the sample is almost purely capacitive and is being effectively heated dielectrically. The impedance meter was also used during matching procedures to ensure that the power source was seeing a 50 Ω, 0° impedance at the sample.

Periodically, in addition to the temperature and impedance measurements, water content samples were taken to determine the extent of the dry zone around the inner electrode. Since the size of the water content samples were small compared to the size of the whole sample their removal was not considered to have a significant affect on heating. Water content is defined as the mass of water as a percentage of the mass of solid material (ASTM 1992a). The sampling tool was a simple steel pipe, 1.7 cm in diameter, with a sharpened end. Nine samples were taken, three deep at three locations on a radial line between the inner and outer electrode (Figure 4.3).

Since the power had to be turned off to carry out the described monitoring procedures they were done with all deliberate speed. The time to measure impedance and temperatures was typically 5 minutes. If water content samples were taken as well the procedure took 30 minutes. Temperatures were restored to pre-sampling levels within 20 minutes.

4.1.2 Sample Preparation

Samples were prepared in the laboratory by mechanically mixing dry powdered solid material with distilled water. The samples were mixed to approximately their optimum water content. After mixing the soil was hermetically sealed and left in a temperature and humidity controlled chamber, 8°C, 100 %, for at least 24 hours. Finally the soil was compacted into the sample holder according to standard compaction procedures (ASTM 1992b). The compaction energy was scaled according to the volume of the sample holder. The material was placed in five lifts, each approximately 3.5 cm in height. The sample was again placed in the cold room overnight.

4.1.3 Geotechnical Properties of Soils

Four types of soil were tested: Athabasca clay, Devon silt, bentonite and kaolinite. Their geotechnical properties are summarized in Table 4.1.

Athabasca Clay: The material originates from the Athabasca formation. The soil is classified as CL by the Unified Soil Classification (USC) system. The soil's strength is sensitive to moisture content.

Devon Silt: The silt is extracted from a borrow pit just north of Devon, Alberta. It is classified as CL on the USC system. The silt is frost susceptible and is typical of silts in northern Canada.

Bentonite (montmorillinite): The clay structure consists of a sheet of alumina octahedrons between two sheets of silica tetrahedrons. In the octahedral sheet there is partial substitution of alumina by magnesium. The space between the combined sheets is occupied by water and cations. The bond between the combined sheets is weak and thus a considerable amount of water can be absorbed causing the clay to swell.

Kaolinite: The clay structure consists of a single sheet of silica tetrahedrons combined with a single sheet of alumina octahedrons. The combined sheets are tightly held together by hydrogen bonds.

Table 4.1: Geotechnical parameters of the tested soils

Material	Atterberg limits (%)		owc	ρ_{dry}	mean sample values			
	LL	PL	(%)	(g/cm^3)	wc (%)	n	e	S (%)
Athabasca clay	43	21	22	1.65	24.3	0.39	0.66	97
Devon silt	46	20	21	1.63	22.8	0.41	0.68	99
bentonite	500	35	N/A	N/A	213	0.86	6.31	97
kaolinite	58	31	38	1.24	38.5	0.52	1.10	91

where:
LL-liquid limit
PL-plastic limit
owc-optimum water content
ρ_{dry}-optimum dry density
wc-water content
n-porosity
e-void ratio
S-saturation

4.2 Experimental Results and Discussion

4.2.1 Electrical Properties of Soils

The relative dielectric constant (ε_r) for all the soil samples varied inversely with frequency. Athabasca clay, Devon silt and kaolinite with water contents 24.3, 22.8 and 38.5% respectively, had values of ε_r of similar magnitude, from 50 down to 25 (Figure 4.4a, 4.5a and 4.6a). Bentonite with water content 213% had a much higher dielectric constant, ranging from 210 to 80 (Figure 4.7a).

Electrical conductivity increased roughly linearly with increasing frequency for all samples. The magnitude however was significantly different. Bentonite with the highest water content easily had the highest conductivity (Figure 4.7b). However kaolinite, which had a higher water content than either Athabasca clay or Devon silt, had the lowest conductivity (Figure 4.6b). This is a reflection of the secondary effects of salinity, mineralogy and organic matter etc. on conductivity. This was also emphasized by Athabasca clay and Devon silt where Athabasca clay had a higher conductivity despite having a similar density and water content as Devon silt (Figure 4.4b and 4.5b).

The dry soil samples did not show any significant variation in dielectric constant over the frequency range tested. The results for dry samples also varied little between soil type. Table 4.2 contains the average dielectric constant over the frequency range measured.

Table 4.2: Dielectric constant of dry soils, 10-100 MHz.

Soil	ε_r
Athabasca Clay	3.4
Devon Silt	3.4
Bentonite	3.7
Kaolinite	2.8

The conductivity of dry samples was extremely low and could not be measured accurately using available instruments.

4.2.2 Drying Experiments

Electrically all of the samples reacted in a similar manner when heated (Figures 4.8 to 4.12). Initially sample resistance was low and the sample was slightly inductive. With the start of heating the resistance dropped slightly and the sample became even more inductive. As the soil around the electrode dried the sample decoupled, the resistance rose rapidly and the sample quickly became very capacitive (Figure 4.13). Figure 4.14 represents an equivalent circuit of the coaxial capacitor and soil which combine to make up the sample. R_1 and L_1 represent the resistance and the inductance of the electrodes that deliver power to the soil. The electrode resistance is so small that it can be ignored. Initially the resistance of the soil, R_2, is very low so the dominant current is i_1. Heating in this phase is ohmic (Figure 4.13). As the soil along the electrode dries the resistance increases greatly (Figure 4.15) and i_2 increases in favor of i_1. The soil has decoupled, that is the heating mechanism has changed from resistive to dielectric (Figure 4.13). Bentonite with exceptionally high water content was initially almost purely inductive, after decoupling almost purely capacitive (Figure 4.12b). The kaolinite sample decoupled more smoothly compared to the other samples (Figure 4.11).

The time of significant decoupling indicated by the impedance measurements in Figures 4.8 to 4.12 corresponded with the time at which the temperature at the inside electrode rose past 100°C (Figure 4.16 to 4.20). The soil heated up to 100°C and dried out. The sample decoupled when a zone of dry soil was formed around the inner electrode.

Water content profiles illustrate the growth of the dry zone that has caused the decoupling (Figures 4.21 to 4.25). This dry zone results in the increase of the resistance of the sample and marks the beginning of dielectric heating. This dry layer will be critical in the future to the development of uniform axial heating (Maslowski *et al* 1992 and Nachai *et al* 1992)

All the soils were successfully heated and partially dried out. Bentonite of course, with its considerable amount of water, took much longer to dry out than any of the other samples. Most of the energy that goes into a sample is to heat and evaporate the water (the heat capacity of water is over four times that of soil). Therefore water content exerts the major control over the time it takes to heat a sample.

During a test there are several areas of energy loss. A certain amount of power is reflected back from the sample due to imperfect impedance matching. Energy is also lost to heat to the air and through the insulation. As a sample dries out these energy losses increase, reducing the efficiency of heating. As well energy is dissipated in the transmission line and matching network. Energy efficiency is defined as the percentage of the net energy delivered by the power source that causes heating of soil or the heating or evaporation of water. The energy delivered to the sample is calculated by subtracting the reflected from the forward power level (measured by the RF directional wattmeter) and multiplying by the time the power is on. The energy absorbed by the soil can be calculated using the temperature measurements and the water content data to determine the energy absorbed by the soil and water and the energy consumed to turn water into vapor. Table 4.3 illustrates where the energy was being absorbed throughout one of the tests on Devon silt. Note the increasing amount of energy that was applied to the evaporation of water. As the dry zone expanded the heat losses increased and there was a corresponding decrease in efficiency.

Table 4.3: Devon silt (DS3)-energy efficiency during the heating test

Time (min)	m_{water} (kg)	E_{in} (kJ)	E_{soil} (kJ)	E_{water} (kJ)	E_{evap} (kJ)	eff (%)
0	3.95	0	0	0	0	N/A
80	3.29	6894	1451	1320	1490	61.8
160	2.05	7008	786	526	2799	58.7
260	0.44	8760	1093	339	3636	57.8

where:

m_{water}-mass of water
E_{in}-energy into the sample
E_{soil}-energy absorbed by the silt
E_{water}-energy absorbed by the water
E_{evap}-energy to turn water into steam
eff-energy efficiency

The following tables summarize the geotechnical data before and after testing. All parameters are based on simple mass and volume measurements plus water content measurements (ASTM 1992a).

Table 4.4: Pre-test geotechnical parameters for the drying experiments

Sample	m_i (kg)	V (cm^3)	ρ (g/cm^3)	wc_i (%)	e	n	S (%)
AC1	17.42	8825	1.97	25.7	0.68	0.41	99.6
DS1	21.17	11031	1.92	26.4	0.75	0.43	93.8
B1	13.12	10791	1.22	213.0	6.12	0.86	96.3
K1	21.20	11194	1.89	38.3	0.93	0.48	109.0
B2	13.44	11713	1.15	222.0	6.76	0.87	90.8
AC2	19.83	10999	1.80	24.9	0.83	0.45	79.3
DS2	22.13	11031	2.01	22.1	0.61	0.38	95.6
DS3	22.96	12070	1.90	20.8	0.68	0.41	80.7

where:
m_i-initial mass
V-sample volume
ρ-density
wc_i-initial water content
e-void ratio
n-porosity
S-saturation
AC-Athabasca clay
DS-Devon silt
B-bentonite
K-kaolinite

Table 4.5: Post-test geotechnical parameters for the drying experiments

Sample	m_f (kg)	wc_f (%)	r (%)
AC1	14.60	5.4	79.2
DS1	15.96	0	100.0
B1	12.04	187.1	12.1
K1	16.35	6.6	82.7
B2	6.83	63.5	71.4
AC2	16.49	3.9	84.5
DS2	19.50	7.6	65.7
DS3	18.70	2.3	89.0

where:
m_f-final mass
wc_f-final water content
r-water removal
sample symbols as in Table 4.4

Table 4.6: Water removal calculated for the drying experiments

Sample	P_{for} (W)	P_{ref} (W)	time (hour)	E_{in} (MJ)	E_{ab} (MJ)	r (%)	eff (%)
K1	1500	41	4.25	22.3	14.8	83	66
B2	1500	68	5.00	25.8	18.9	71	73
AC2	1500	38	4.75	23.6	10.9	84	46
DS2	1500	39	4.08	19.7	9.7	66	49
DS3	1500	45	4.33	22.7	13.6	89	59

where:
P_{for}-forward power
P_{ref}-reflected power
time-heating time
E_{in}-energy in
E_{ab}-energy absorbed
r-water removal (water removed as a percent of initial water)
eff-energy efficiency
sample symbols as in Table 4.4

The energy efficiency calculations are averages over the length of the test. Because of the variable nature of the time increments between temperature measurement and water content sampling these numbers are not absolute quantities and should not be strictly compared.

4.2.3 Vitrification Experiments

The vitrification experiments used much thinner electrodes to create a very high electric field intensity near the inner electrode. The high intensity field resulted in much higher temperatures than were achieved during the drying tests. These higher temperatures were also reached in much shorter periods of time. Usually, after just 5 to 10 minutes of heating, considerable steam and fumes were observed. Power was usually delivered for less than 1.5 hours. Often the continuity of the inner electrode had been destroyed (it had melted). Plate 4.2 shows small seams of copper on the edge of the solidified material. The highest measured temperature near the inner electrode exceeded the thermocouple's range of 700°C. The temperature was likely significantly higher but unfortunately the power had to be turned off during temperature measurements and the sample always cooled significantly before temperatures could be measured. Thus, the actual temperature during melting could not be measured. Due to the nature of these tests no water content samples could be taken.

Athabasca clay and Devon silt have been successfully heated to their melting point. After cooling the result is a glass like lump of very hard material (Plates 4.1, 4.2, and 4.3). Less success was achieved with bentonite which only produced a brittle glass shell (Plate 4.4). This is due to the lack of solid material in the sample; the void ratio was 6.05. There is simply very little clay to vitrify. Apparently kaolinite did not reach its melting point as it did not vitrify.

The following tables summarize the geotechnical parameters and post experimental data.

Table 4.7: Pre-test geotechnical parameters for the vitrification experiments

Sample/ electrode	m_i (kg)	V (cm^3)	ρ (g/cm^3)	wc_i (%)	e	n	S (%)
AC/Cuϕ7	22.94	10370	2.21	23.6	0.48	0.32	131
DS/Cuϕ7	7.6	4011	1.89	21.9	0.70	0.41	82
K/steelϕ3	6.53	3925	1.66	38.1	1.19	0.54	84
B/steelϕ3	4.46	3741	1.19	203.7	6.05	0.86	93
K/Tgϕ3	6.51	3861	1.68	39.2	1.18	0.54	88
AC/weld	7.14	3701	1.93	24.2	0.70	0.41	91
AC/weld	7.61	3741	2.03	23.0	0.60	0.37	102

where:
m_i-initial mass
V-sample volume
ρ-density
wc_i-initial water content
e-void ratio
n-porosity
S-saturation
AC-Athabasca clay
DS-Devon silt
B-bentonite
K-kaolinite
Cuϕ7-copper electrode, 7 mm diameter
steelϕ3-steel electrode, 3 mm diameter
Tgϕ3-tungsten electrode, 3 mm diameter
weld-coated welding rod #7018

Table 4.8: Post-test geotechnical parameters for the vitrification experiments

Sample/ electrode	m_f (kg)	wc_f (%)	r (%)	P_{for} (W)	P_{ref} (W)	time (min)
AC/Cuϕ7	22.73	22	5	500-1500	20-200	120
DS/Cuϕ7	7.45	19	11	1000	20	45
K/steelϕ3	6.18	31	19	1000	20	45
B/steelϕ3	4.26	190	7	500-1000	100	90
K/Tgϕ3	6.19	33	17	1000	125	90
AC/weld	6.39	11	54	1500	25	60
AC/weld	N/A	N/A	N/A	1500	150	40

where:

m_f-final mass
wc_f-final water content
r-water removal (water removed as a percent of initial water)
P_{for}-forward power
P_{ref}-reflected power
time-heating time
sample and electrode symbols as in Table 4.7

4.3 Summary

The complexity of earth materials are such that predicting electrical parameters strictly on the basis of density, water content and other parameters is impossible. To establish the electrical properties of a soil a thorough testing program is required at varying temperature, water content and frequency.

To establish dielectric heating of a volume of soil it must be decoupled from the power source. That is accomplished by having dry soil surrounding the electrode to provide a low conductivity dielectric layer to reduce the current through the soil to almost zero.

Athabasca clay, Devon silt and bentonite can be vitrified (solidified) into glass at temperatures greater than 700°C.

5.0 ENGINEERING SCALE RADIO FREQUENCY HEATING OF CLAY

An engineering scale test was designed to simulate a section of an array of electrodes. The proposed field configuration would simulate two parallel conducting plates in the ground with two rows of closely spaced electrodes (Figure 5.1). The configuration in the laboratory represents a "piece of the field". The amplifier and matching network were the same as those described in Section 4.1.1.3. Athabasca clay was chosen for these tests. No specific measurements of the electrical parameters of the clay were run for these experiments but it was felt that the clay would be close to what was measured for Athabasca clay in Section 4.2.1. The forward power delivered by the power source was 1500 W for all tests to be described here. Since the experiment was at a larger scale than the previous coaxial tests, a lower frequency of 6.8 MHz was used in order to achieve more penetration of energy. The lower frequency ensures a larger distance of penetration of the EM energy than was the case at 14 MHz for the previously described drying tests (Section 4.2.2). Heating took place in two stages: Stage 1 to decouple the electrodes, Stage 2 to heat the sample.

5.1 Experimental Design

5.1.1 Apparatus

5.1.1.1 Sample Holder

The inside dimensions of the sample holder are 150 cm long x 60 cm wide x 30 cm deep (Figure 5.2). Figure 5.3 defines the X, Y, Z co-ordinates used for this test. The temperature data from these tests will be displayed in the form of contour plots of cross-sections through the box that will be identified by the X, Y, Z co-ordinate system. The box is made of wood and is lined with 4 cm thick styrofoam thermal insulation. Two "real" electrodes are placed in the middle on either side of the length of the box. These electrodes represent electrodes in the field. During Stage 1 heating took place between these two electrodes. For Stage 2 a plate was inserted at one end of the box to serve as the ground electrode and the two "real" electrodes became high tension electrodes. This plate takes advantage of the symmetry of the electric field about the plane y=75 cm, and thus simulates the heating in the entire space between the two rows of electrodes (Figure 5.1). The other half of the box was required to simulate fringing of the electric field in the space exterior to the region between the electrodes, and to simulate the heat sink represented by the surrounding soil. Note also that planes x=0 cm, x=60 cm and y=75 cm are planes across which, due to symmetry, no heat flow takes place (Figure 5.1).

Stage 1: During this stage adjacent electrodes alternate between ground and high tension. Since the spacing between the electrodes in a row is less than the spacing between rows, current flow and heating occur predominantly between electrodes in a row. Figure 5.4 illustrates the electric field that is created. The purpose of this stage of heating is to dry the soil in the immediate vicinity around the electrodes. The formation of this dry zone decouples the soil from the electrodes and creates the heating described by Nachai *et al* 1992.

Stage 2: For this stage the electrodes are re-connected to the power source so that all the electrodes in one row are high tension electrodes, while in the other row, the plate electrode, is the ground (Figure 5.5). The dried out zone established in Stage 1 has created the transverse inhomogeneity that leads to inter-leafing of standing waves and uniform heating along the length of the electrodes that is described by Maslowski *et* *al* 1992 (Section 2.5.1).

5.1.1.2 Electrical Components

The electrical components are essentially the same as in Section 4.1.1.3 except for the matching network which has been altered to include a number of discrete capacitors. The experimental configuration is slightly different because of the larger size of the sample and the fact that it is in a protective cage, a screened room, which contains any stray radiation. A 4 m 50 Ω coaxial cable leads from the power amplifier into the cage and to the matching network. The matching network now requires a short, 20 cm, piece of coaxial cable between itself and the sample. Plate 5.1 displays the sample holder, without the insulation lining, with the matching network in place. The door to the protective shield is open to display the variable capacitor and inductor. The power amplifier and signal generator are in the background.

5.1.1.3 Monitoring Instrumentation

Principally two parameters are monitored during a test, impedance of the sample and temperature within the sample. For obvious safety reasons these measurements can only be taken when the power is turned off. It was therefore important to minimize the time it takes to record the data. This restriction made it unreasonable to take water content samples during the test and limited the number of temperature data points that were monitored in the sample. Alcohol thermometers would have been the instrument of choice but they were of limited use given their 110°C temperature limit, and that they could only be inserted to a depth of a few centimeters before their scale was obscured. J-type thermocouples (TCs), which have to be inserted into the sample after the power is shut off, and withdrawn before turning the power on again, were used to monitor locations where temperatures were expected to increase beyond

110°C, and also at all deep locations (z=5 cm) in the sample. In all there were 23 thermometers and 18 TCs (Figure 5.6). A few thermometers were located in the region outside of the RF heating zone to monitor the temperature there. Plate 5.2 displays the sample holder prior to a test with thermocouples and thermometers installed. Just prior to the start of the test the clay surface was covered with vermiculite insulation.

During power off intervals, every 2 to 4 hours, the alcohol thermometer temperatures were recorded. The TCs were inserted and a HP 3052A Automatic Data Acquisition System recorded all of the TC temperatures simultaneously. Lastly the impedance of the sample was measured using an HP 4815A RF vector impedance meter. Since the measurements had to be taken with the power turned off they were conducted with all due speed, in a time of approximately 9 minutes. The measurements were taken approximately every 2 to 4 hours depending upon the expected change of the parameters.

At the end of the test, water content samples were taken using the same tool as described in Section 4.1.1.4. The samples were taken at the same locations as the temperature monitoring points plus additional samples outside the heated zone to determine the amount of water removed and the migration of water. Particular attention was given to the amount of water drawn into the heated zone.

Energy efficiency calculations were performed as described in Section 4.2.2.

5.1.2 Clay and Sample Preparation

5.1.2.1 Mixing

The Athabasca clay was first dried so that the water content was 0%. The clay was then crushed and ground into powder. Since a large volume of clay was needed a concrete mixer was required. The clay was mixed with distilled water in batches of 30 to 50 kg. The water was added gradually over a 2 to 3 minute period. The clay was mixed for another 10 to 15 minutes or until the clay appeared homogeneous. The batch was then sealed and placed in cold storage for several days.

5.1.2.2 Preparation and Compaction

The clay was retrieved from the cold room and was placed in the sample box in lifts 7.5 cm thick, approximately 120 kg of soil per lift. The sample box was enclosed in a protective cage for safety during heating. This cage restricted the use of bulky compaction tools. Also, the box itself is made of wood and was unlikely to withstand violent compaction techniques. The clay was compacted manually to a reasonable density with the aid of an 8 kg hammer. The surface was then scored and the process repeated until the sample was 30 cm in height. Finally the clay was covered with vermiculite to provide thermal insulation during heating.

5.2 Experimental Results and Discussion

5.2.1 Experiment 1

5.2.1.1 Trial 1

Stage 1:
The Athabasca clay was mixed rather wet (wc=29%, ρ_{dry}=1.48 g/cm^3). The forward power delivered by the source for this experiment, as for all the experiments, was 1500 W. At this time the matching box was positioned outside the protective cage, close to the amplifier but far from the sample. Initially the sample, being so wet, was inductive (Figure 5.7b). For the first 7:00 hours the sample readily absorbed RF energy and the coaxial cables were handling the load. As the clay dried out however the sample impedance increased, the sample became more capacitive, and the load on the cables was greatly increased due to the increase of reflected power. The cables began to heat up. Over the next 5:00 hours of heating the dielectric insulation in several cables broke down and had to be replaced. A significant part of the problem seemed to be the position of the matching network. The length of cable between the matching network and the load was subjected to a large amount of reflected power and heated up to the point of failure.

The highest temperature within the sample was 98°C at both the high tension and ground electrodes. It was decided that the test could not proceed until adjustments had been made to obtain a better impedance match to deliver more energy into the clay. Despite the problems of power delivery the energy delivery efficiency was relatively high at 58%.

The sample was left at room temperature for several weeks while adjustments in the apparatus were made to allow for the matching network to be located inside the protective cage, close to the sample. The matching network could still be manipulated from outside the cage.

5.2.1.2 Trial 2

Stage 1:

Water content samples were taken from the previously heated sample after it had cooled for several weeks. The water content increased in the direction away from the electrodes. Water content was 27% at locations furthest removed from the electrodes and 24% in regions adjacent to the electrodes. The average water content was 26%.

The sample was still dry in the immediate area around the electrodes so the sample input impedance was immediately capacitive. Heating was continued and initially proceeded as before. After 2:00 hours the sample impedance became more resistive and more capacitive (Figure 5.8) than during the previous trial and the cables did not overheat. After 5:00 hours temperature measurements indicated that the sample was experiencing considerable heat loss through the top surface and also a significant asymmetry in temperature developed between the high tension and ground poles. The region adjacent to the high tension electrode was entirely dry which was not the case near the ground electrode (Figure 5.9). After 7:00 hours it became evident that current return to the ground electrode was not restricted to paths through the load, but also occurred through air, wood, insulation *etc.*. The result of this was the very significant decrease in the rate of heating at the ground electrode in relation to that of the high tension electrode (Figure 5.10). This asymmetry is correctable but is not detrimental to the interpretation of the results. After almost 12:00 hours the ground electrode started to dry out. The sample impedance at this time was almost 400 Ω and the sample was almost purely capacitive. The coaxial cable broke down again. The cable between the network and the sample was put under increasing stress as the sample impedance increased and became capacitive, creating an electrical mismatch. A surface plot of the sample temperature illustrates that considerable heating had taken place perpendicular to the plane y=0 (Figure 5.11). Since the ground electrode had just dried out the decision was made to switch over to Stage 2.

The reflected power during Stage 1 averaged 68 W. The energy efficiency of the stage was 49%.

Stage 2:

The electrical configuration of the sample was changed for the start of the second stage of heating as described previously. The impedance of the sample was much lower, 200 Ω at -40°, for this configuration than for Stage 1 so there was less stress on the coaxial cable. The sample was heated successfully for almost 3:00 hours. It was decided to heat for two more days.

Day 2: The sample was heated for almost 7:00 hours.

Day 3: The half of the sample lying in the region of strong electric field was at a fairly uniform temperature at the start of Day 3 of heating (Figure 5.12). The sample was heated for 8:00 hours and temperature measurements were taken every 2:00 hours (Figures 5.13 to 5.16). The heating proceeded as expected, most intensely around the high tension electrodes. The matching network performed adequately keeping the reflected power to, on average, 49 W.

The water content samples taken after the test show that a considerable amount of water was removed, 37 kg or 34%. This was surprising considering that most of the heated half of the sample did not reach temperatures above 100°C. The water content of the heated half was reduced to 15% (Figure 5.17). The uniformity of the water content suggests that there has been a considerable migration of water during the overnight breaks in heating. The gradient of water content in the half of the sample outside the heated zone illustrates more clearly the migration of water into the heated zone. The immediate areas around the electrodes were completely dry except near the surface. The water content on average for the whole sample was 17%. Plate 5.3 illustrates the cracking on the surface of the sample.

5.2.2 Experiment 2

Stage 1:

The experimental equipment configuration was the same as in Experiment 1 but included an increased amount of insulation on the surface of the sample. Athabasca clay was used again but was mixed to 23% water content. The compaction of the slightly drier clay was more difficult so the dry density was only 1.41 g/cm^3. As before the forward power was 1500 W and the frequency 6.8 MHz.

Initially the sample was just slightly capacitive, -7° (Figure 5.18b). After 2:00 hours the phase angle was -64° and the temperature was on average 90°C at the electrodes. The resistance was stable at approximately 60 Ω. After 4:01 hours of heating the resistance had increased significantly and the sample was nearly purely capacitive (Figure 5.18). The region around the high tension electrode had dried out (Figure 5.19). In time the resistance continued to increase but at a decreasing rate. After 5:59 hours the high tension electrode was very dry and very hot, 110 to 180°C. There was considerable heat loss to the top and bottom of the sample (Figure 5.20). The sample was now purely capacitive. After 8:02 hours the high tension electrode was hotter, 180 to 250°C, however the region near the ground electrode was still not dry (Figure 5.21). After 12:01 hours the coaxial connector failed. As before when the coaxial cable broke down the sample resistance was 400 Ω. The ground electrode had just dried out (Figure 5.22). The water content in the middle had only dropped to 19.8%. A plan view, Figure 5.23, illustrates how much heating had taken place transverse to the y=0 plane. The next morning an attempt was made to continue Stage 1 but after only an hour the coaxial cable broke down again. The resistance was again close to 400 Ω. It appears that the impedance limit of the equipment was reached.

The reflected power on average was 41 W. The energy efficiency was the highest so far, 72%. The increased energy efficiency was almost certainly the result of the test being free of the breakdowns in the dielectric cable that plagued the previous experiment.

Stage 2:

Heating started in the new geometry just 1 hour after the restart of Stage 1 was completed, so the former high tension electrode was still very hot (Figure 5.24). The resistance was much lower for this configuration than for the configuration of Stage 1 but the sample was still very capacitive (Figure 5.25). After only 2:03 hours the heating pattern was close to symmetric with respect to the two high tension electrodes. There was some preferential heating on the wetter side (Figure 5.26). Heating proceeded systematically until 15:17 hours (Figure 5.27) as the clay around the electrodes dried out and the resistance increased. Heating proceeded very slowly until 33:14 hours (Figure 5.28). The sample was fairly stable at 200 Ω resistance from 15:17 to 33:14 hours. Although the temperatures changed little for up to 33:14 hours, at 23:00 hours a crack opened up at the y=30 to 36 cm mark of the heated zone. By 33:14 hours the temperature of the clay between the electrodes and the crack was approaching the 100°C threshold (Figure 5.28). By 38:19 the clay between the electrodes and the crack had entirely dried out and was very hot, 105 to 150°C. The clay beyond the crack was starting to cool slightly. By 41:26 the dry clay was hotter still while the wet clay beyond the crack had cooled slightly (Figure 5.29). The plan view of the final water content distribution shows a sharp gradient across the crack between the dry and wet zones (Figure 5.30). The test was halted due to excessive fumes from the melting insulation.

The plan view water content contour plot clearly shows there has been migration of water into the heated zone (Figure 5.30).

The final water content of the sample was, on average, 12%, which represents a removal of 47%. The energy efficiency for Stage 2 was 47%.

5.3 Summary

The test has effectively demonstrated the removal of water from Athabasca clay. The electric field however was not intense enough and the power level not high enough to dry the entire sample. Clearly the frequency of the energy and the power level must be carefully chosen with regard to the character and volume of soil to be heated.

During the two RF heating experiments considerable migration of water took place. This circulation of water worked to cool the high temperature zone of the sample close to the high tension electrodes and to heat the sample close to the ground electrode where the electric field was less intense. This migration was not a direct of result of the thermal gradient but rather was the result of the water content gradient that resulted from the heating. The dry zone that formed around the high tension electrodes resulted in considerable capillarity driven flow of water towards the heated zone. The water circulation was completed by water vapor that was driven away from the heated zone by a vapor density gradient (Mitchell 1993). The movement of vapor away from the heated zone indicates the importance of vacuum extraction. In a field application the vapor gradient must be to the surface and/or towards the vapor collection system.

6.0 MODELING AXIAL UNIFORM HEATING OF PARALLEL PLATE CONDUCTORS

6.1 Modeling Technique

The engineering scale test simulates an electrode array in two dimensions, length and width, perpendicular to the electrode. Since it was impractical to simulate the third dimension, depth, in the laboratory, a computer model is required to simulate heating along the electrode.

TMCOPTER (Nachai 1991b) numerically simulates the radio frequency heating of porous, lossy materials within an azimuthally symmetric coaxial geometry. Temperature and water content are predicted at all positions in the coaxial geometry as functions of time by solving the interrelated electrical and thermal problems. An EM field solution is explicitly coupled with a heat conduction equation solver.

The program is a two-dimensional finite difference approximation of Maxwell's equations and energy and mass balance equations. The model is based on the array configuration depicted in Figure 6.1. The boundaries of the cell are by symmetry surfaces across which no current, heat or fluid will flow. Given the nearly symmetrical manner in which current will be distributed around the inner conductor, the process can be studied satisfactorily using the very simple coaxial cell illustrated by the circle circumscribing the outer conductors in Figure 6.1. Thus electrically, the computational cell can be taken as equivalent to a coaxial cable, filled with a generally lossy inhomogeneous dielectric material.

The cell is azimuthally symmetric and can be solved in r-z space (Figure 6.2). Within each grid block all thermal and electrical parameters are assumed constant although they may differ from block to block. To begin the initial temperature, water content etc. are used to evaluate necessary thermal and electrical parameters (such as the temperature and water dependent heat capacities and thermal and electrical conductivities) for each grid block. The EM field in the cell is calculated. The energy accumulation in each grid block is determined from the energy dissipated and conductive and convective heat flows into the grid block. Electrical and thermal parameters are computed using "beginning of timestep" temperature and fluid saturation. Heat flow terms in the energy balance equation are expressed in terms of unknown "end of time step" temperatures. This is only a partially implicit solution. It is necessary to use small time steps to limit changes in key parameters, such as electric conductivity, to less than 5%. Energy associated with phase change must be accounted for to determine new saturation levels. A second time step is then initiated to recalculate thermal and electrical parameters for each grid block. For grid blocks 2,2 to (M-1)(N-1) this results in an (M-2)(N-2) system of algebraic equations in the unknown "end of time step" temperature at the center of each grid block. The system is solved using the Alternating Direction Implicit (ADI) method, using a combination of n and n+1 level temperatures to reduce the system to elementary tridiagonal form.

Assumptions:

1. The conductors are electrically perfect and thermally they are perfect insulators. They are impervious to the flow of fluids. The source and load ends are also assumed to be bounded by a no heat and no fluid flow boundary.
2. Fluid flow to and from grid blocks is negligible below steam temperature.

3. No steam is generated until a grid block has reached steam temperature.
4. Upon reaching steam temperature, the temperature is constant until the water has evaporated. If a wet grid block reaches steam temperature it continues to boil for the duration of the current time step.
5. Energy, electrically generated and due to thermal conduction, that is deposited into a steaming grid block is consumed to convert water to steam. Steam temperature is stable until the water is gone. That is to say that the "end of time step" temperature is known in the boiling grid blocks and thus the number of unknowns is reduced.
6. Steam simply moves to the perforated inner conductor and escapes.

This model will not approximate a situation where convective cooling due to fluid flow is significant.

The goal was to simulate heating between two parallel plates in the ground. In order to achieve this the geometry of the coaxial cell was manipulated to approach parallel plate conditions. By expanding the diameter of the cell the inside and outside electrode approach parallel plate conditions. The diameter of the inside conductor was chosen to be 5 m and that of the outside conductor 6.5 m. At this size there is still a significant fall off in the intensity of the electric field between the inner and outer electrode but larger dimensions cause the solution to become unstable. The 1.5 m spacing between electrodes simulates the spacing of the engineering scale test (Section 5.0) (Figure 5.1). The frequency, 6.8 MHz, and net absorbed power level, 800 W, were also chosen to match the engineering scale test. The simulated heating time of 41.7 hours was roughly the same heating duration of Experiment 2, Stage 2 (Section 5.2.2). With the assistance of Dr. Peter Stroemich, of the Department of

Electrical Engineering University of Alberta, a simulation was run for the case of a 15 m electrode. In Section 4.2.1 tests to determine the electrical conductivity and dielectric constant of wet and dry Athabasca clay were carried out. An binomial expression with a temperature factor, based upon the tests in Section 4.2.1 and previous experience of Dr. Stroemich, was used to predict the change in the electrical conductivity and dielectric constant of Athabasca clay with respect to water content.

$$\sigma = (1 + \alpha(T - 40))[1 \times 10^{-5} + wc^2(3.75 \times 10^{-4})] \qquad [S/m]$$

$$\varepsilon_r = 4 + wc^2(0.13)$$

Alpha was assumed to be 0.024 $°C^{-1}$ for these simulations. Temperature does not have a significant effect on dielectric constant in these temperature ranges. At low frequencies, <10 MHz, measuring the residual conductivity of Athabasca clay was impossible given the equipment available. An estimate of residual (dry) conductivity of Athabasca clay was made by extrapolating from the data available. A second case was run using a higher estimate of the residual conductivity.

$$\sigma = (1 + \alpha(T - 40))[1 \times 10^{-3} + wc^2(3.75 \times 10^{-4})] \qquad [S/m]$$

The simulation includes a dielectric layer along both the high tension and ground electrodes. The dielectric layer is dry clay that represents the dry zone that was created in Stage 1 of the engineering scale tests (Section 5.1.1.1). Without the dielectric coating along the electrodes the electric field skin depth for case 1 is only 3 m. Thus very little heating to depth will take place.

6.2 Results and Discussion

Case 1: 15 m long electrode, conductivity of dielectric coating = 1 x 10^{-5} S/m

After 10.8 hours the zone of dry clay has expanded downward to between the 15 m to 10 m depth along both of the inner and outer electrodes (Figure 6.3). After 24.2 hours the dry zone was continuing to expand in a wedge like fashion down both of the electrodes (Figure 6.4). At the end of the simulation, 41.7 hours, there remains a thin zone of wet clay between the electrodes (Figure 6.5).

Case 2: 15 m long electrode, conductivity of dielectric coating = 1 x 10^{-3} S/m

The water content at the end of the simulation was far greater than in the lower conductivity simulation (Figure 6.6 and 6.5). The assumption of a higher conductivity for dry Athabasca clay has resulted in a much slower rate of drying.

6.3 Summary

The RF heating simulations illustrate that a low conductivity dielectric layer of material introduced into a parallel plate waveguide will promote uniform heating along the waveguide. The higher the electrical conductivity of the dielectric layer the less effective is the penetration of energy.

7.0 CONCLUSIONS

7.1 Electrical Parameters of Soil and their Effect on RF Heating

7.1.1 Electrical Conductivity and Dielectric Constant

1. Measurements of dielectric constant and electrical conductivity conducted in the frequency range of 10 to 100 MHz on Athabasca clay, Devon silt, kaolinite and bentonite indicate that dielectric constant decreases over the range while electrical conductivity increases. This behavior is similar to tests on other earth materials such as oil sand (Chute *et al* 1979).

2. Secondary effects of soil composition, such as salinity and organic matter content, have a significant effect on the electrical conductivity of soil. Water content and density alone cannot be depended upon to determine the electrical parameters of soil.

7.1.2 Drying Experiments

1. Experiments in RF heating at 14 MHz of 11 000 cm^3 of soil in a coaxial configuration at forward power levels of 1500 W, showed that on average the soil was 75% dry in a period of 4.5 hours.

2. For all heating experiments it was observed that initially the input impedance to the sample was resistive and inductive. As heating progressed the resistive

part of the input impedance increased and the initial inductive behavior changed to capacitive. This was because the soil surrounding the inner electrode had heated up past 100°C and had dried out. As the soil continued to increase in temperature the dry zone expanded enveloping the inner electrode. The dry zone was highly resistive and capacitive and dominates the sample impedance.

7.1.3 Vitrification Experiments

1. Vitrification of Athabasca clay, Devon silt and bentonite has been accomplished on a small scale using RF energy at 14 MHz and power levels of 500 to 1500 W. The temperatures attained were greater than the 700°C maximum temperature range of the thermocouple. The resulting glass lumps, 100's of cm^3, of Athabasca clay and Devon silt are hard and competent and could well serve as ground anchors. Due to the high void ratio of bentonite, it vitrified into a fragile glass shell. Kaolinite did not vitrify despite the destruction of the tungsten electrode, which has a melting point of greater than 3000°C.

7.2 Electrode Array Geometry

1. Two "piece of the field" laboratory tests were conducted on samples of Athabasca clay, water content 25 and 23% respectively. The volume of both samples was 0.270 m^3. The sample was heated with RF energy at 1500 W for up to 42 hours to a maximum temperature of 314°C. Up to 47% of the water

was removed reducing the average water content of the sample to as low as 12%. Power was applied via high tension and ground electrodes. Heating was conducted in two sequential stages. Stage 1 was designed to partially decouple the electrodes from the sample. Stage 2 was designed to allow the partially decoupled electrodes to heat the bulk of the sample. The high tension electrode decoupled quickly during Stage 1 compared to the ground electrode which took much longer. This disparity in time is because a significant fraction of the return current bypassed the ground electrode. The result is that the electric field, and heating, is less intense around the ground electrode than at the high tension electrode.

2. There was considerable migration of water within the sample. The high temperature gradient in the sample results in a water content gradient that results in capillarity driven flow of water towards the heated zone. Water vapor, driven by the vapor density gradient, flows away from the heated zone. The circulation of water resulted in the heating of a greater volume of soil, but it also diminished the heating intensity nearer the high tension electrodes, restricting the rate of drying.

3. The results of these experiments prove the feasibility of heating and drying soil with RF energy.

7.3 Axial Uniform Heating along an Electrode

1. A dielectric coating of dry material between the electrode and the bulk of the

sample causes the phenomena explored by Maslowski *et al* (1992) and Nachai *et al* (1992) that allows significant heating along the length of an electrode; as demonstrated within this thesis by numerical model.

2. The residual electrical conductivity of dry clay (the dielectric layer) has a significant effect on the depth to which heating can take place along the length of the electrode. The higher the conductivity the less the energy penetration to depth.

8.0 RECOMMENDATIONS

1. A full study of the electrical conductivity and dielectric constant of a number of soils should be carried out over a large range of frequencies, water content, density and temperature.

2. More data is required to clarify the dependence of RF electrical properties of soil on salinity, mineralogy, organic matter and other secondary soil parameters.

3. At low frequencies, <10 MHz, the resistance of most soils is very high and therefore they will conduct very little current. At such low conductivities a very sensitive probe is required to get accurate measurements of the electric and magnetic fields required to determine the electrical properties of the soil. Sensitive measurements are also required to determine the electrical properties of dry soil.

4. A contaminant recovery system would have to maintain the vapor density gradient towards itself.

5. The RF heating model TMCOPTER should be revised to include fluid flow.

6. Additional laboratory, field and pilot tests are required to further assess the potential of RF *in-situ* heating remediation technology.

FIGURES

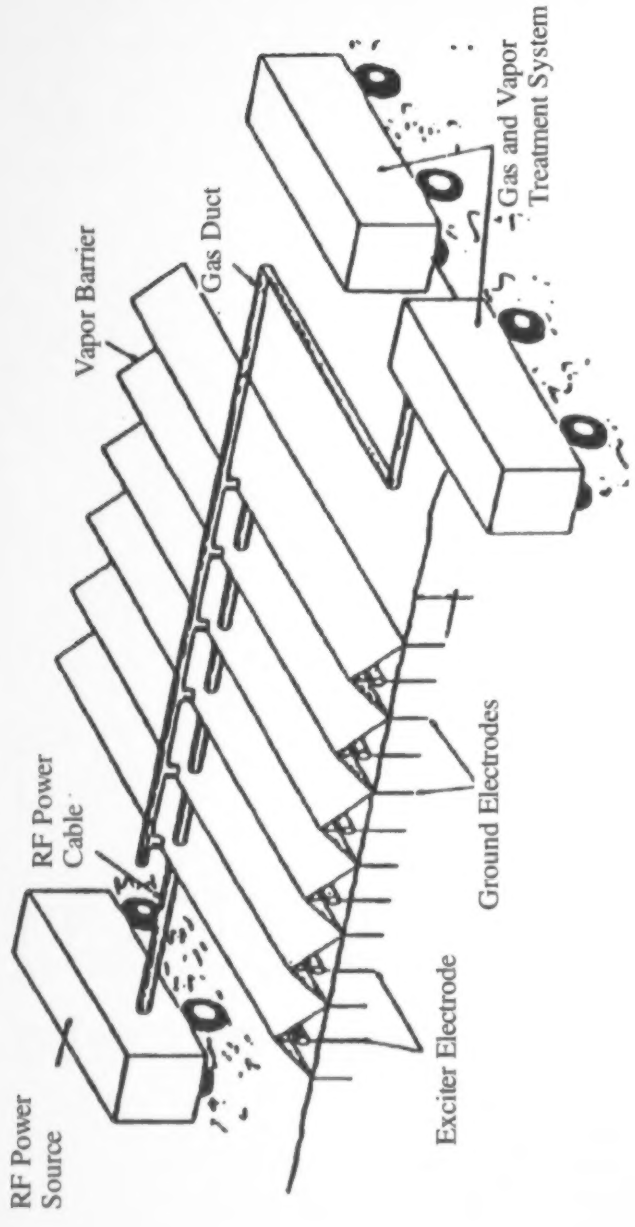
RF Power Source
RF Power Cable
Vapor Barrier
Gas Duct
Gas and Vapor Treatment System
Ground Electrodes
Exciter Electrode

Figure 1.1: RF *in-situ* treatment module (adapted from Dev *et al* 1987).

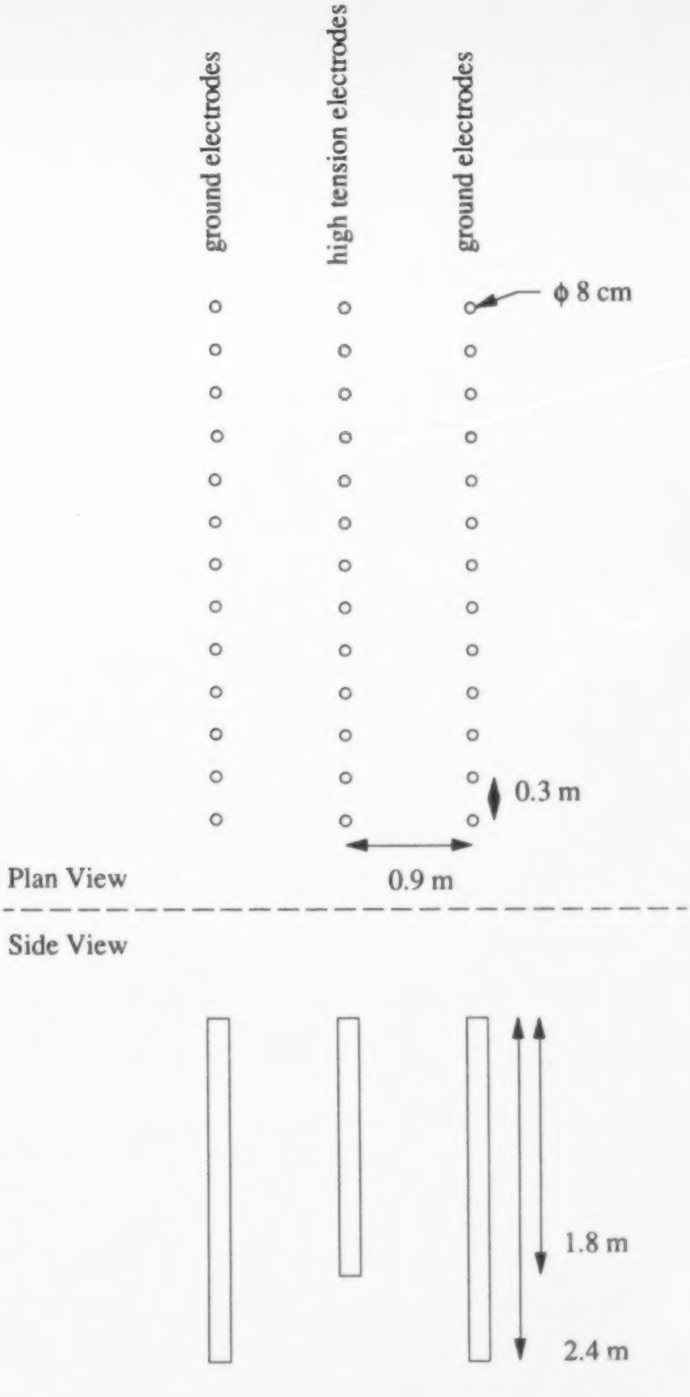
ground electrodes
high tension electrodes
ground electrodes
ϕ 8 cm
0.3 m
0.9 m
Plan View
Side View
1.8 m
2.4 m

Figure 2.1: A tri-plate electrode array (adapted from Dev *et al* 1988).

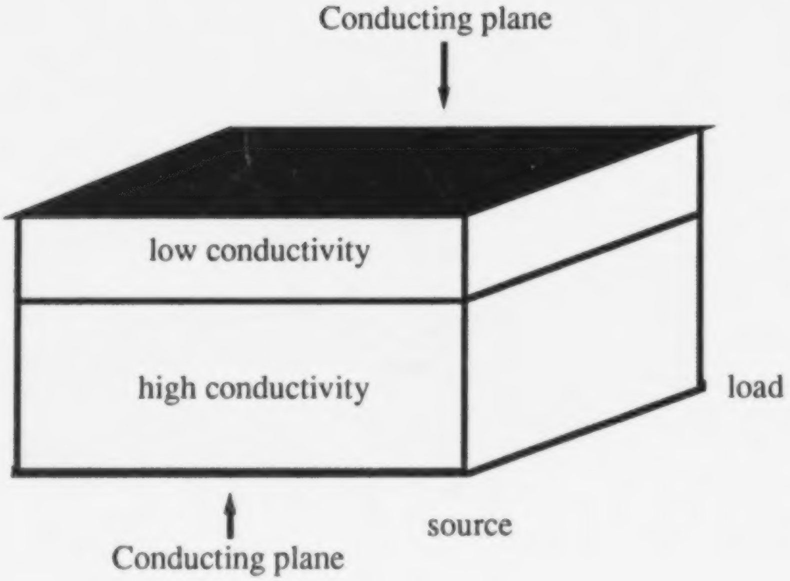
Conducting plane
low conductivity
high conductivity
load
source
Conducting plane

Figure 2.2: Parallel plate waveguide configuration with a low conductivity dielectric layer (adapted from Maslowski *et al* 1992).

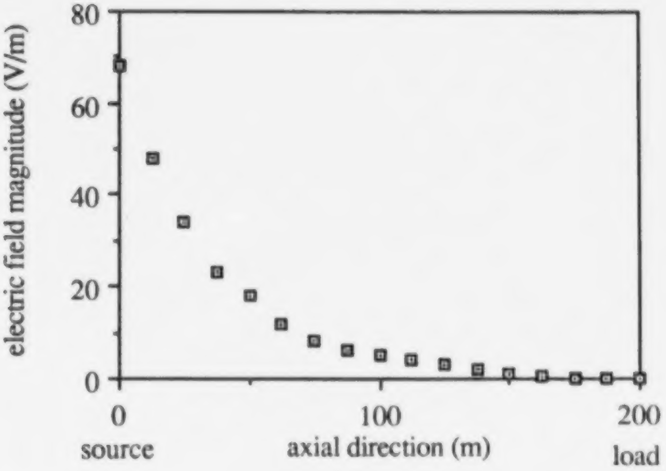

Figure 2.3: Axial variation of the transverse electric field magnitude in a transversely homogeneous medium (adapted from Maslowski *et al* 1992).

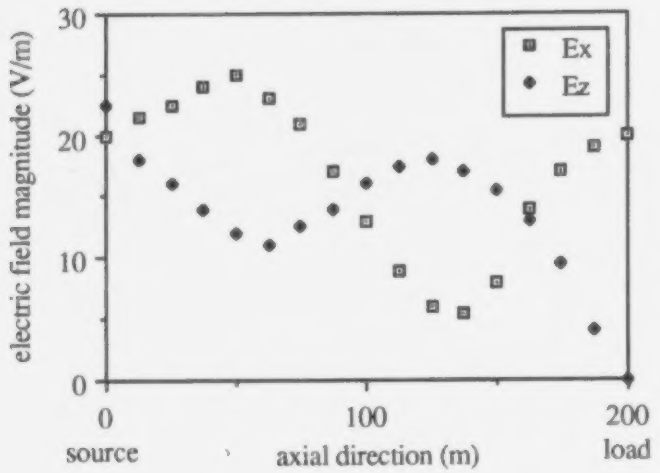

Figure 2.4: Axial variations of the transverse and axial electric field magnitudes after introduction of a low conductivity layer (adapted from Maslowski *et al* 1992).

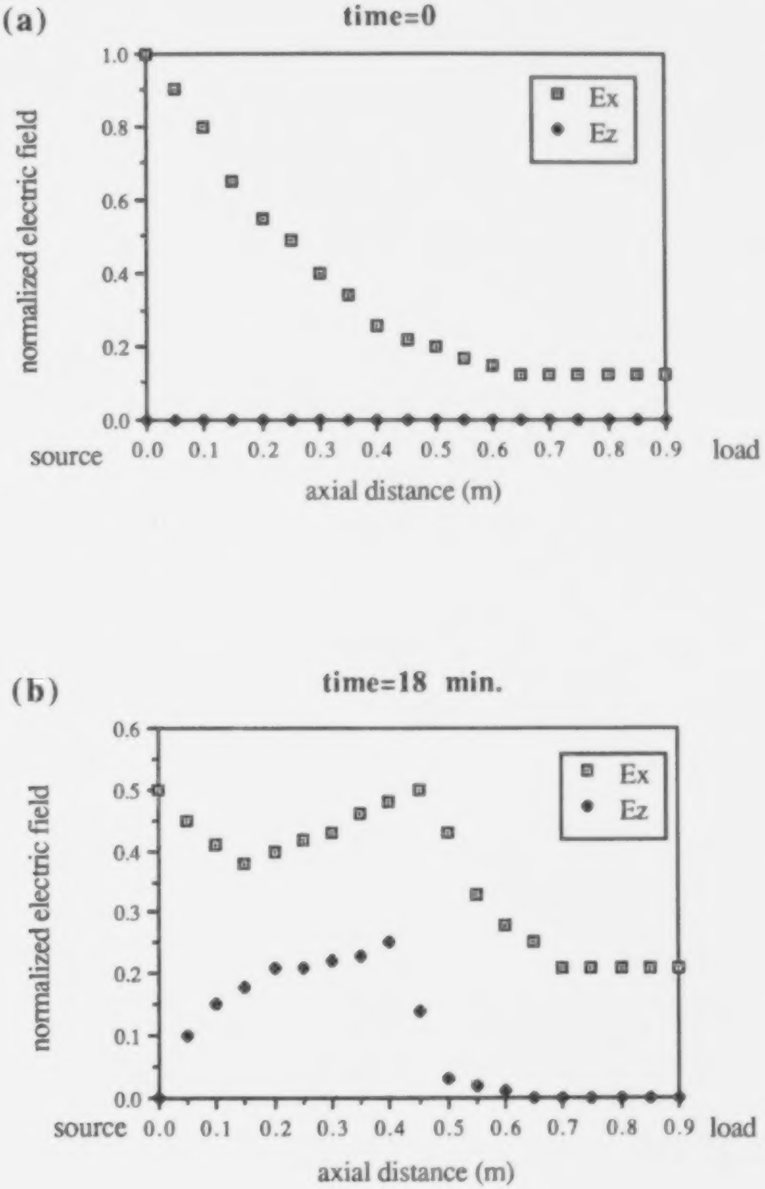

Figure 2.5: Variation of transverse and axial electric field (adapted from Nachai *et al* 1992), (a) time=0, no axial field, (b) time=18 min., growing axial field.

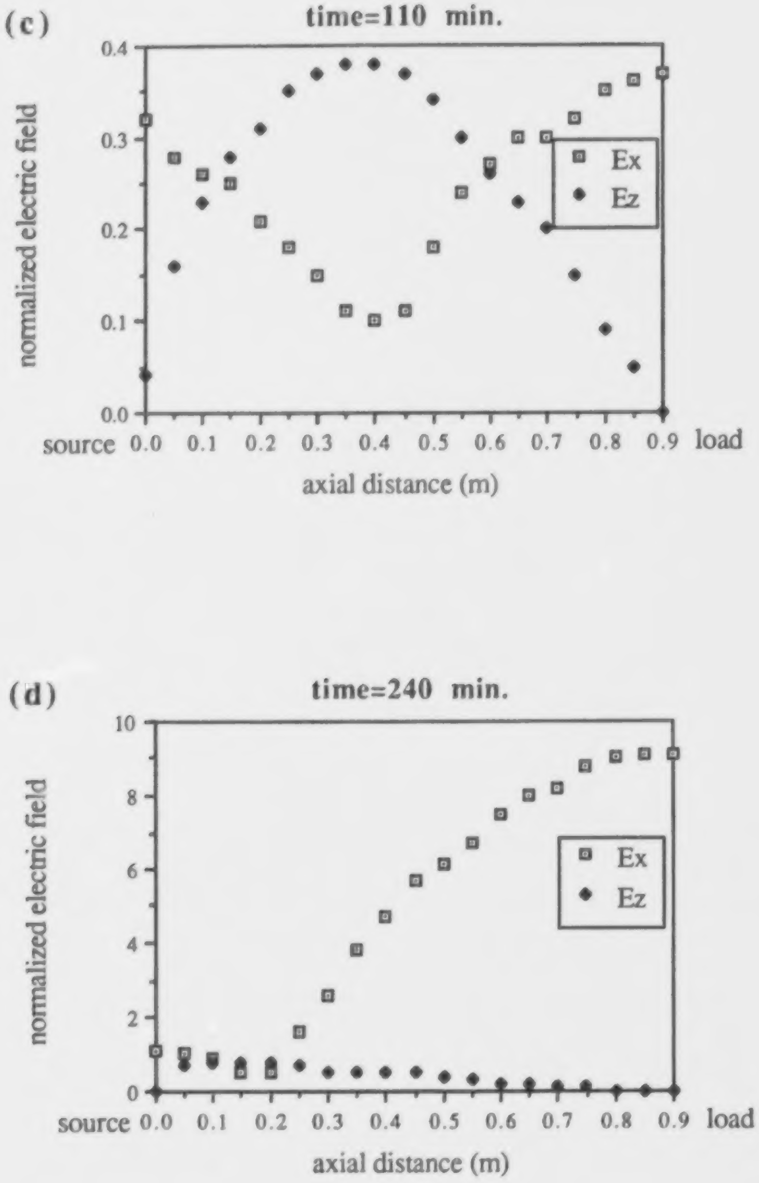

Figure 2.5: Variation of transverse and axial electric field (adapted from Nachai *et al* 1992), (c) time=110 min., full inter-leafing of nodes and anti-nodes, (d) time=240 min., the material has dried out, axial field is negligible.

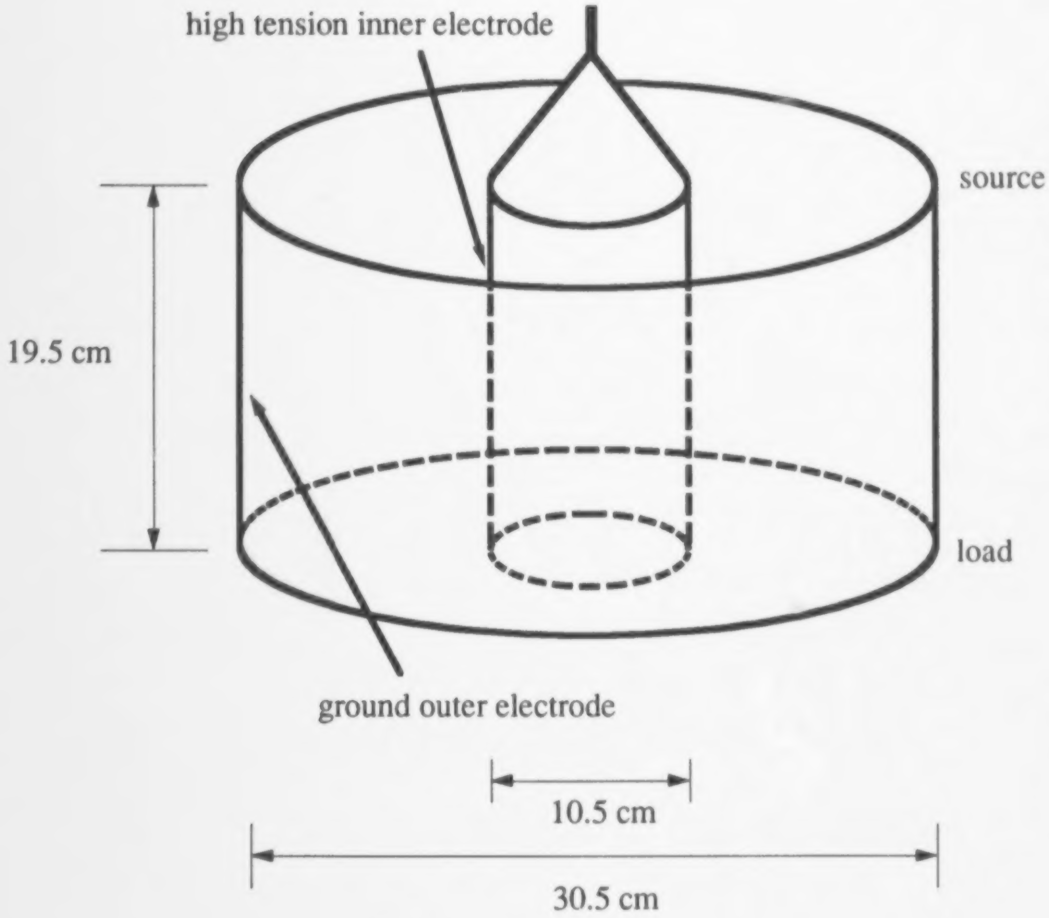
high tension inner electrode
source
19.5 cm
load
ground outer electrode
10.5 cm
30.5 cm

Figure 4.1: Coaxial capacitor used as a sample holder in RF drying experiments.

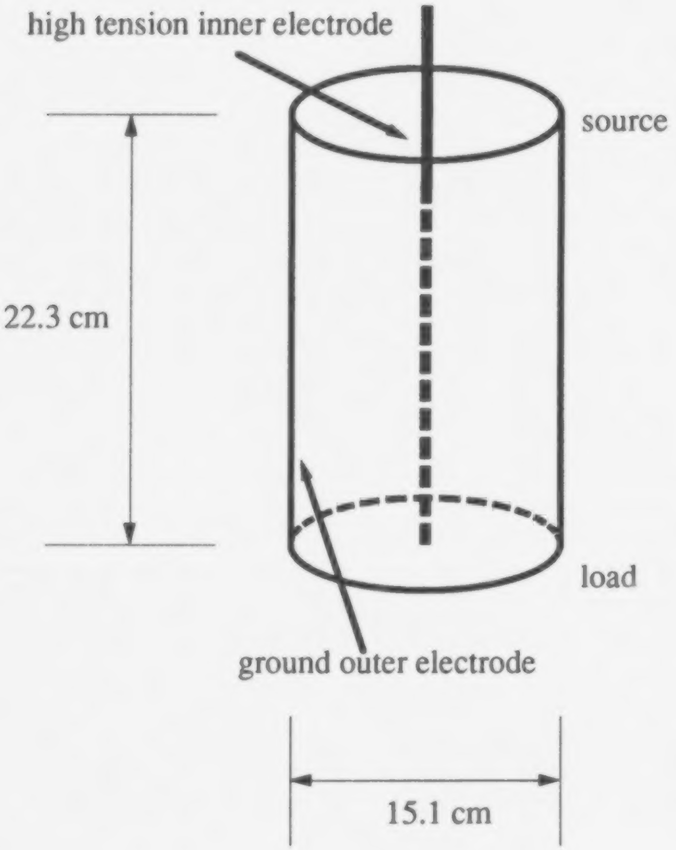
high tension inner electrode
source
22.3 cm
load
ground outer electrode
15.1 cm

Figure 4.2: Coaxial capacitor used as a sample holder in RF vitrification experiments.

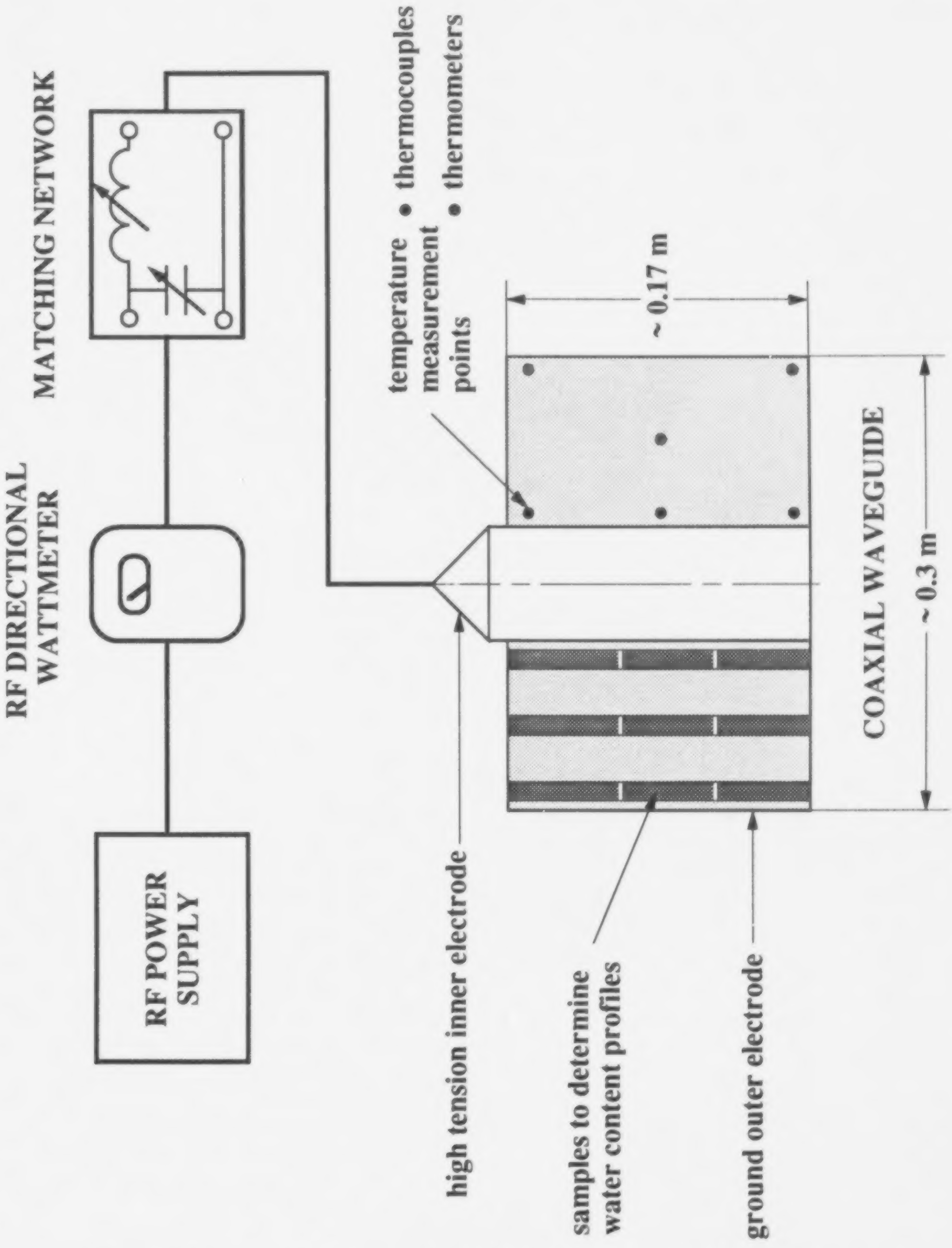
RF POWER SUPPLY
RF DIRECTIONAL WATTMETER
MATCHING NETWORK
temperature measurement points
• thermocouples
• thermometers
~ 0.17 m
high tension inner electrode
samples to determine water content profiles
ground outer electrode
COAXIAL WAVEGUIDE
~ 0.3 m

Figure 4.3: Schematic diagram of the electrical configuration for the drying experiments.

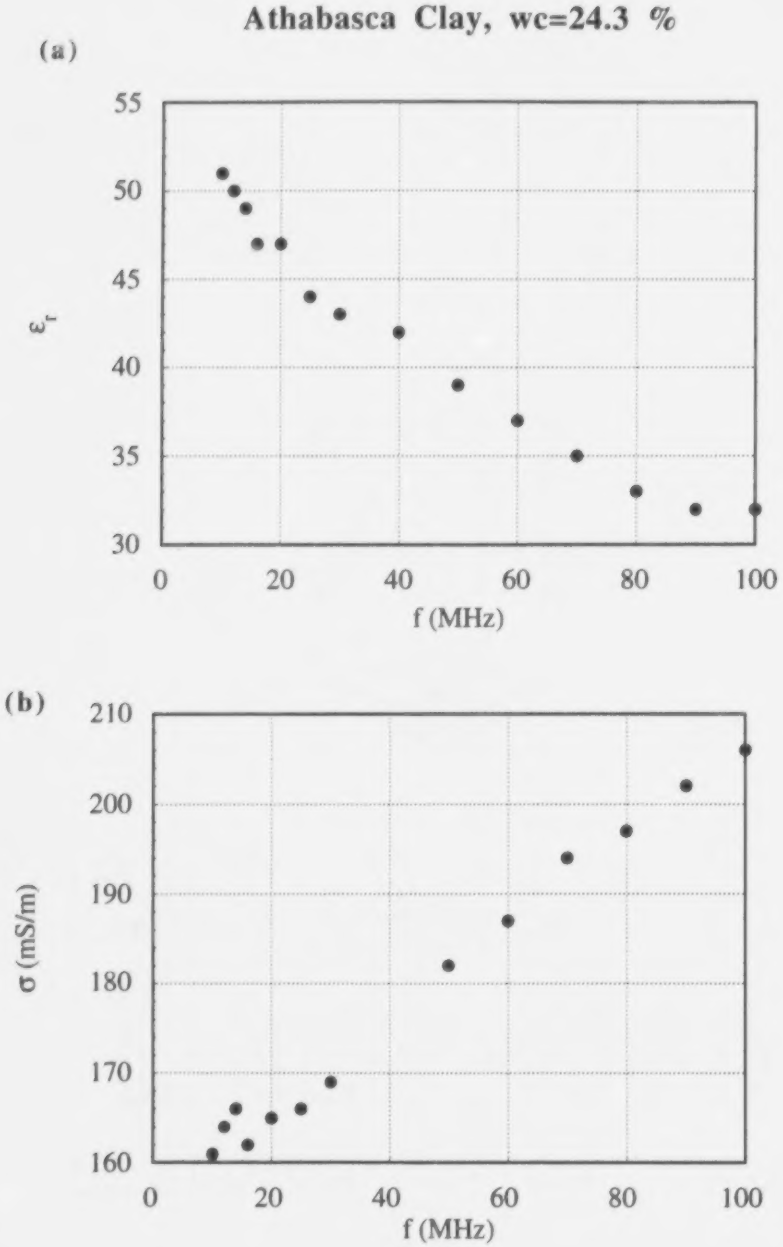

Figure 4.4: Athabasca clay, wc=24.3%, (a) dielectric constant, (b) electrical conductivity.

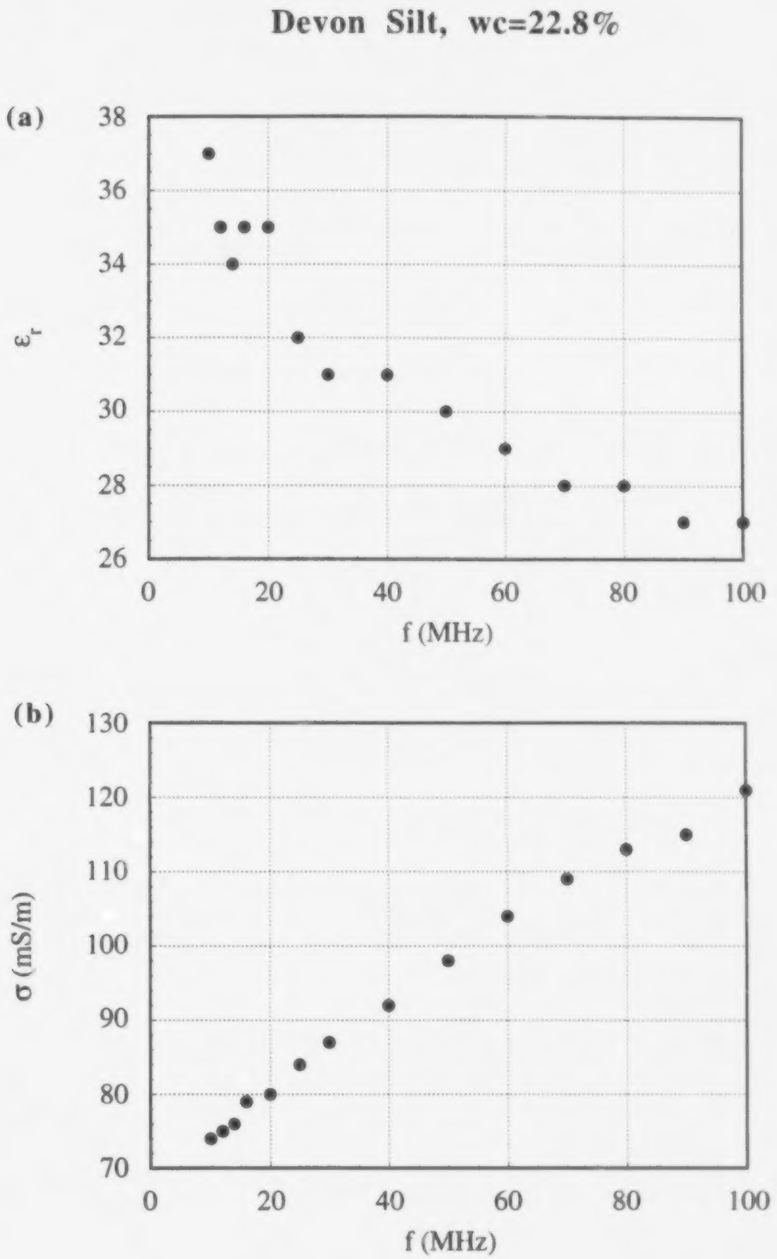

Figure 4.5: Devon silt, wc=22.8%, (a) dielectric constant, (b) electrical conductivity.

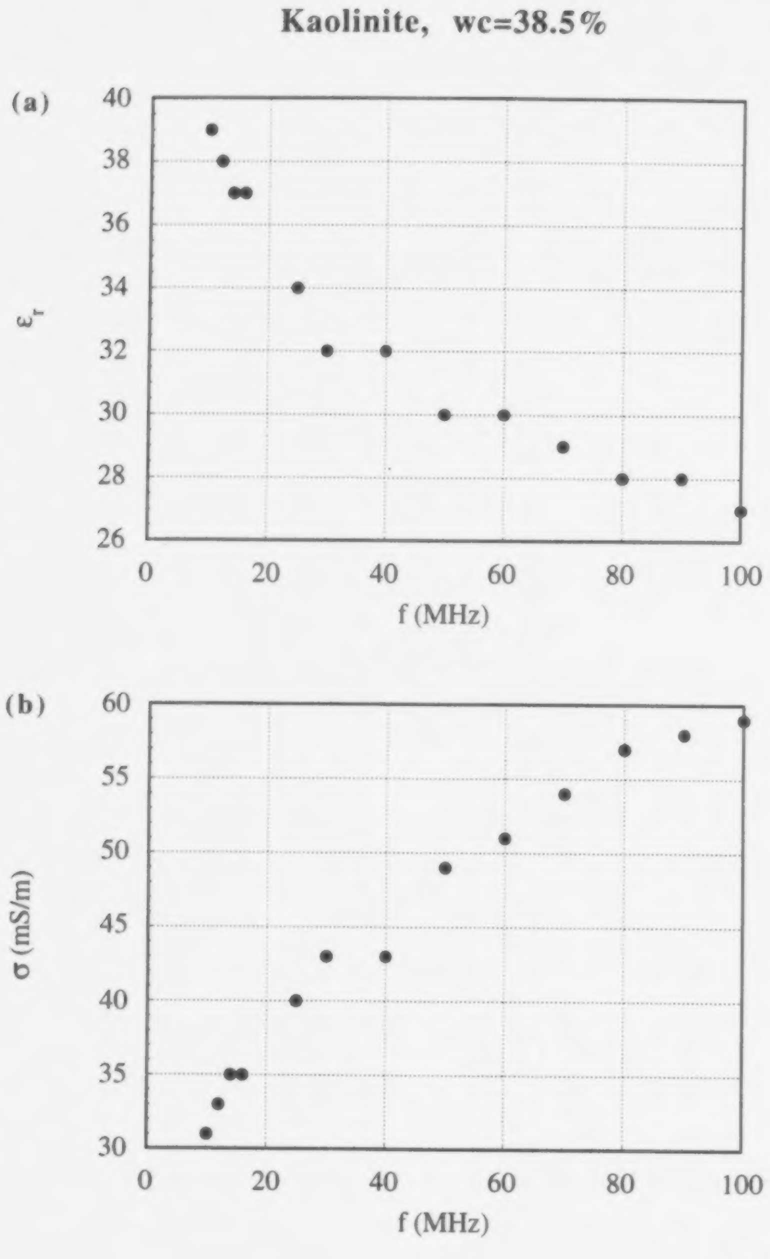

Figure 4.6: Kaolinite, wc=38.5%, (a) dielectric constant, (b) electrical conductivity.

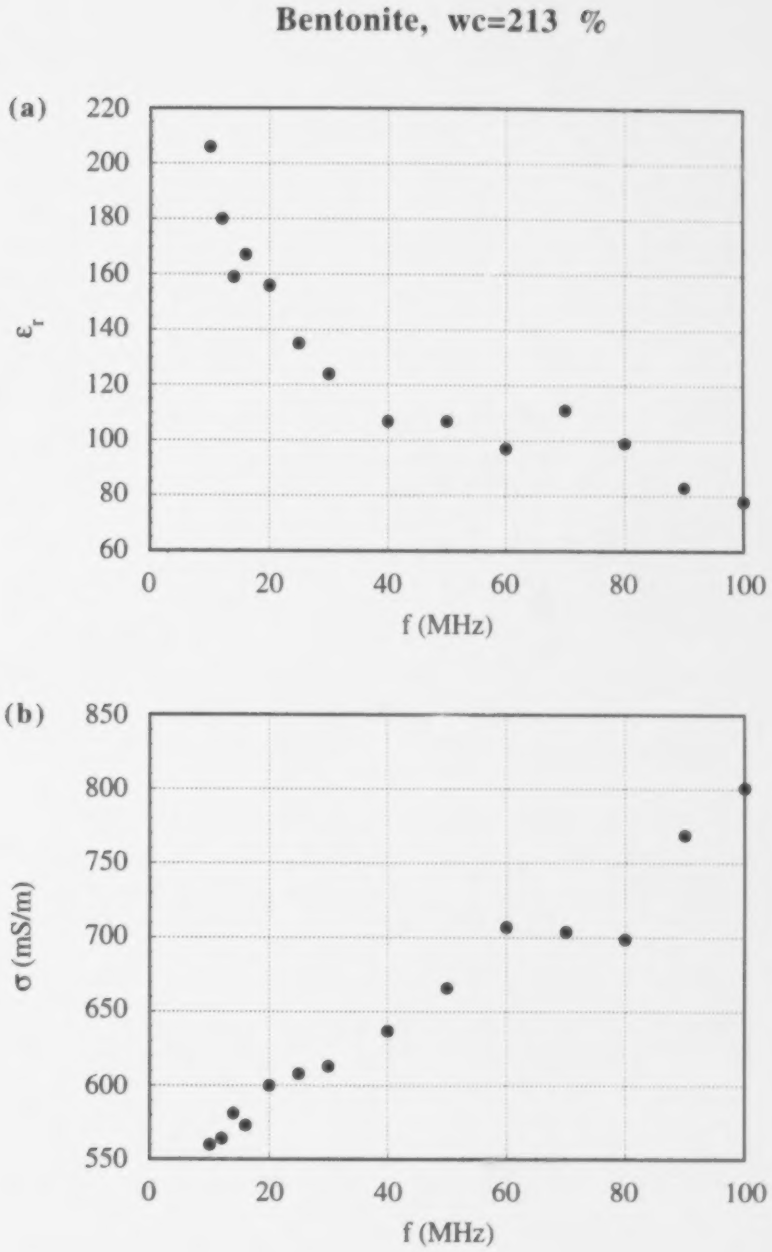

Figure 4.7: Bentonite, wc=213%, (a) dielectric constant, (b) electrical conductivity.

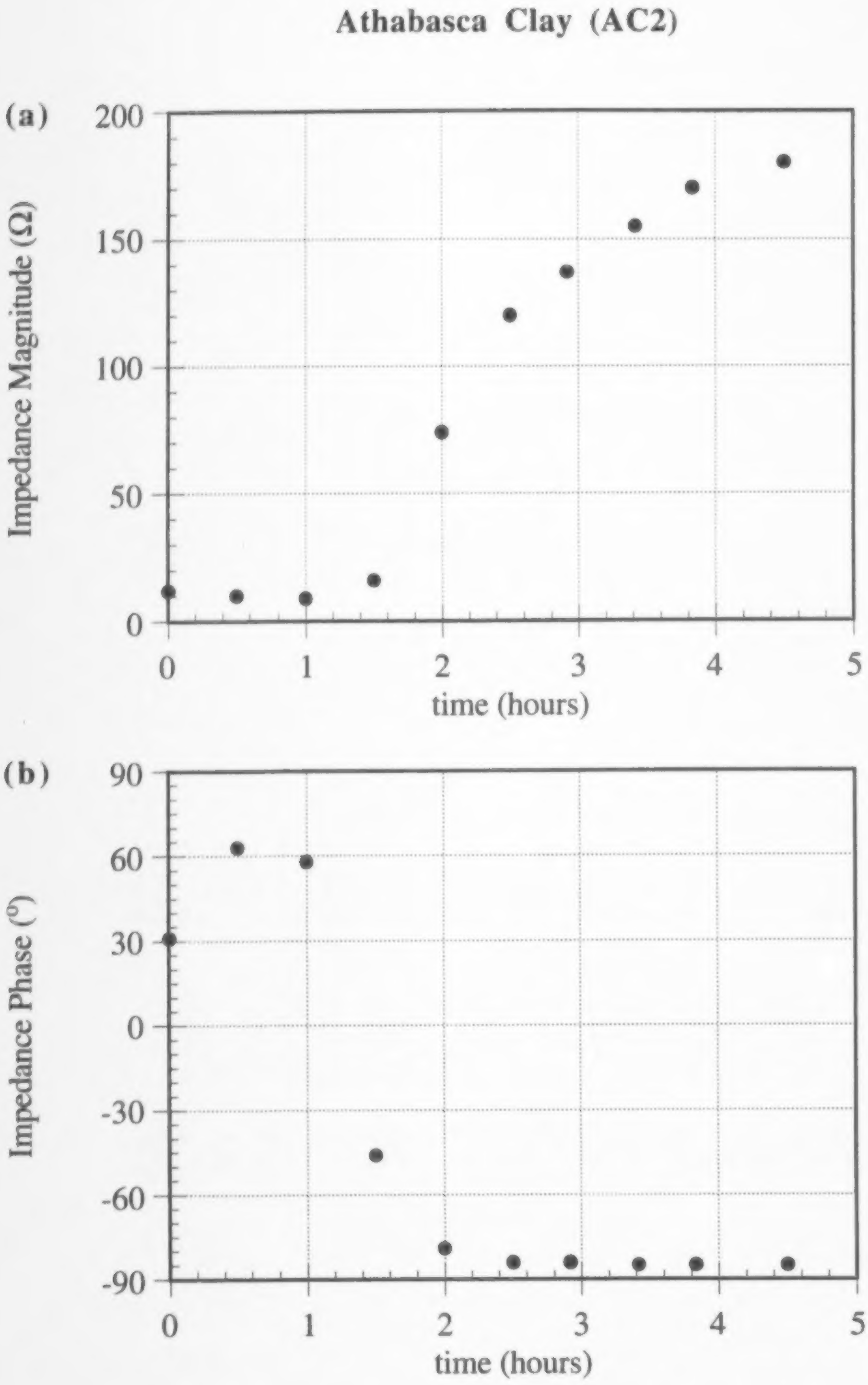

Figure 4.8: Athabasca clay, experiment AC2, impedance, (a) magnitude, (b) phase.

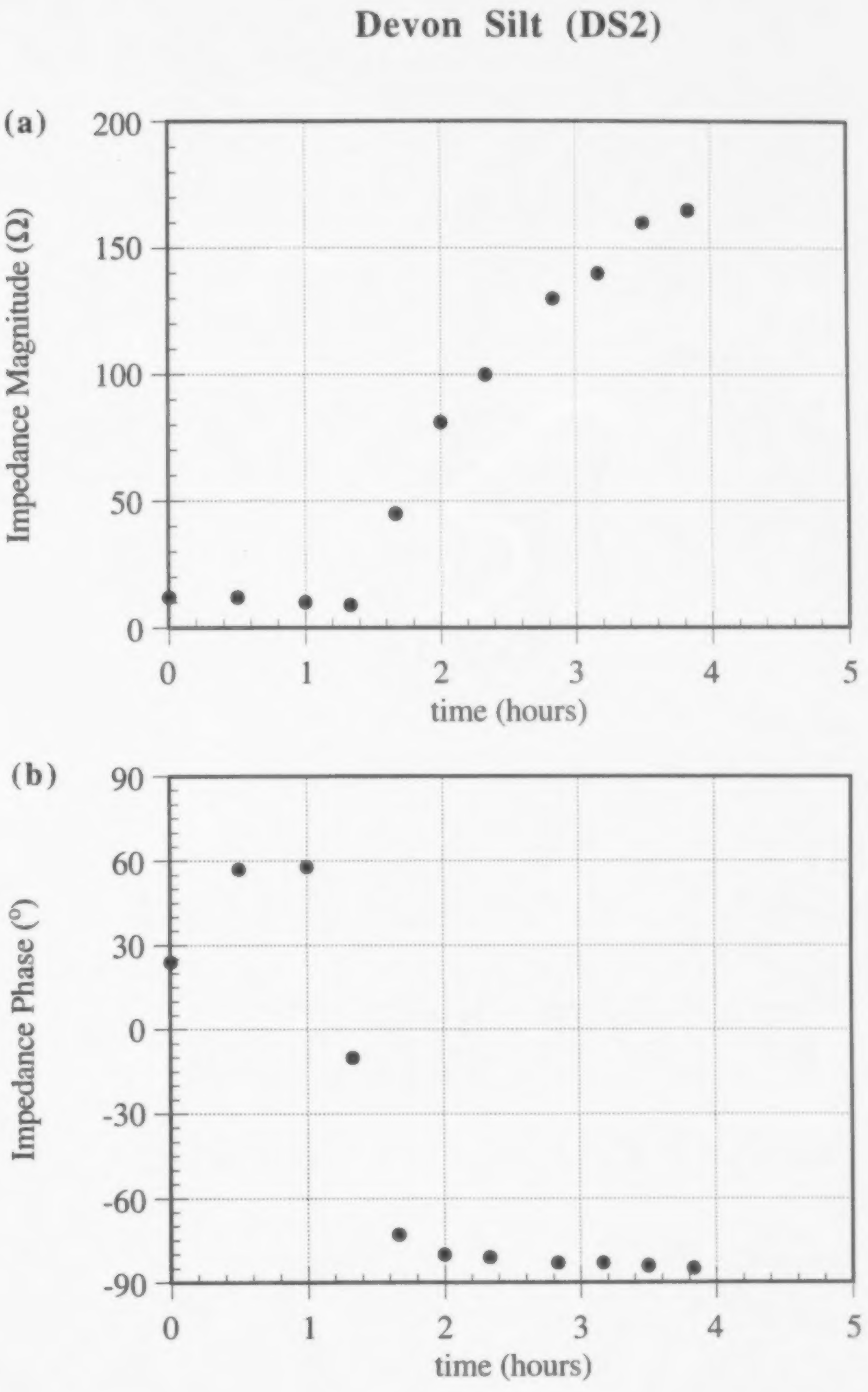

Figure 4.9: Devon silt, experiment DS2, impedance, (a) magnitude, (b) phase.

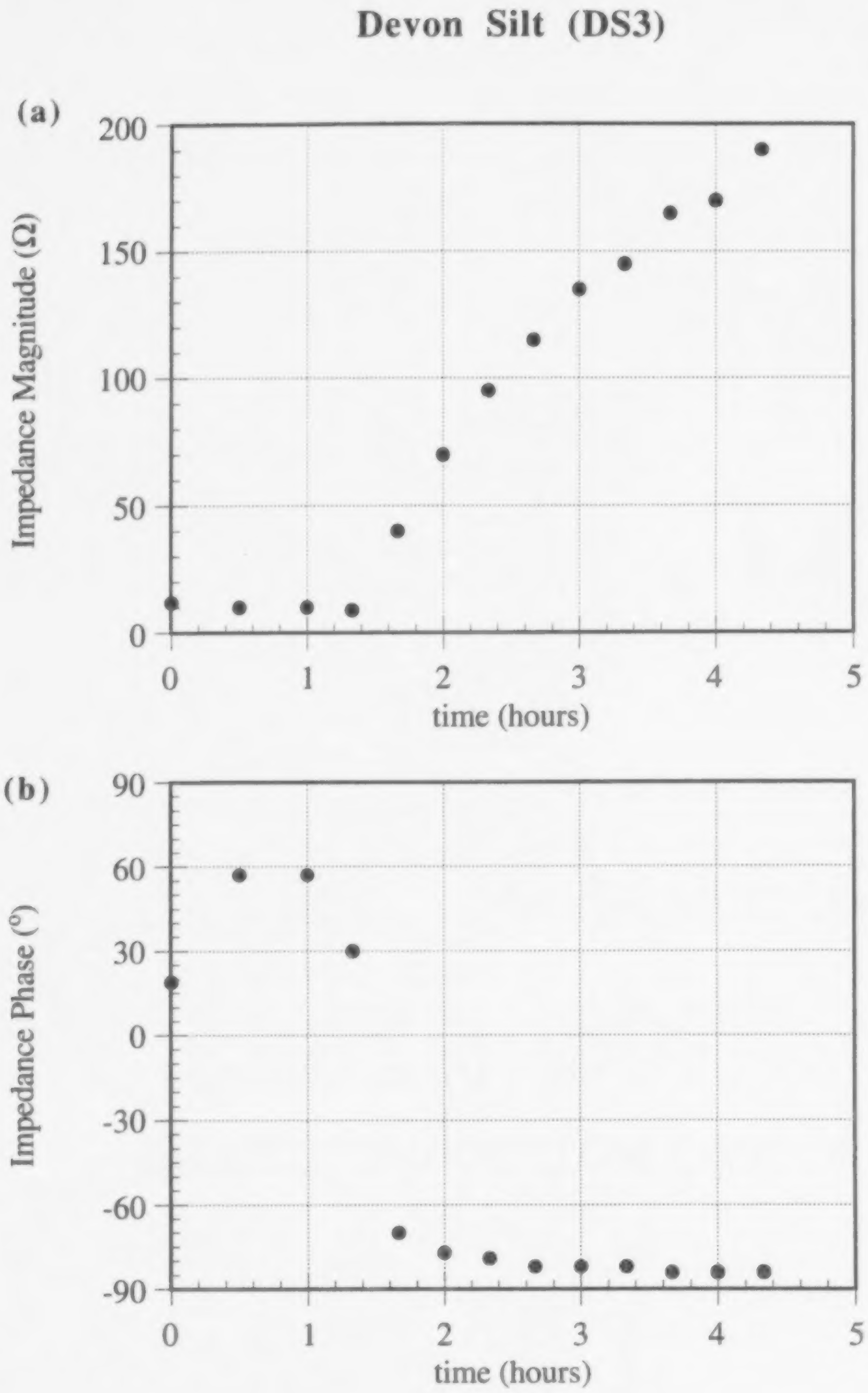

Figure 4.10: Devon silt, experiment DS3, impedance, (a) magnitude, (b) phase.

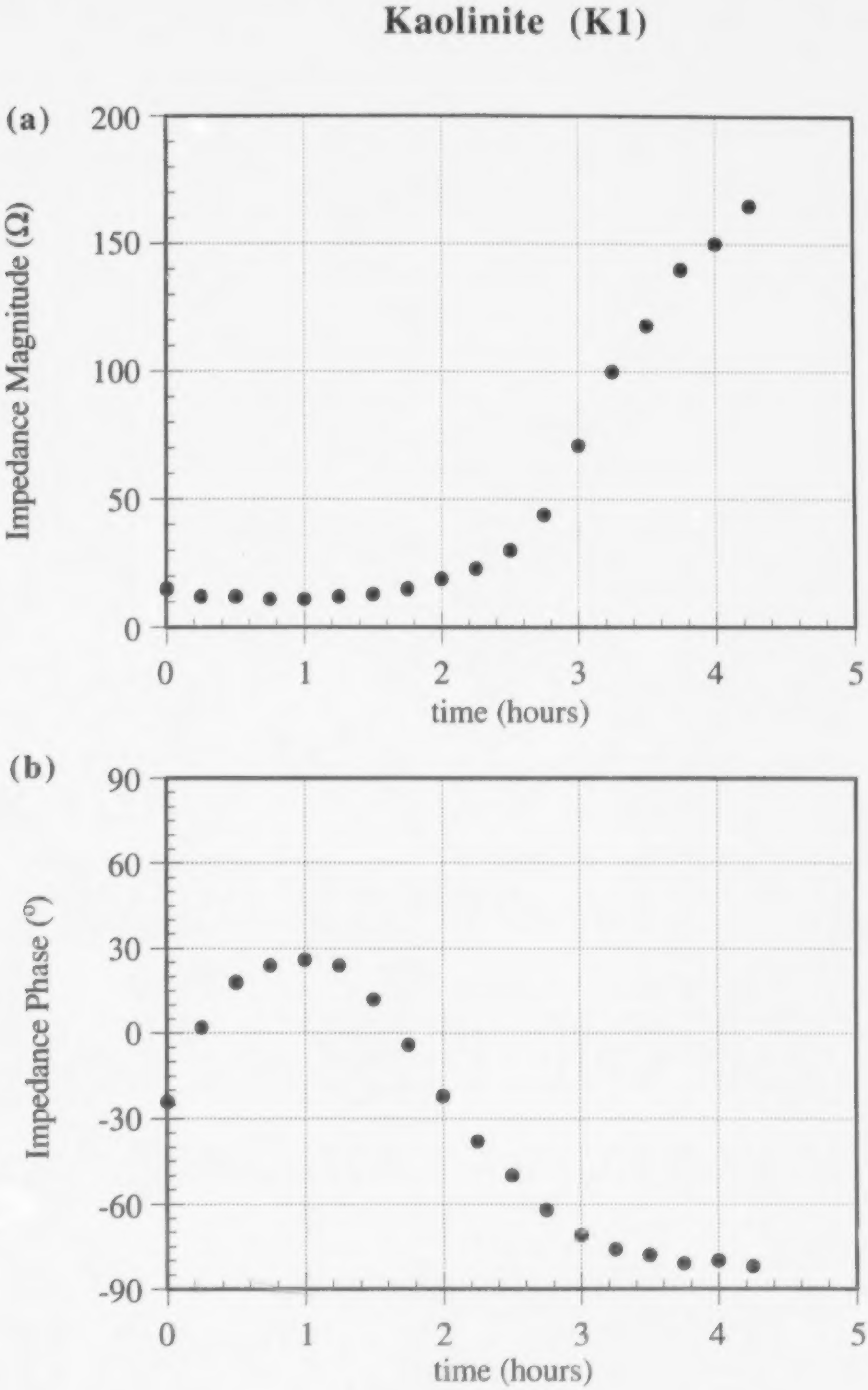

Figure 4.11: Kaolinite, experiment K1, impedance, (a) magnitude, (b) phase.

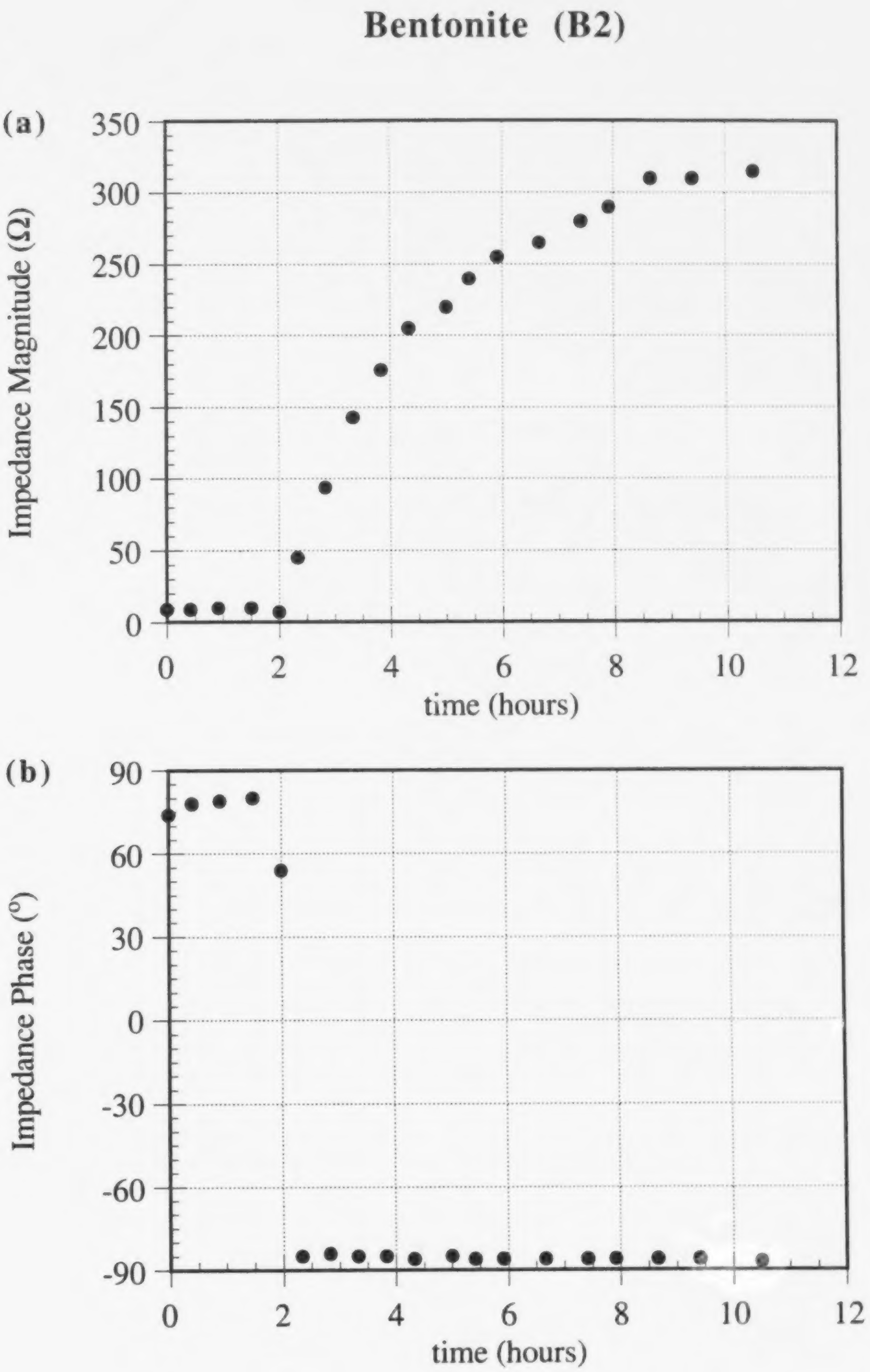

Figure 4.12: Bentonite, experiment B2, impedance, (a) magnitude, (b) phase.

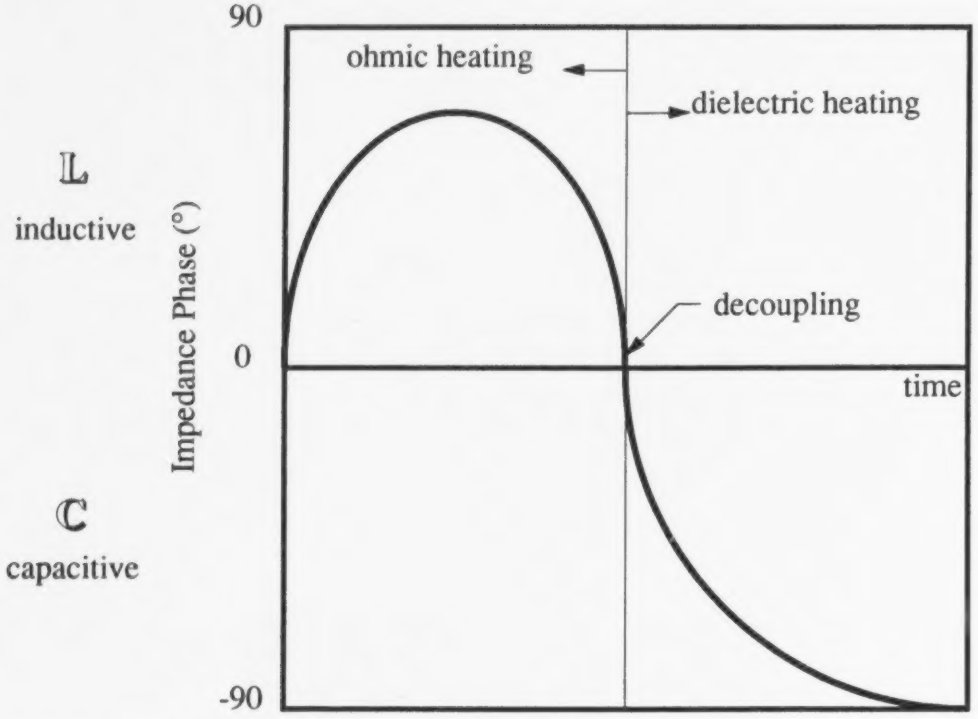

Figure 4.13: Impedance phase of a sample as it decouples.

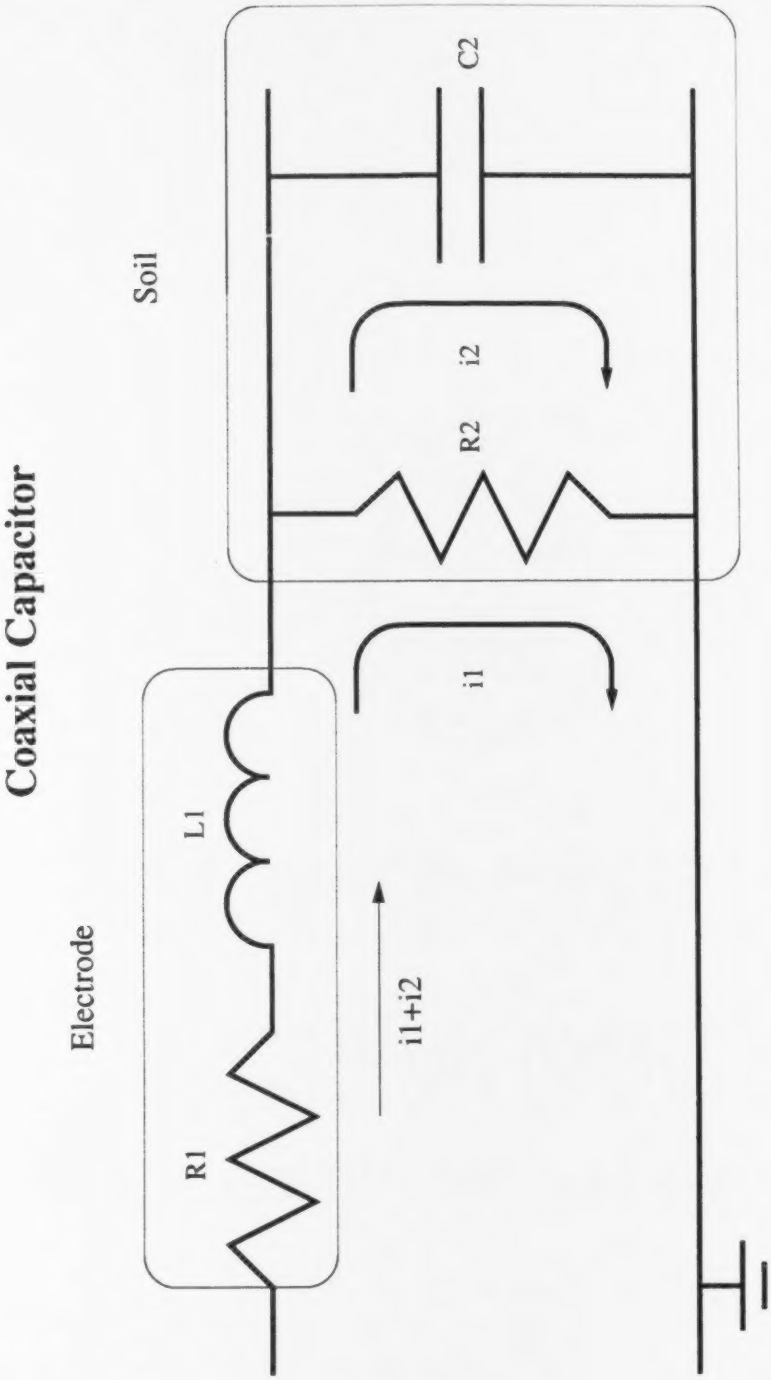
Coaxial Capacitor
Electrode
Soil
R1
L1
i1+i2
i1
R2
i2
C2

Figure 4.14: Equivalent circuit for RF drying and vitrification tests.

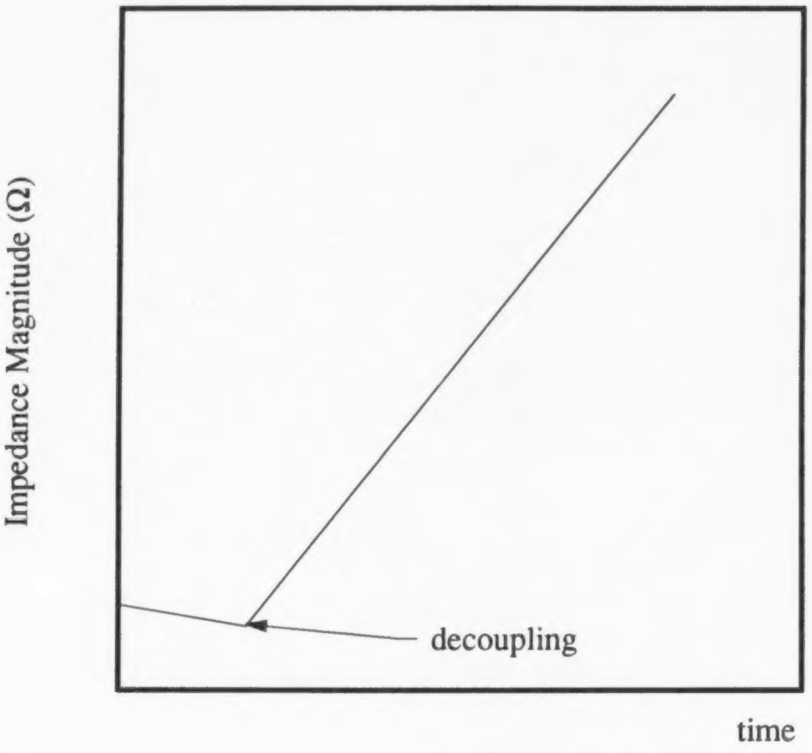

Figure 4.15: Impedance magnitude of a sample as it decouples.

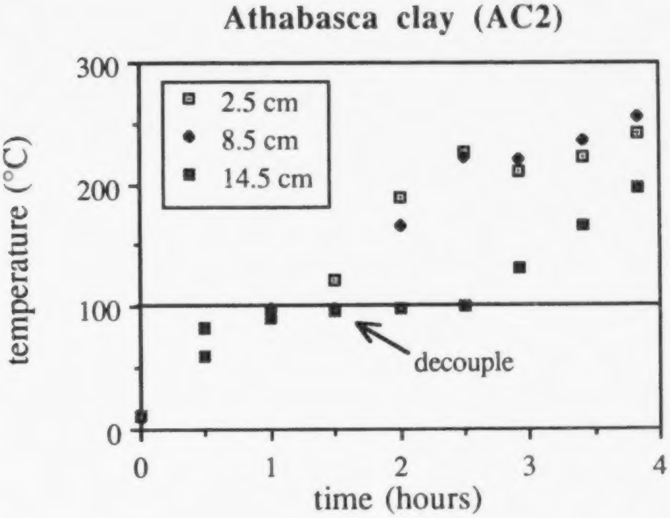

Figure 4.16: Athabasca clay, experiment AC2, temperature at the inner electrode.

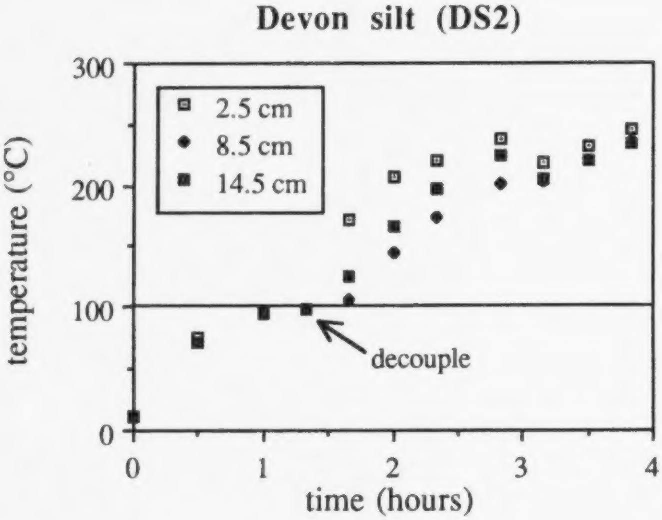

Figure 4.17: Devon silt, experiment DS2, temperature at the inner electrode.

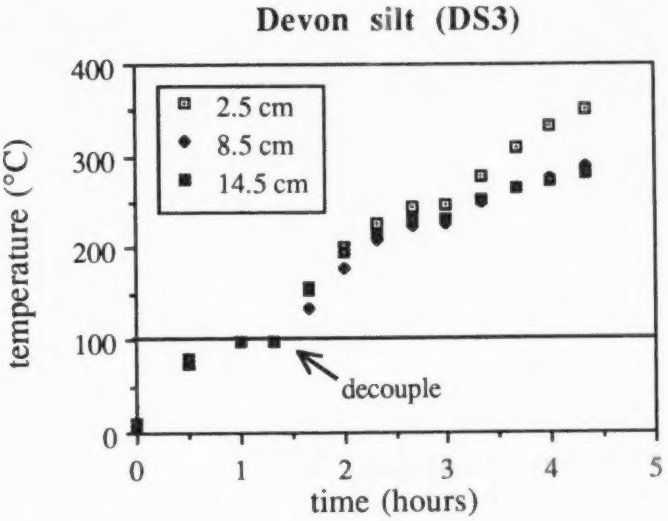

Figure 4.18: Devon silt, experiment DS3, temperature at the inner electrode.

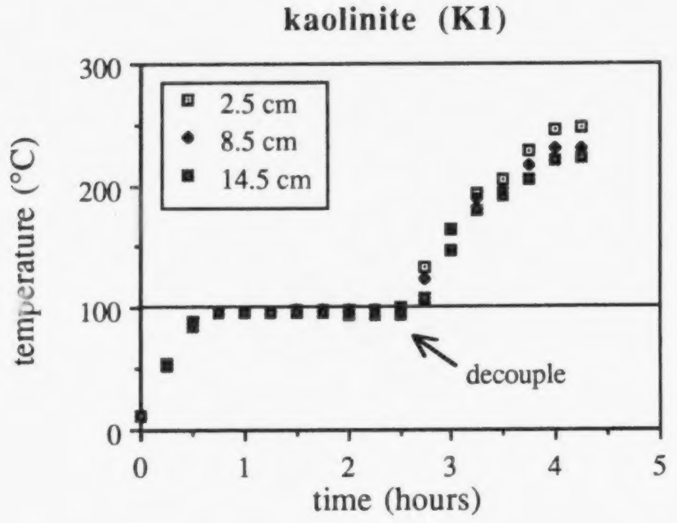

Figure 4.19: Kaolinite, experiment K1, temperature at the inner electrode.

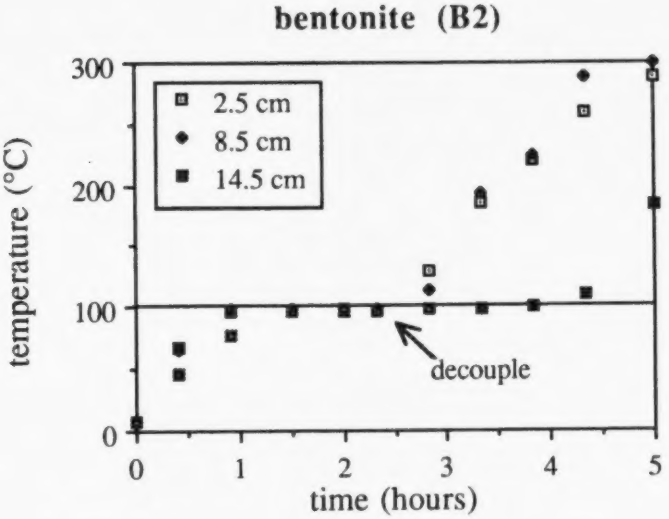

Figure 4.20: Bentonite, experiment B2, temperature at the inner electrode.

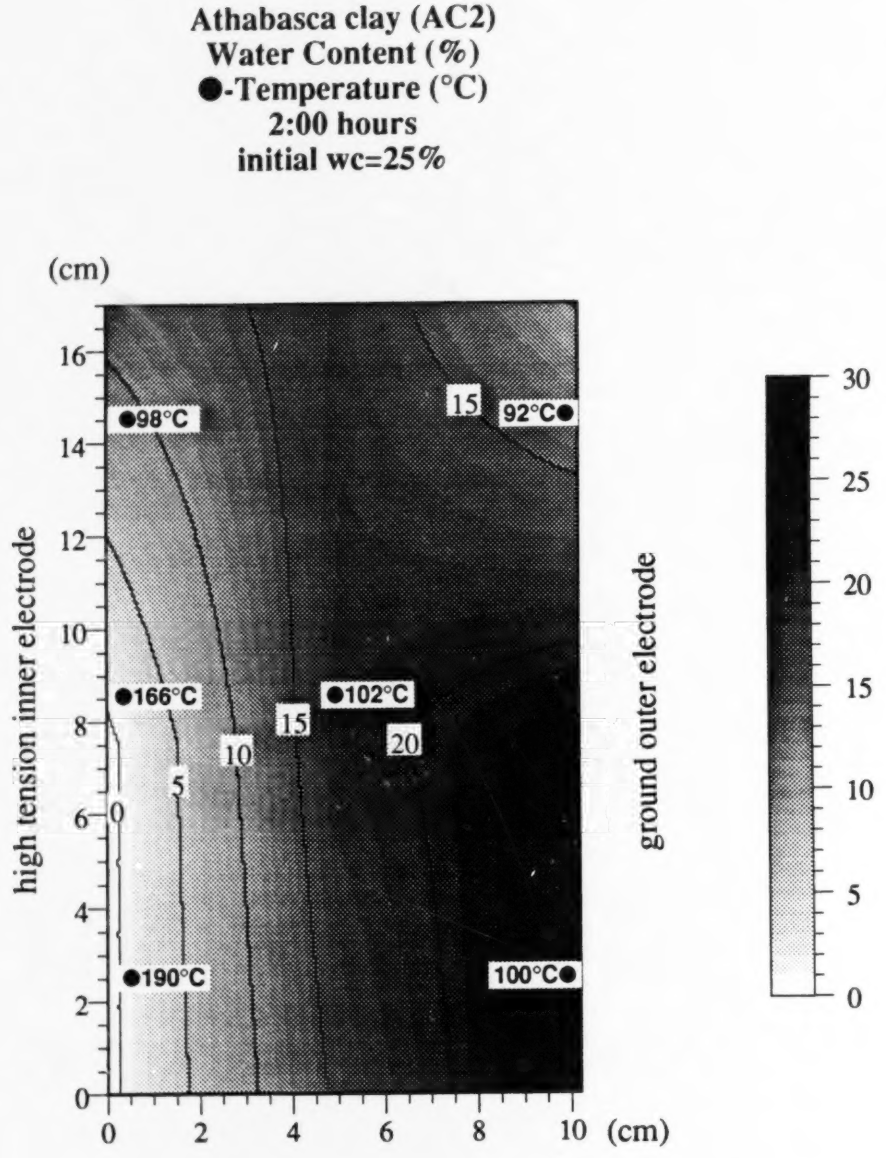

Figure 4.21 (a): Athabasca clay (AC2), water content distribution at 2:00 hours @1500 W.

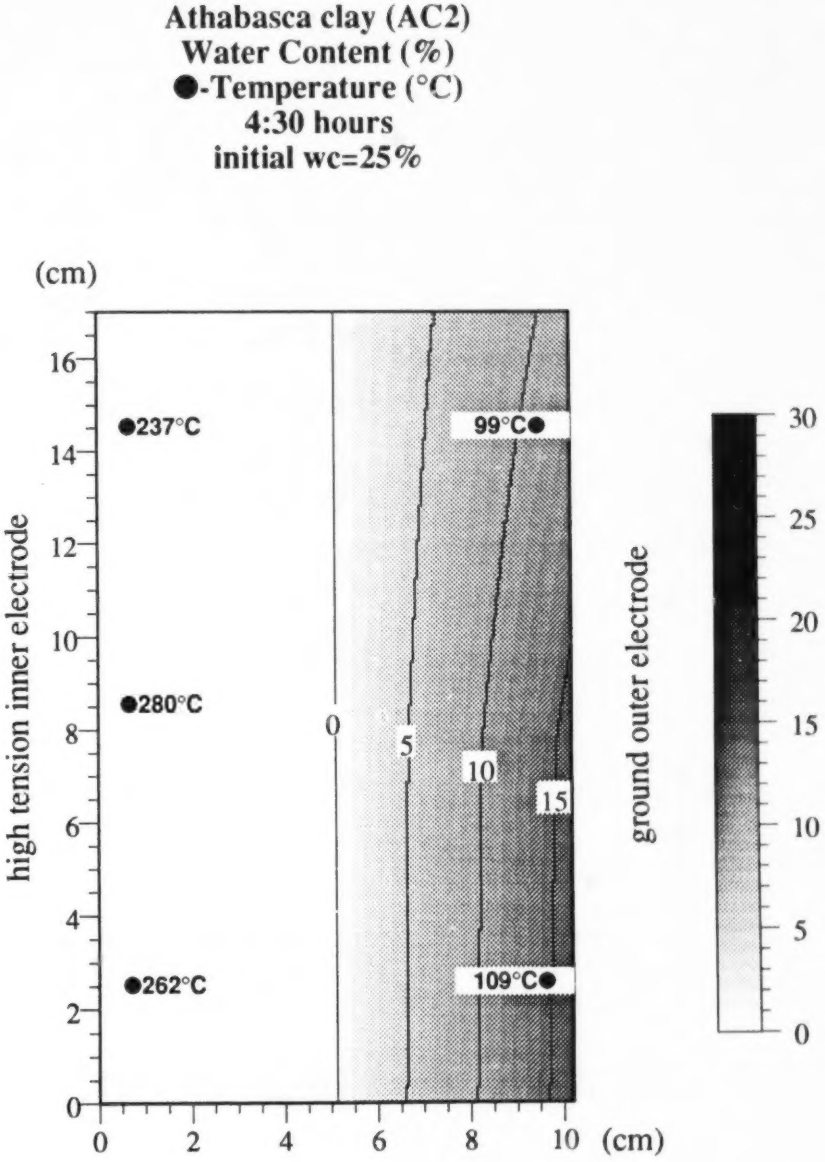

Figure 4.21 (b): Athabasca clay (AC2), water content distribution at 4:30 hours @1500 W.

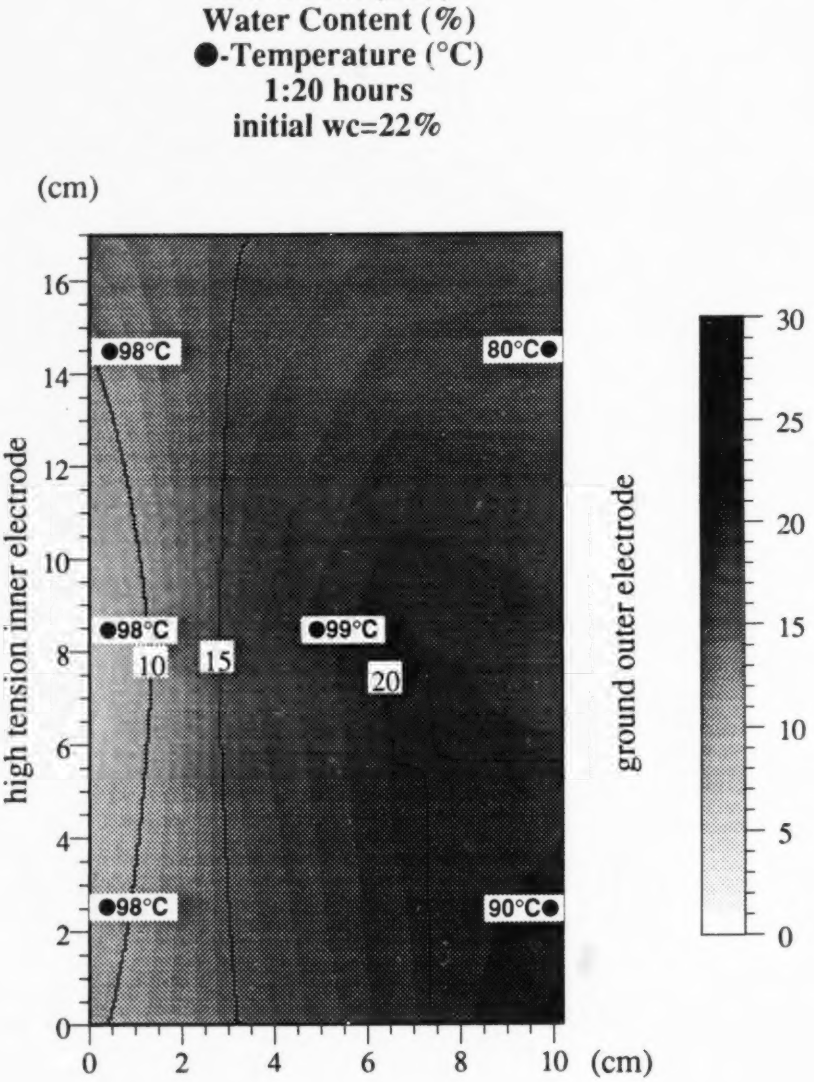

Figure 4.22 (a): Devon silt (DS2), water content distribution at 1:20 hours @1500 W.

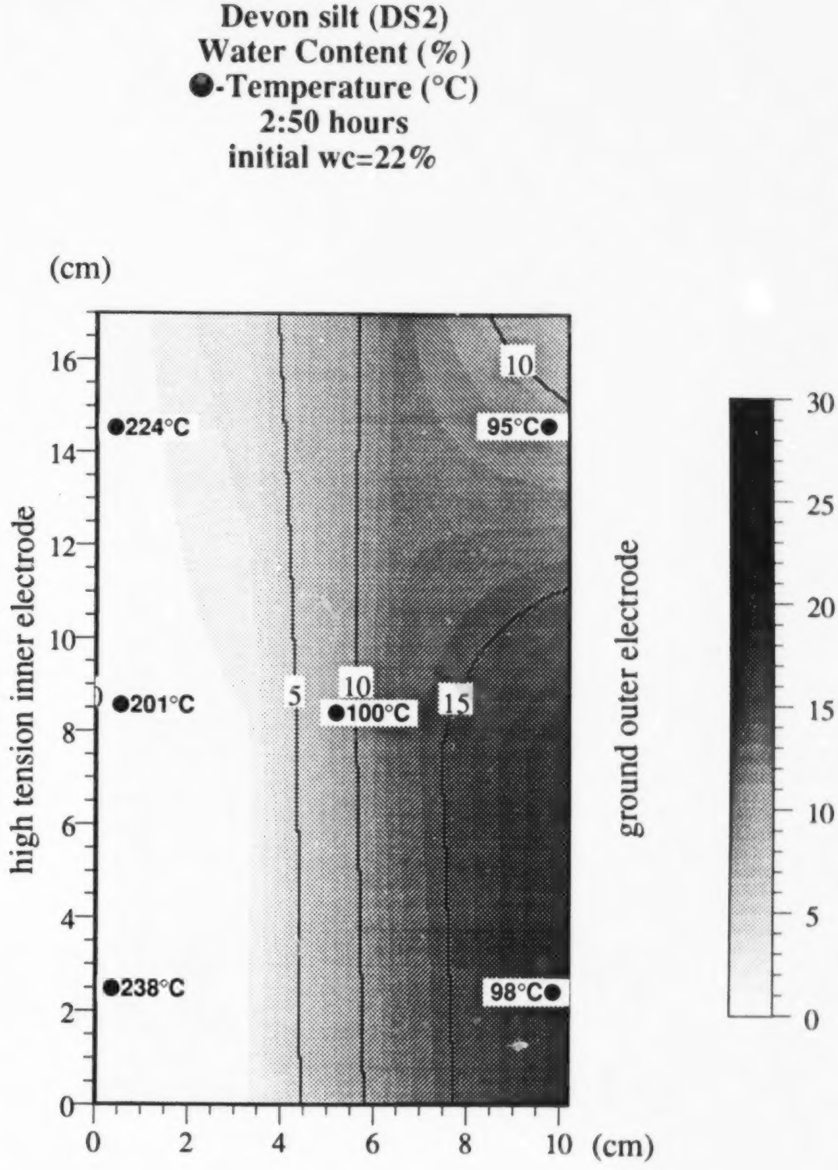

Figure 4.22 (b): Devon silt (DS2), water content distribution at 2:50 hours @1500 W.

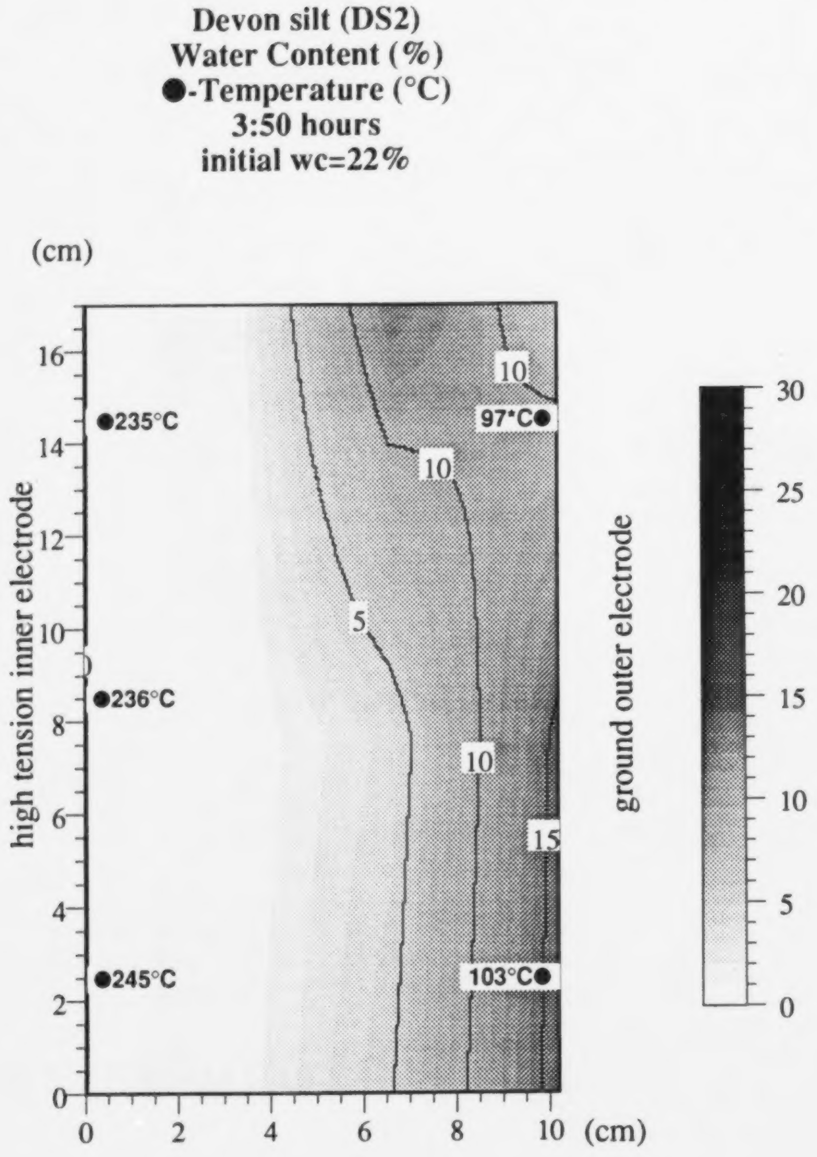

Figure 4.22 (c): Devon silt (DS2), water content distribution at 3:50 hours @1500 W.

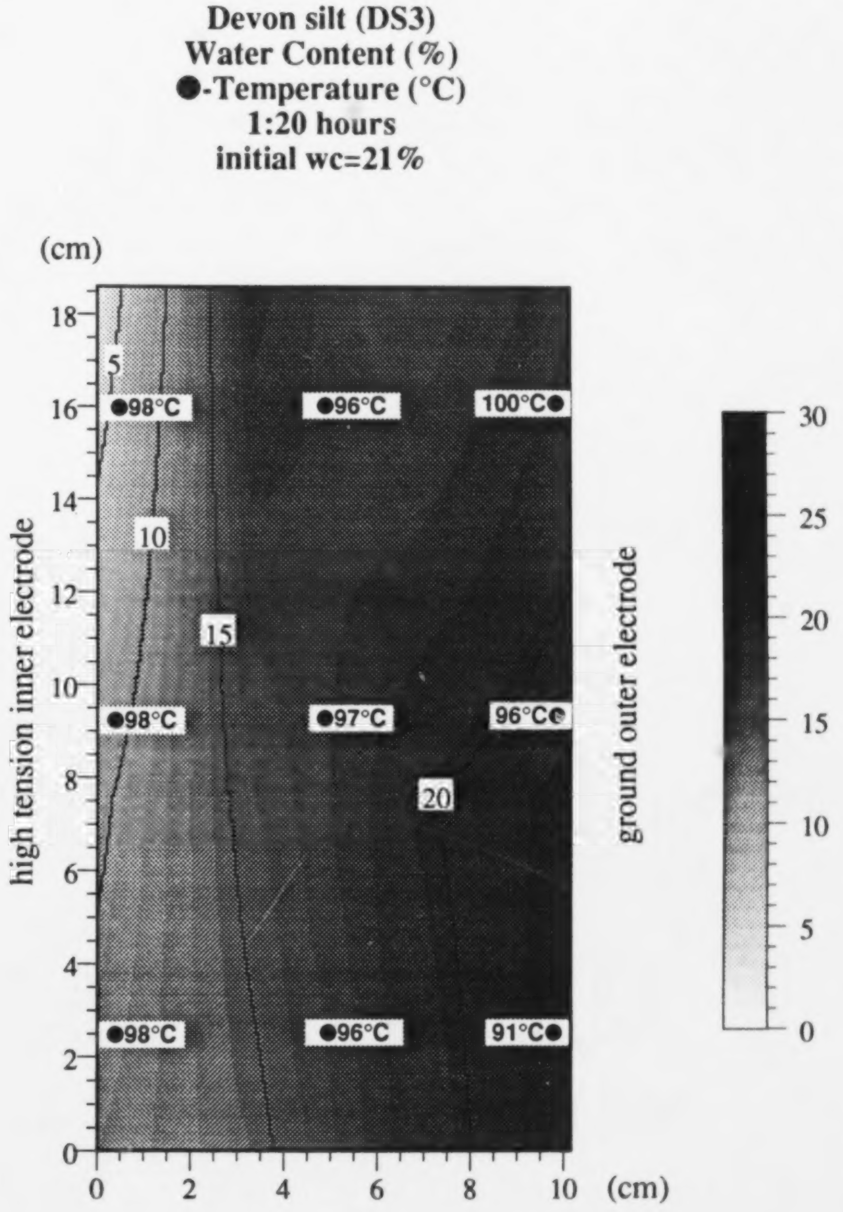

Figure 4.23 (a): Devon silt (DS3), water content distribution at 1:20 hours @1500 W.

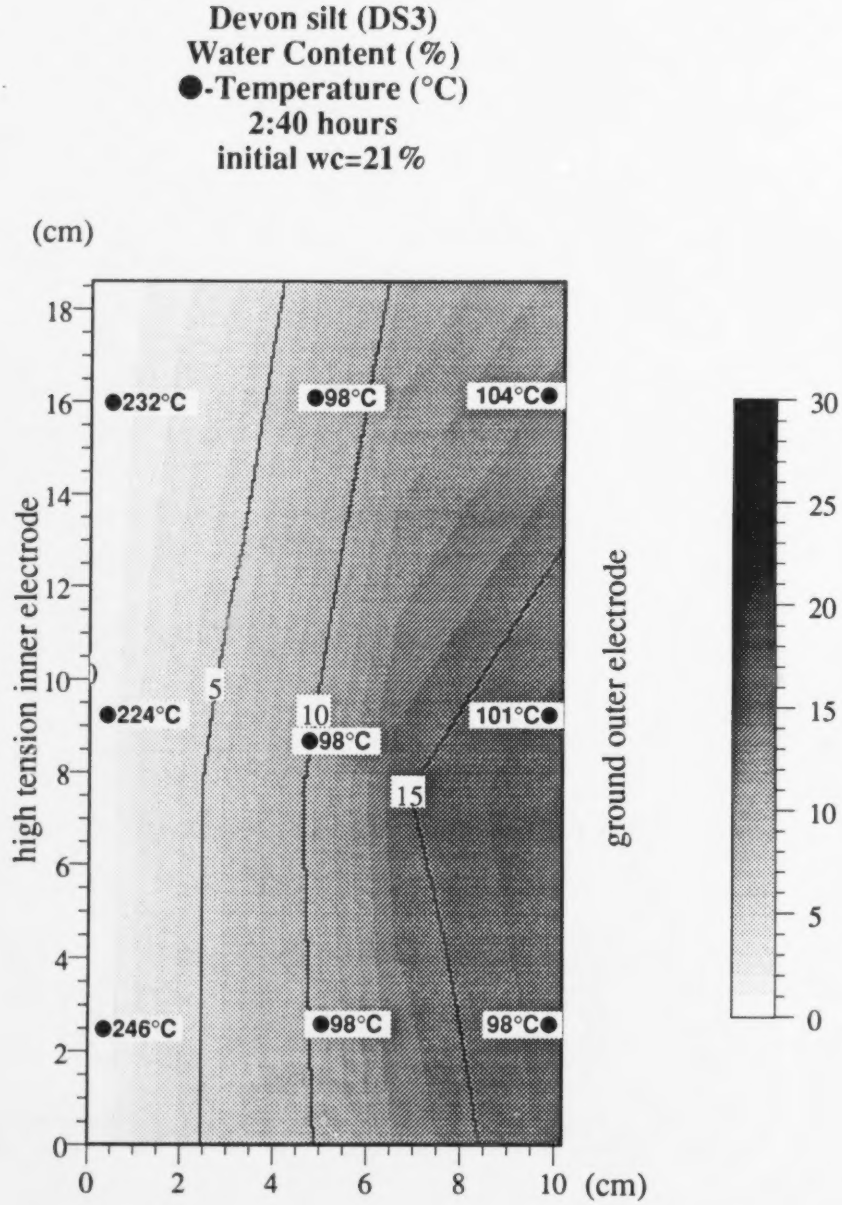

Devon silt (DS3)
Water Content (%)
●-Temperature (°C)
2:40 hours
initial wc=21%

Figure 4.23 (b): Devon silt (DS3), water content distribution at 2:40 hours @1500 W.

Devon silt (DS3)
Water Content (%)
●-Temperature (°C)
4:20 hours
initial wc=21%

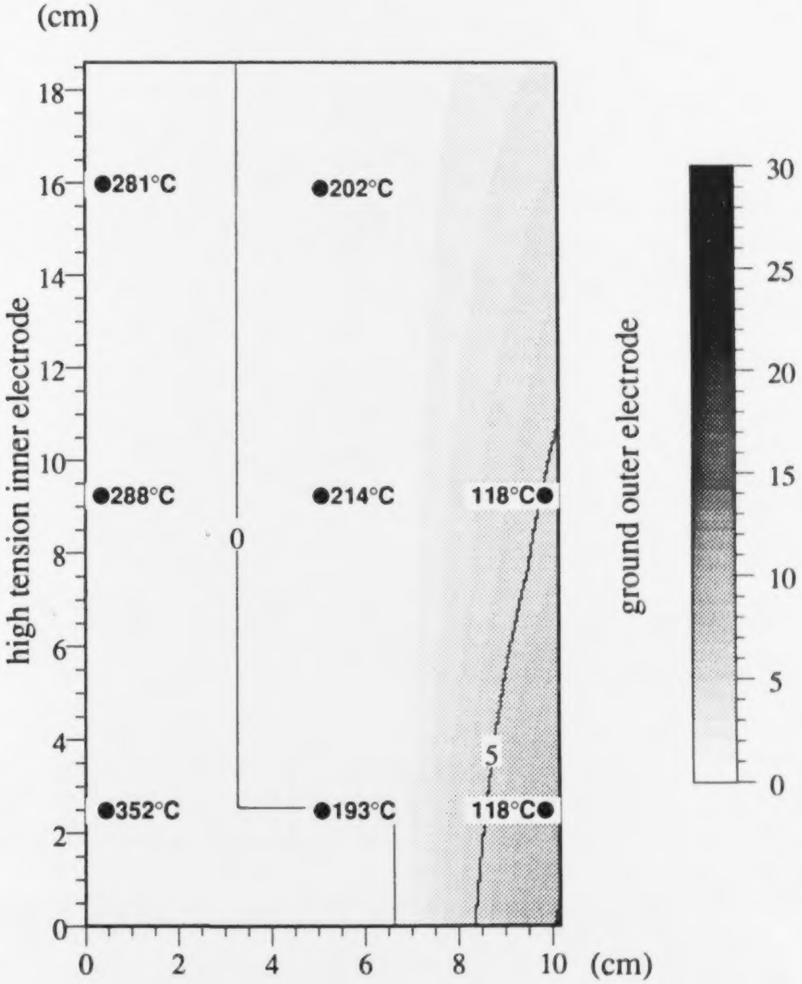

Figure 4.23 (c): Devon silt (DS3), water content distribution at 4:20 hours @1500 W.

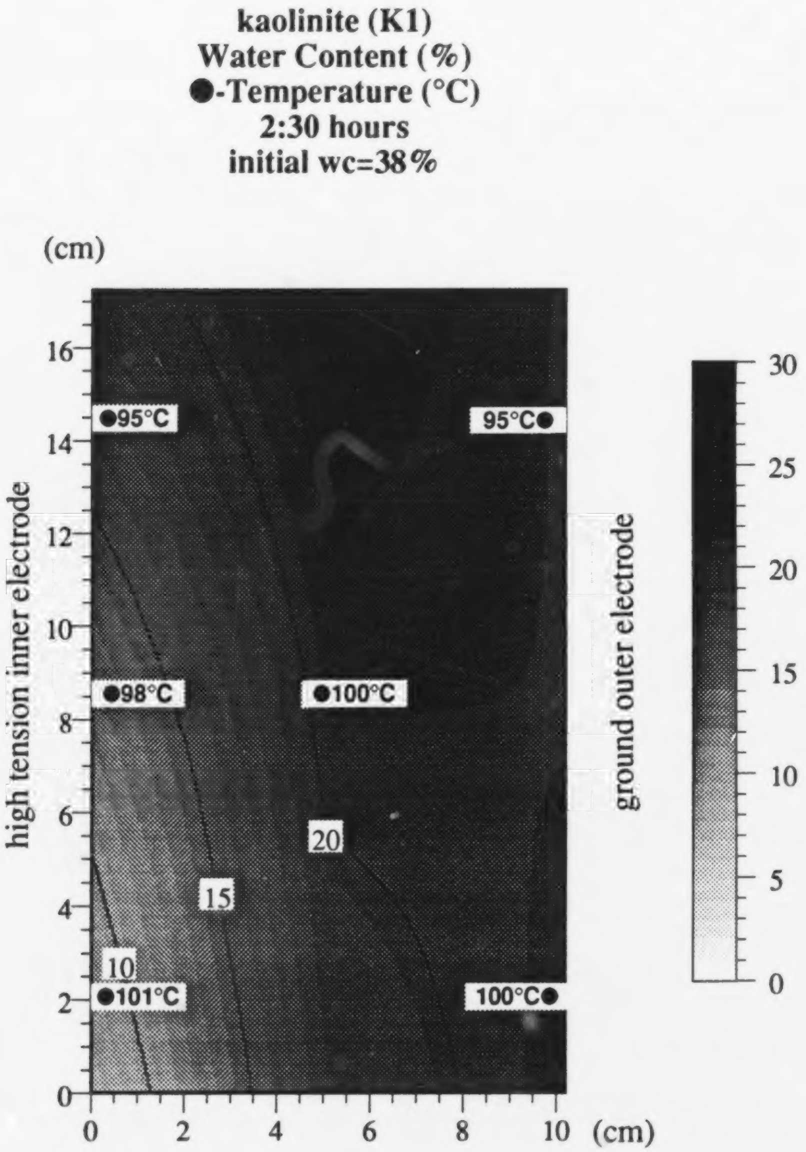

Figure 4.24 (a): kaolinite (K1), water content distribution at 2:30 hours @1500 W.

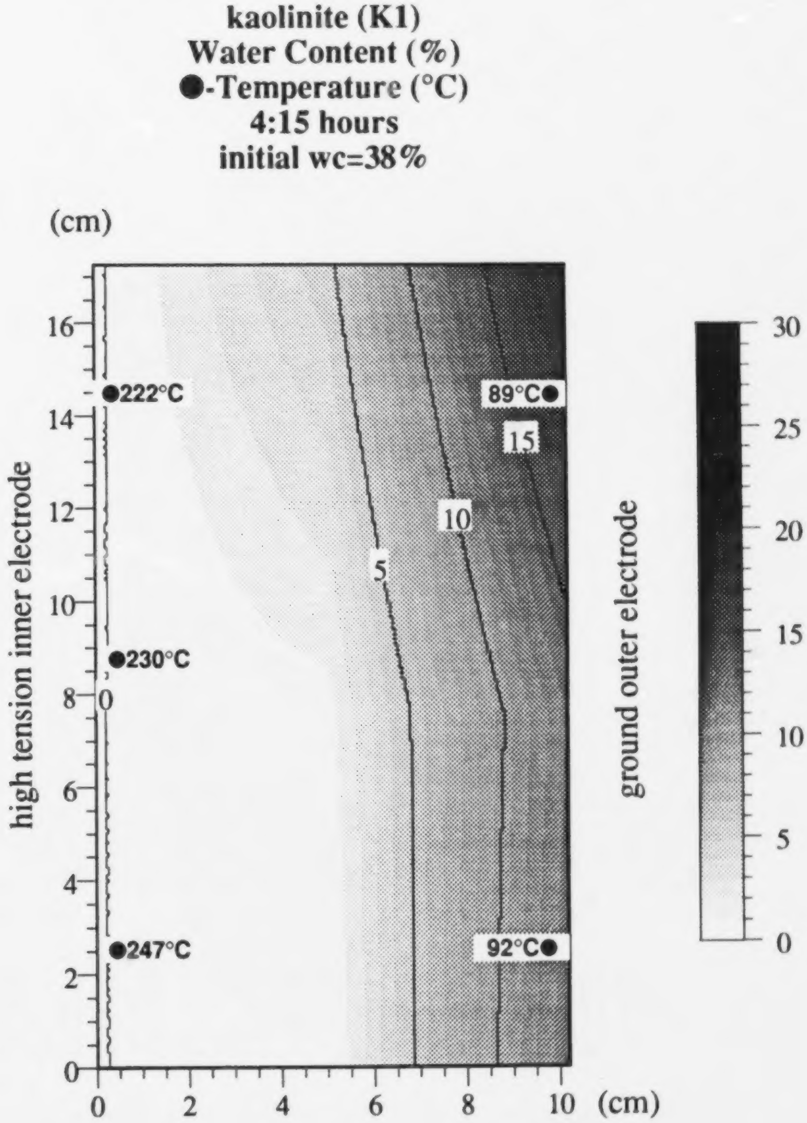
kaolinite (K1)
Water Content (%)
●-Temperature (°C)
4:15 hours
initial wc=38%

Figure 4.24 (b): kaolinite (K1), water content distribution at 4:15 hours @1500 W.

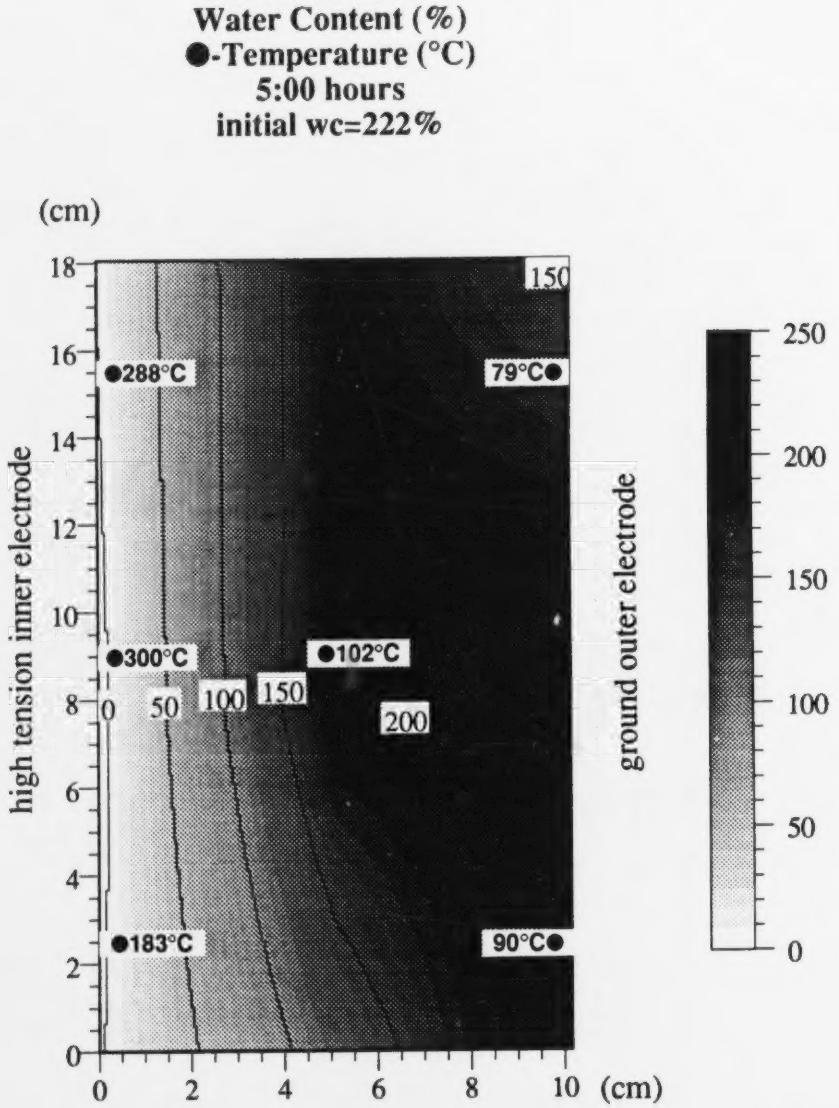
bentonite (B2)
Water Content (%)
●-Temperature (°C)
5:00 hours
initial wc=222%

Figure 4.25 (a): bentonite (B2), water content distribution at 5:00 hours @1500 W.

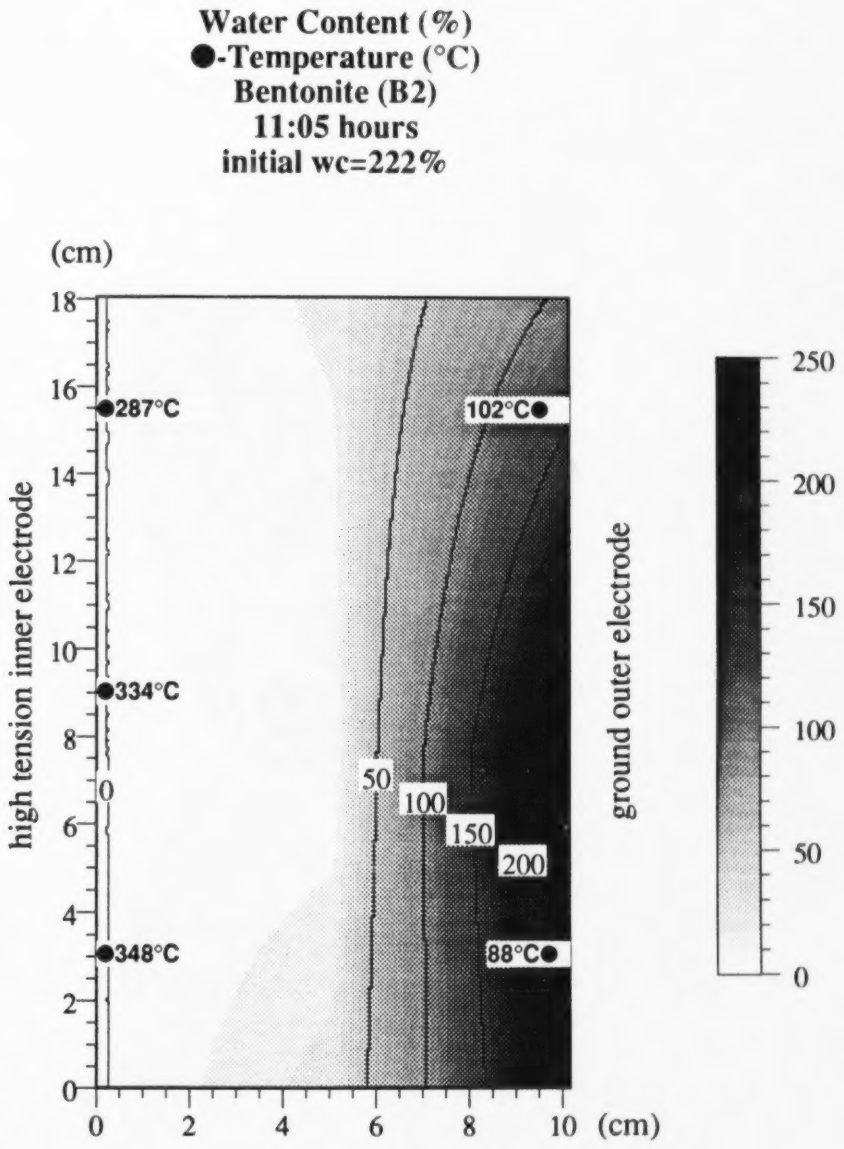

Figure 4.25 (b): bentonite (B2), water content distribution at 11:05 hours @1500 W.

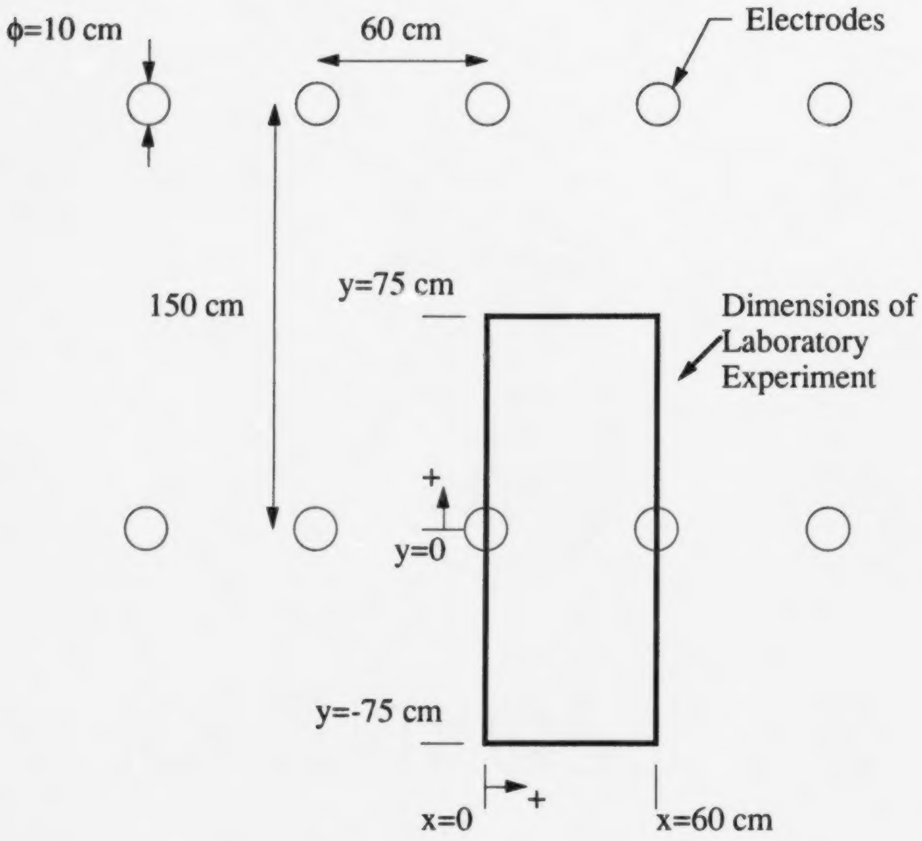
ϕ=10 cm
60 cm
Electrodes
150 cm
y=75 cm
Dimensions of Laboratory Experiment
+
y=0
y=-75 cm
x=0
+
x=60 cm

Figure 5.1: Electrode array, plan view with outline of engineering scale laboratory experiment.

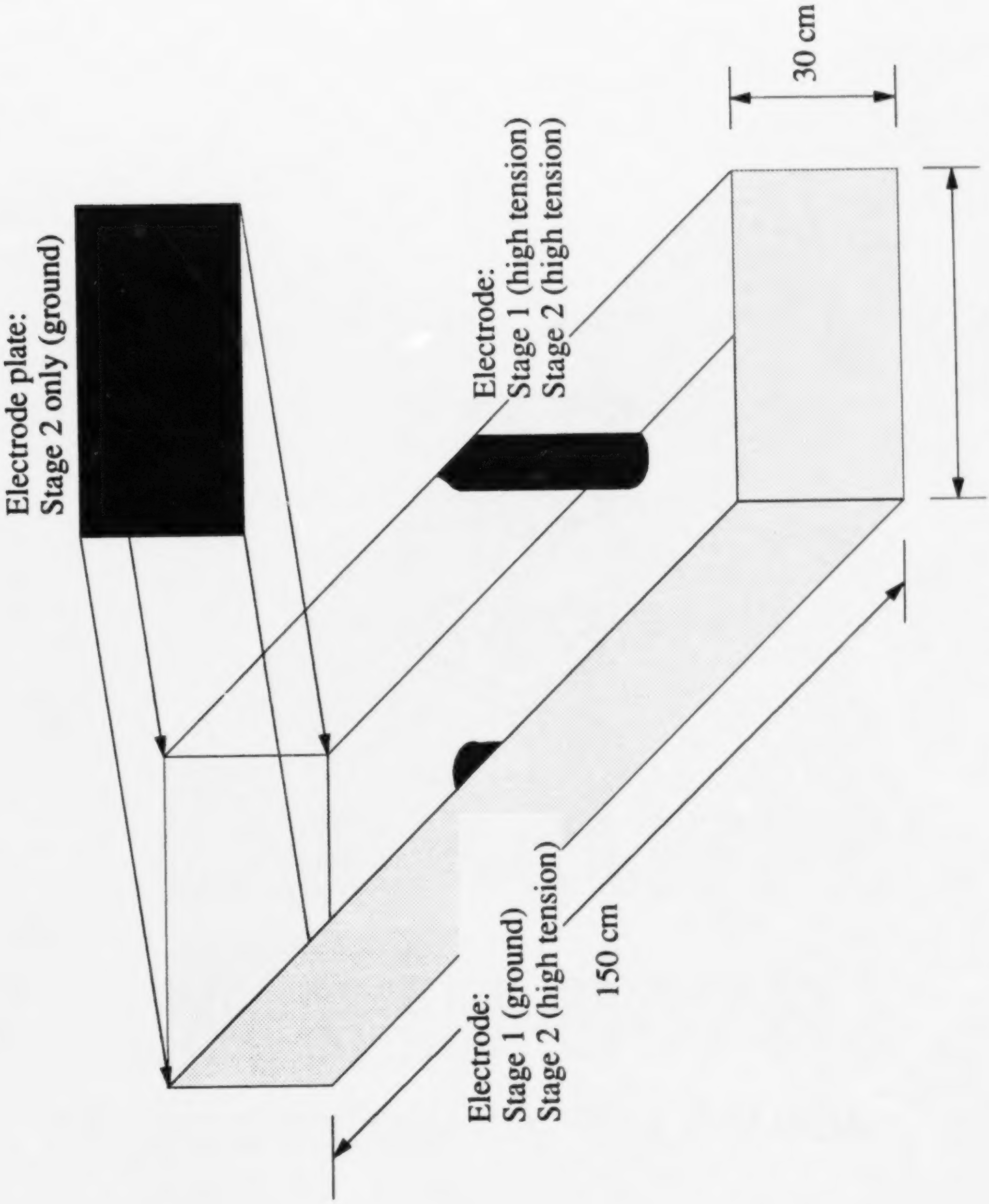
Electrode plate:
Stage 2 only (ground)
Electrode:
Stage 1 (high tension)
Stage 2 (high tension)
30 cm
60 cm
Electrode:
Stage 1 (ground)
Stage 2 (high tension)
150 cm

Figure 5.2: Engineering scale laboratory experiment sample holder.

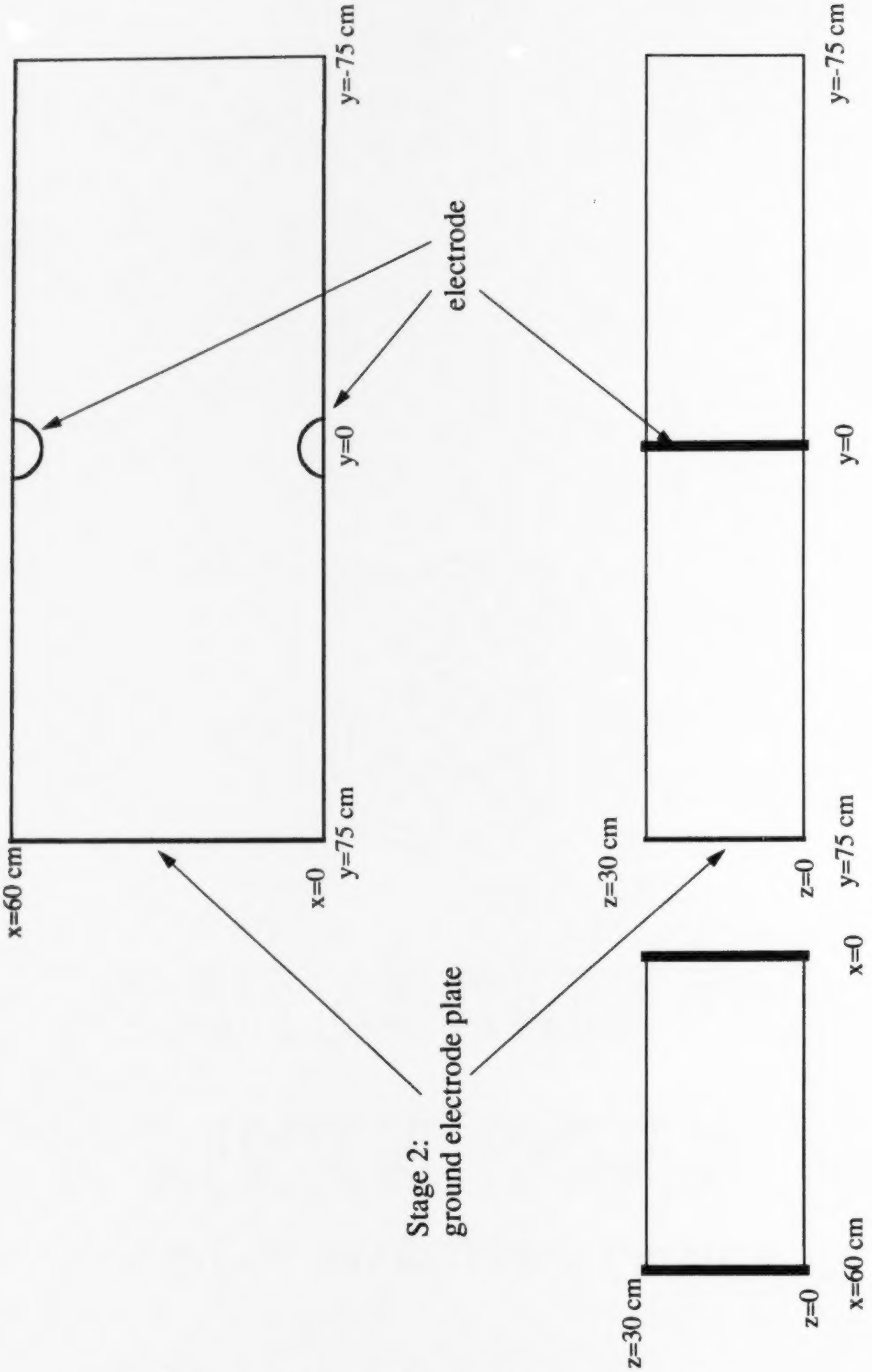
y=-75 cm
electrode
y=0
y=-75 cm
y=0
x=60 cm
x=0
y=75 cm
z=30 cm
z=0
y=75 cm
Stage 2:
ground electrode plate
x=0
z=30 cm
z=0
x=60 cm

Figure 5.3: X, Y, Z co-ordinates of engineering scale test.

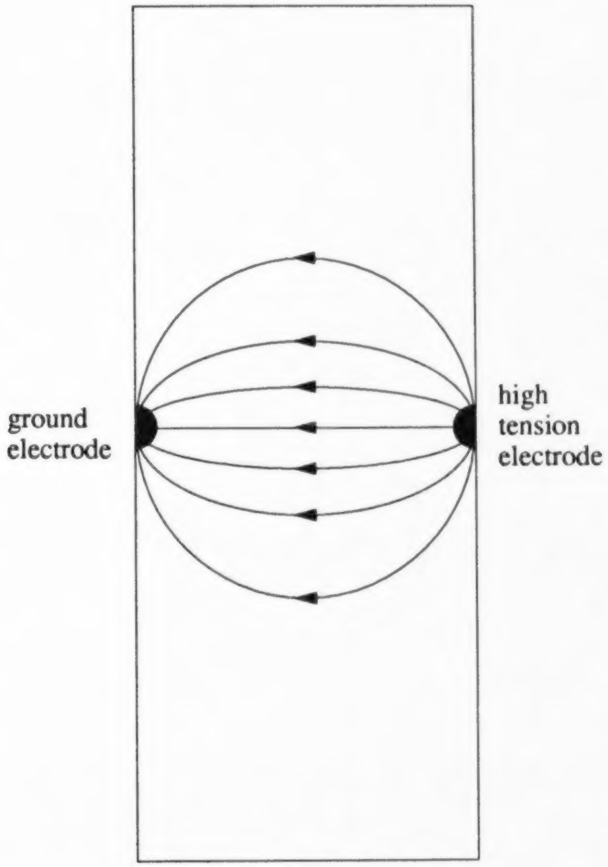
ground
electrode
high
tension
electrode

Figure 5.4: Plan view of the electric field during Stage 1.

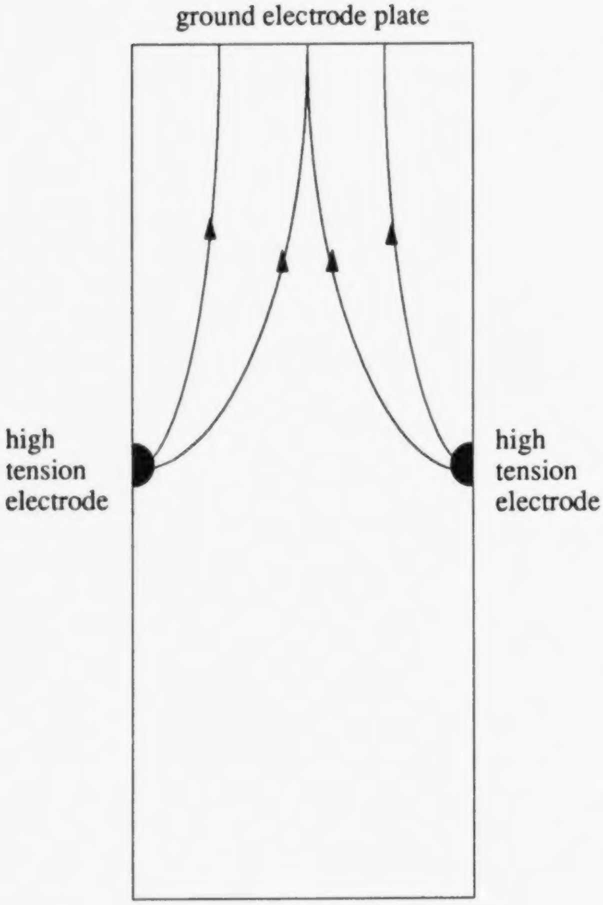
ground electrode plate
high tension electrode
high tension electrode

Figure 5.5: Plan view of the electric field during Stage 2.

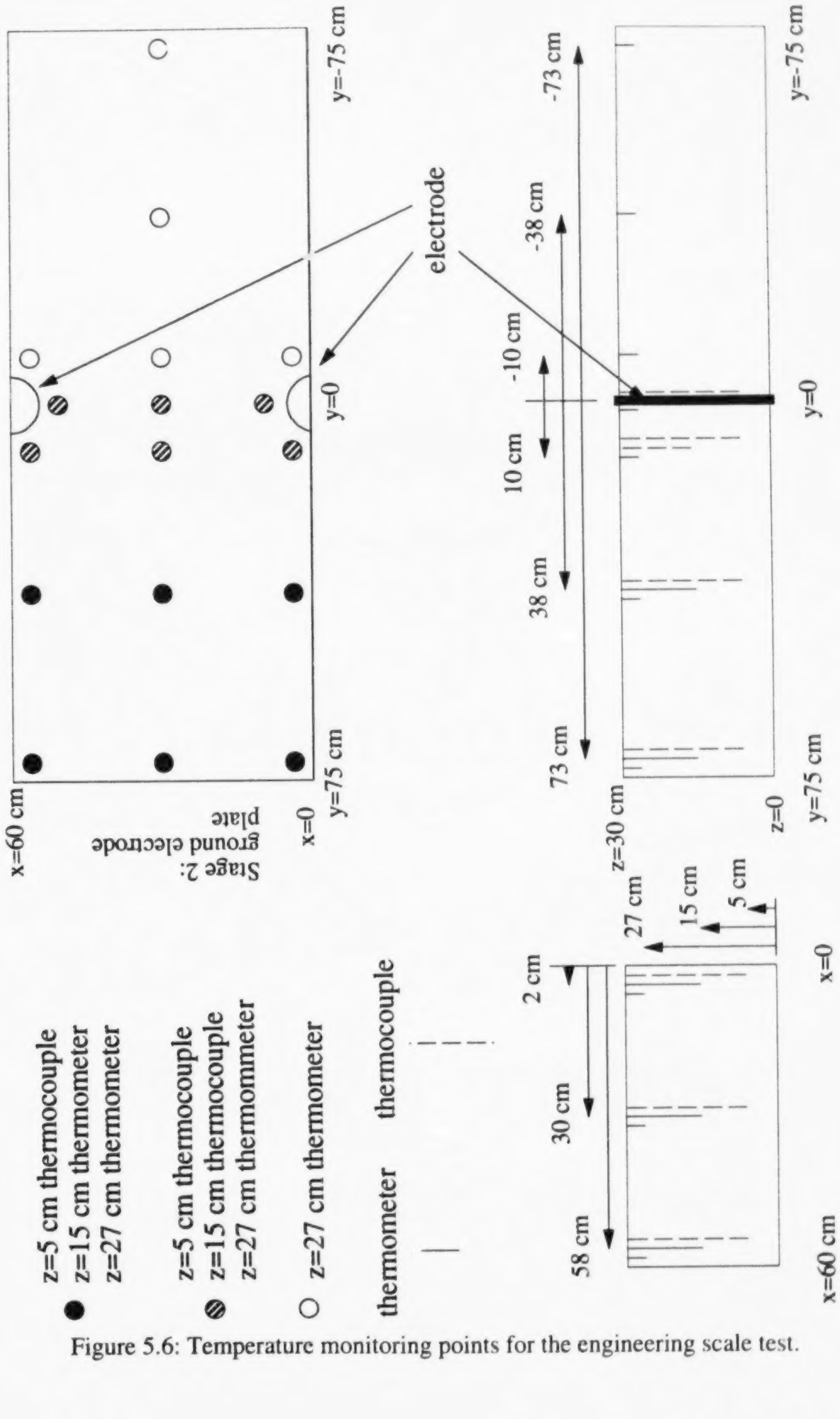

electrode
y=-75 cm
y=0
y=75 cm
x=60 cm
x=0
Stage 2: ground electrode plate
-73 cm
-38 cm
-10 cm
10 cm
38 cm
73 cm
z=30 cm
z=0
y=-75 cm
y=0
y=75 cm
● z=5 cm thermocouple z=15 cm thermometer z=27 cm thermometer
▨ z=5 cm thermocouple z=15 cm thermocouple z=27 cm thermommeter
○ z=27 cm thermometer
thermometer
thermocouple
2 cm
30 cm
58 cm
27 cm
15 cm
5 cm
x=0
x=60 cm

Figure 5.6: Temperature monitoring points for the engineering scale test.

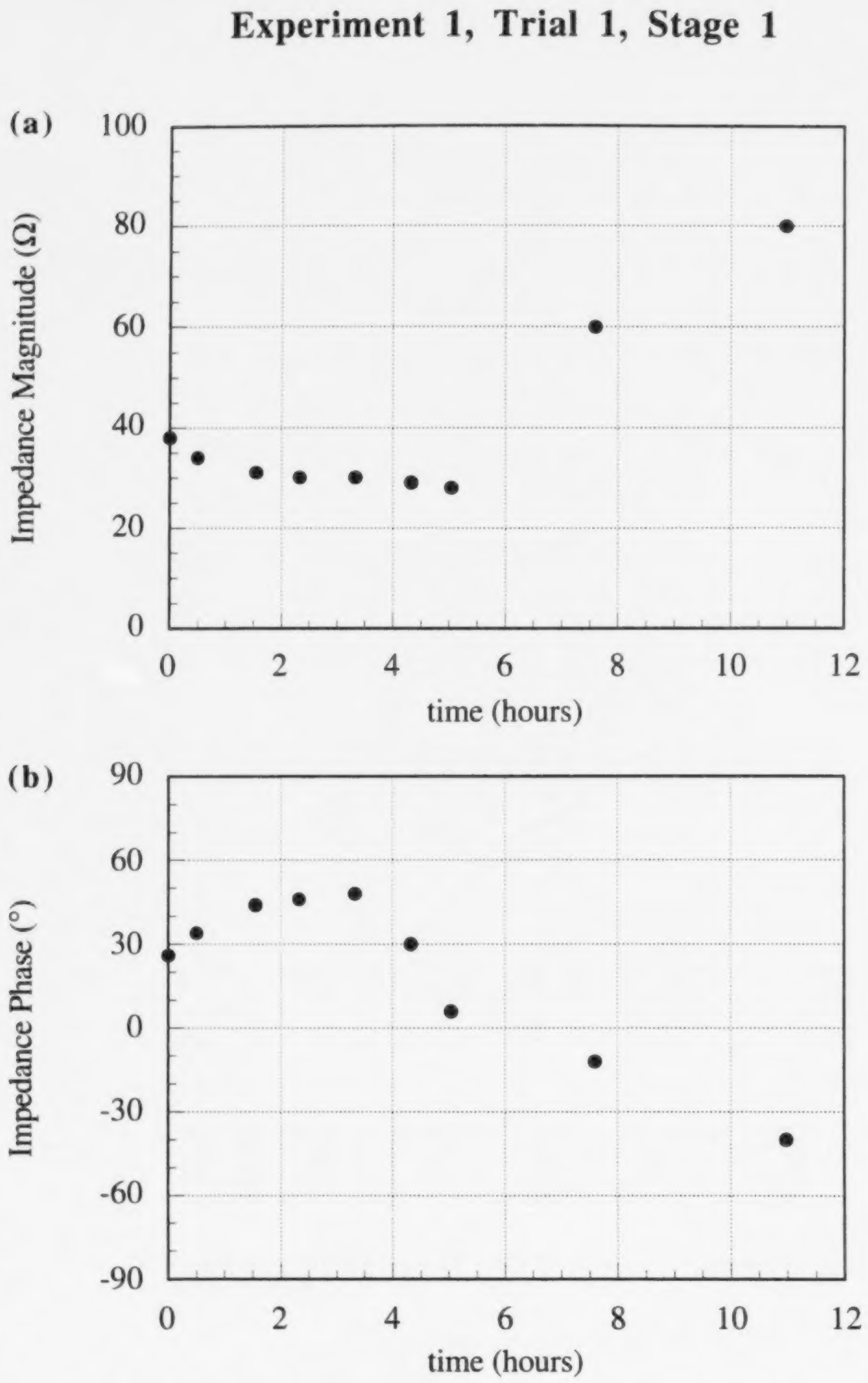

Figure 5.7: Engineering scale test, impedance, experiment 1, trial 1, stage 1, (a) magnitude, (b) phase.

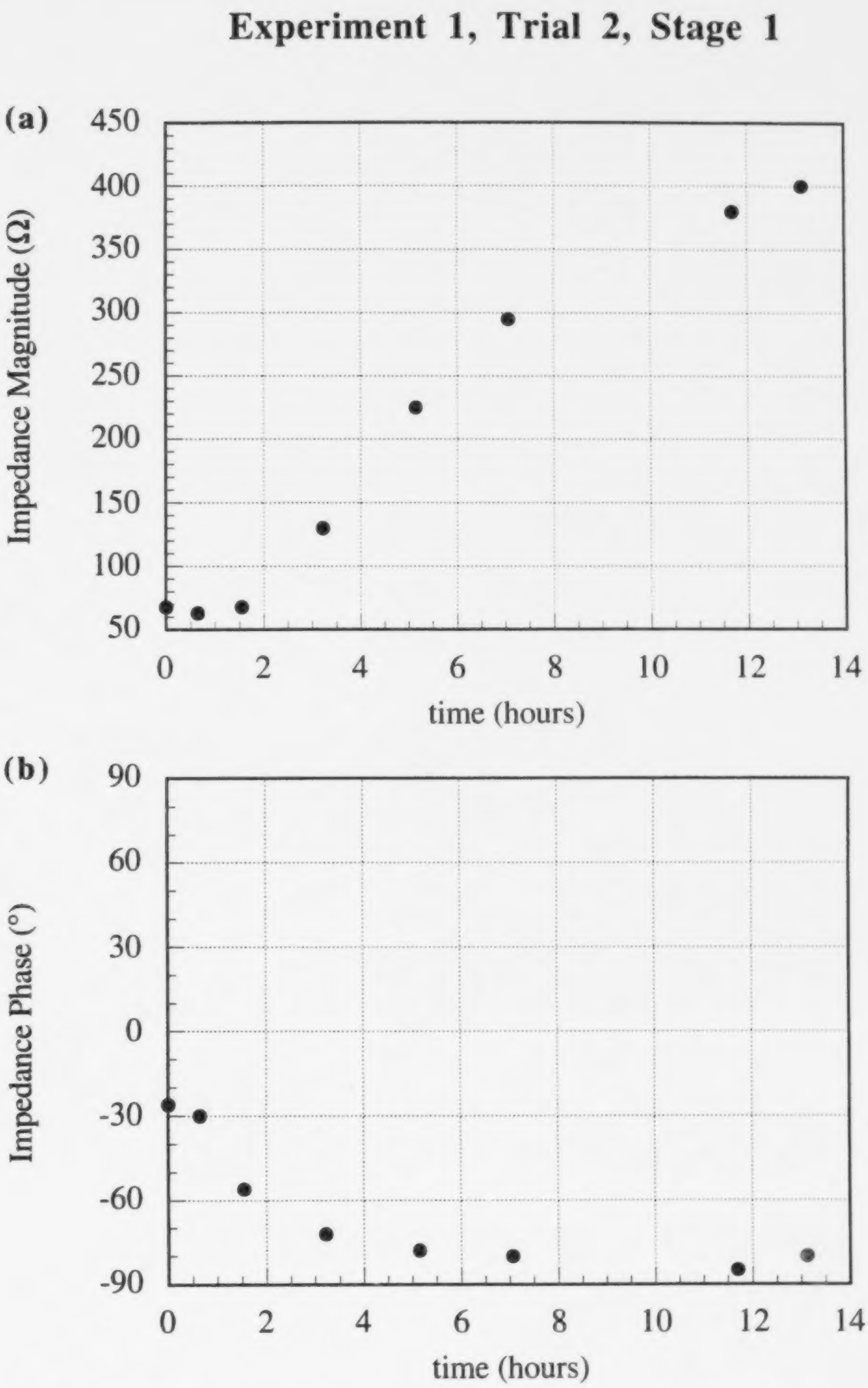

Figure 5.8: Engineering scale test, impedance, experiment 1, trial 2, stage 1, (a) magnitude, (b) phase.

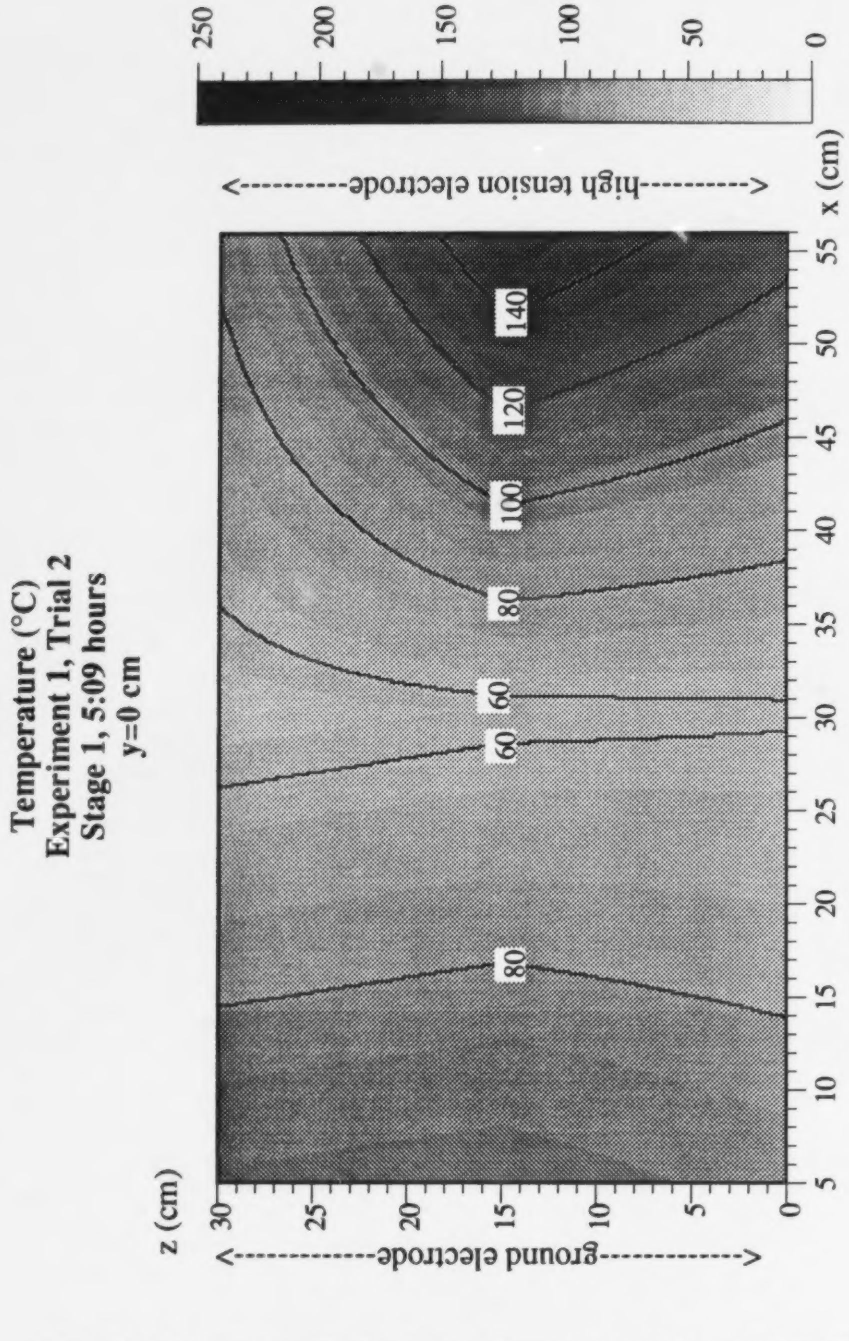

Figure 5.9: Temperature in the plane y=0 cm after 5:09 hours @1500 W, experiment 1, trial 2, stage 1.

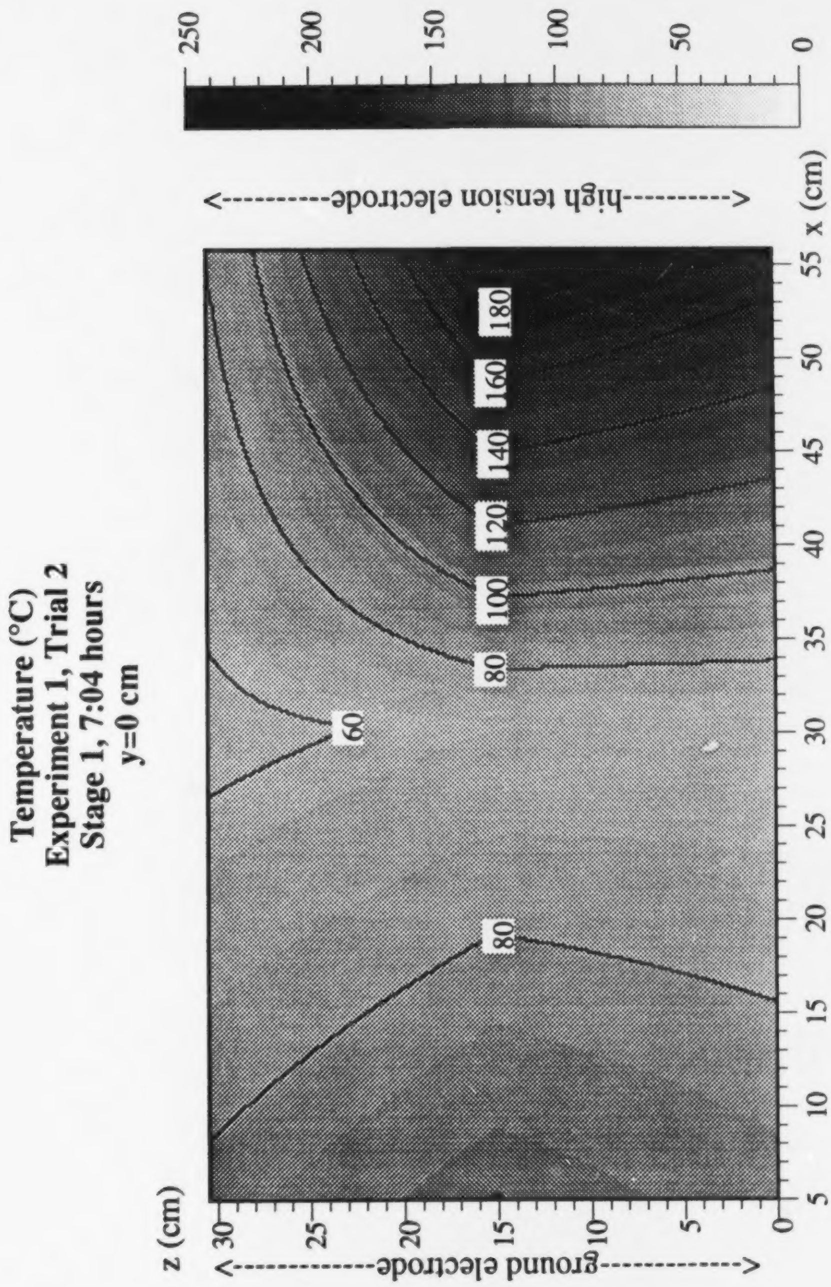

Figure 5.10: Temperature in the plane y=0 cm after 7:04 hours @1500 W, experiment 1, trial 2, stage 1.

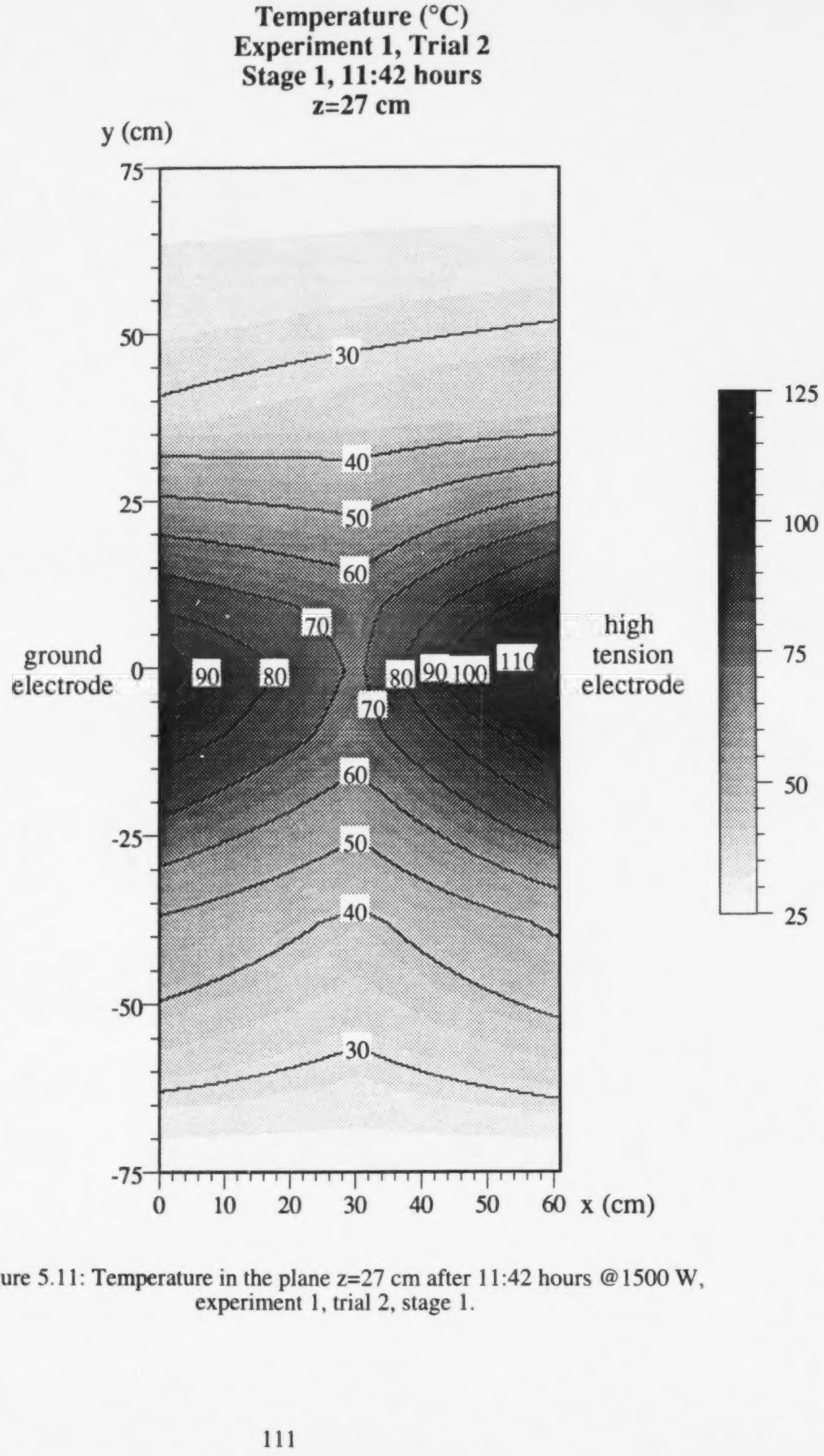

Figure 5.11: Temperature in the plane z=27 cm after 11:42 hours @1500 W, experiment 1, trial 2, stage 1.

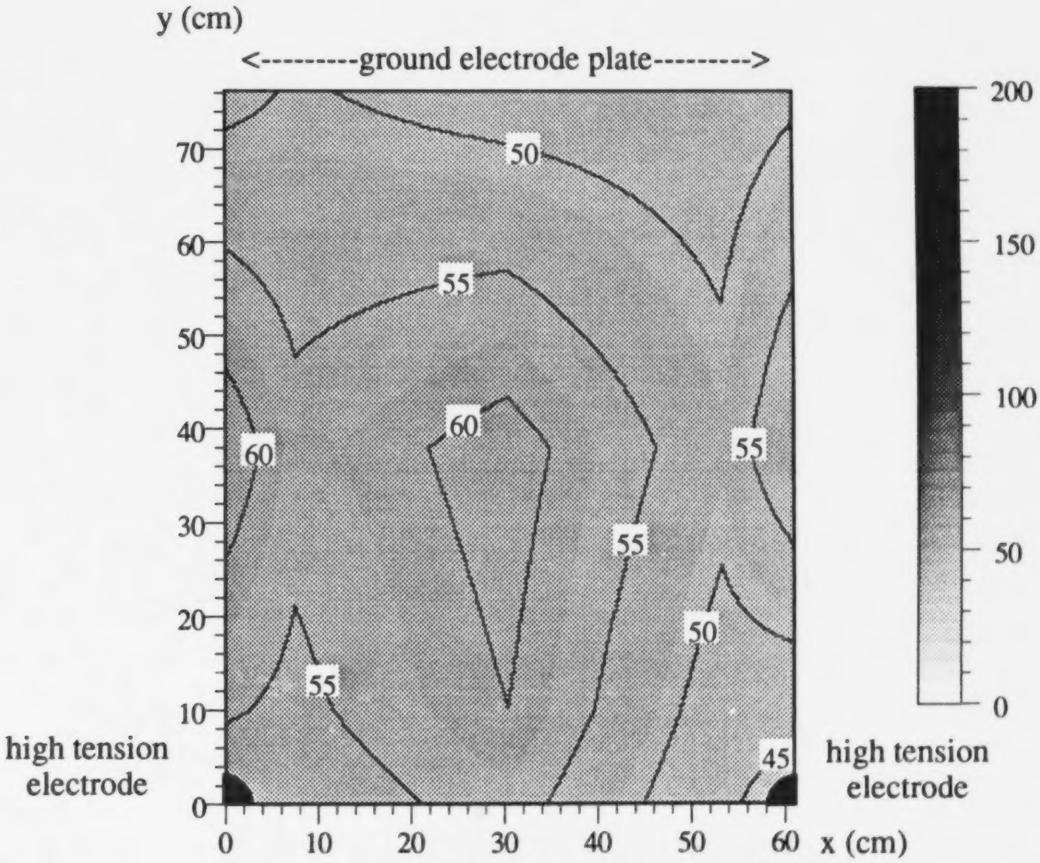

Temperature (°C)
Experiment 1, Trial 2
Stage 2, Day 3, 0 hours
z=15 cm

Figure 5.12: Temperature in the plane z=15 cm after 0 hours, experiment 1, trial 2, stage 2, day 3.

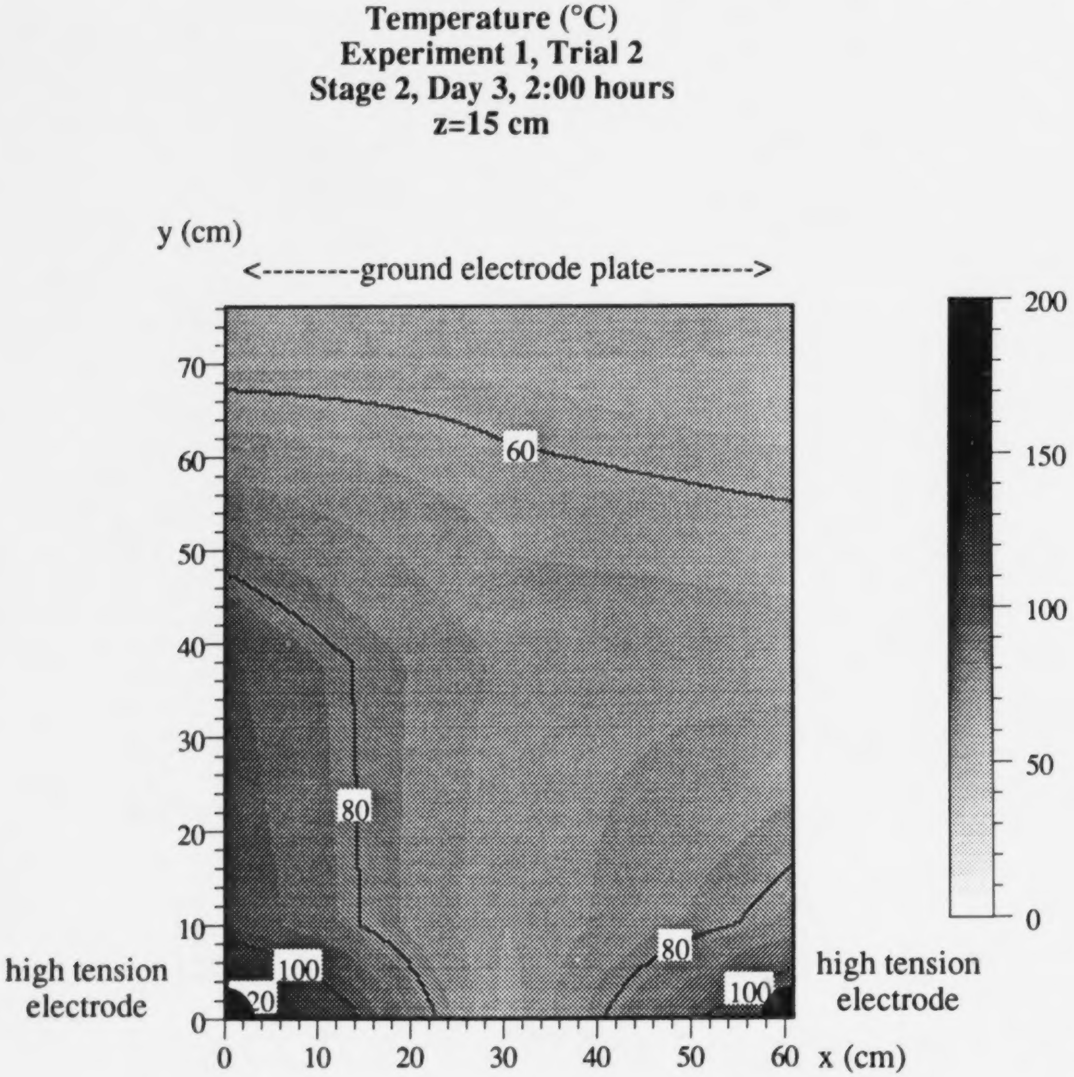

Temperature (°C)
Experiment 1, Trial 2
Stage 2, Day 3, 2:00 hours
z=15 cm

Figure 5.13: Temperature in the plane z=15 cm after 2:00 hours @1500 W, experiment 1, trial 2, stage 2, day 3.

Temperature (°C)
Experiment 1, Trial 2
Stage 2, Day 3, 4:01 hours
z=15 cm

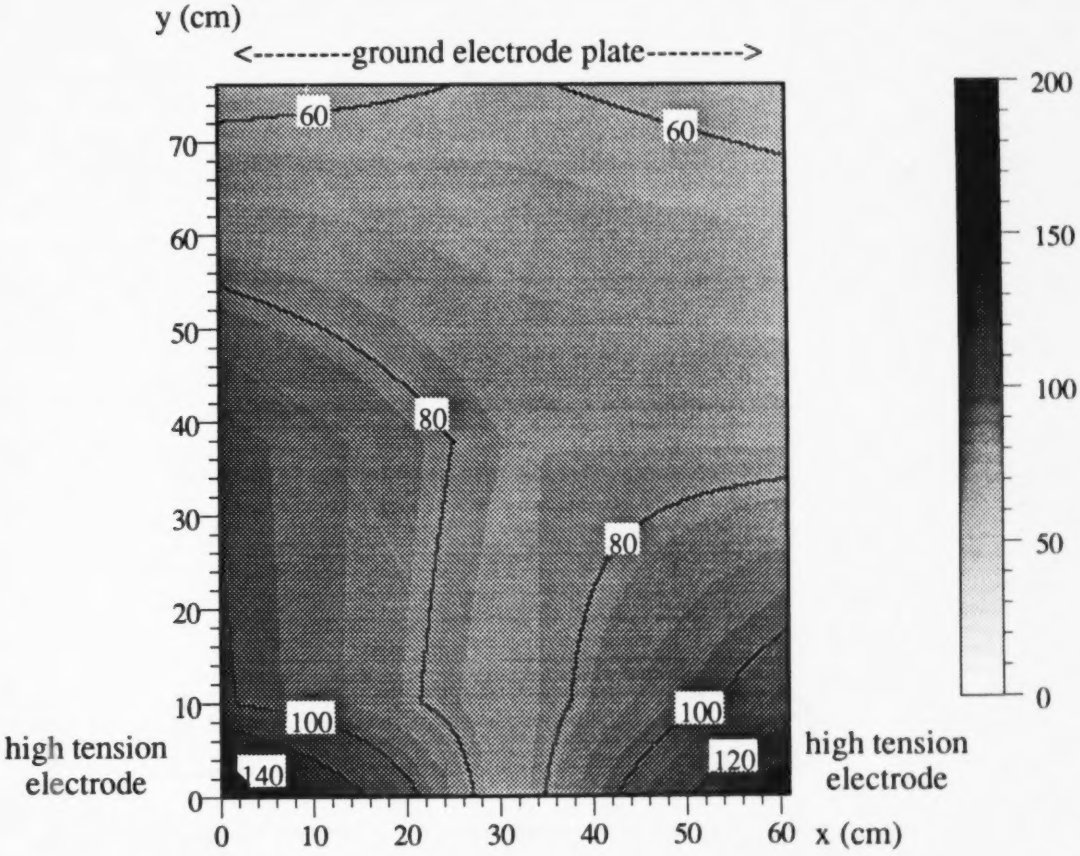

Figure 5.14: Temperature in the plane z=15 cm after 4:01 hours @1500 W, experiment 1, trial 2, stage 2, day 3.

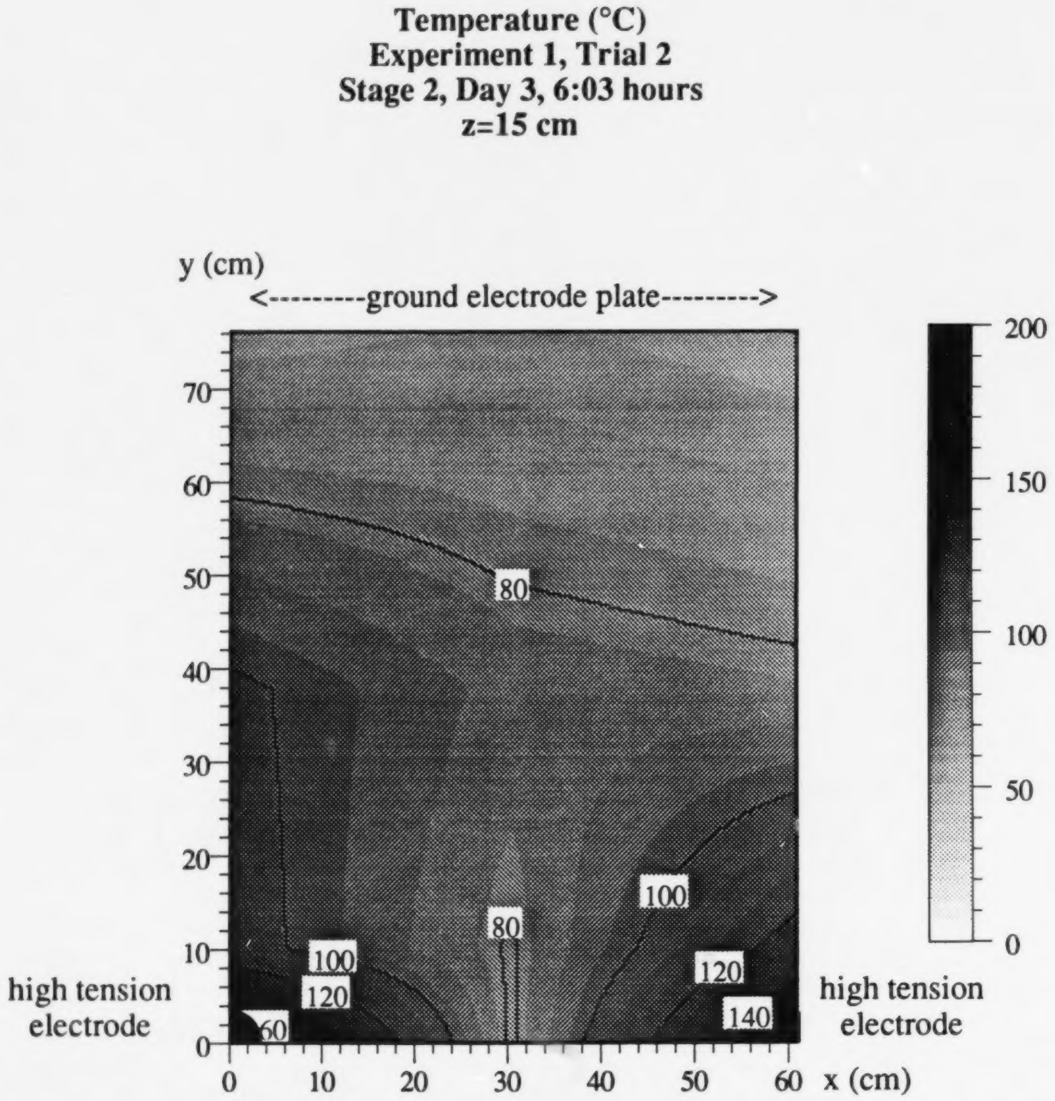

Figure 5.15: Temperature in the plane z=15 cm after 6:03 hours @1500 W, experiment 1, trial 2, stage 2, day 3.

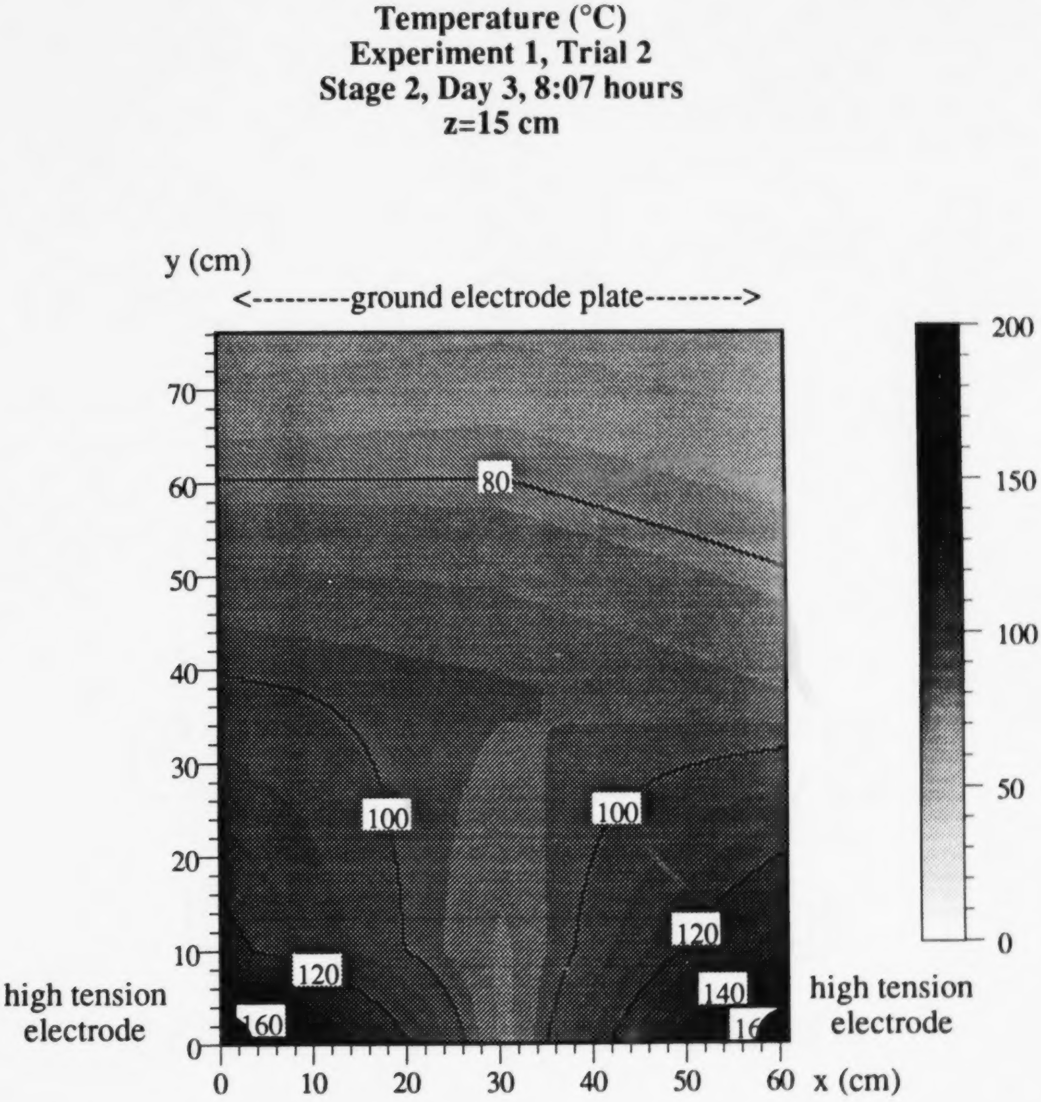

Figure 5.16: Temperature in the plane z=15 cm after 8:07 hours @1500 W, experiment 1, trial 2, stage 2, day 3.

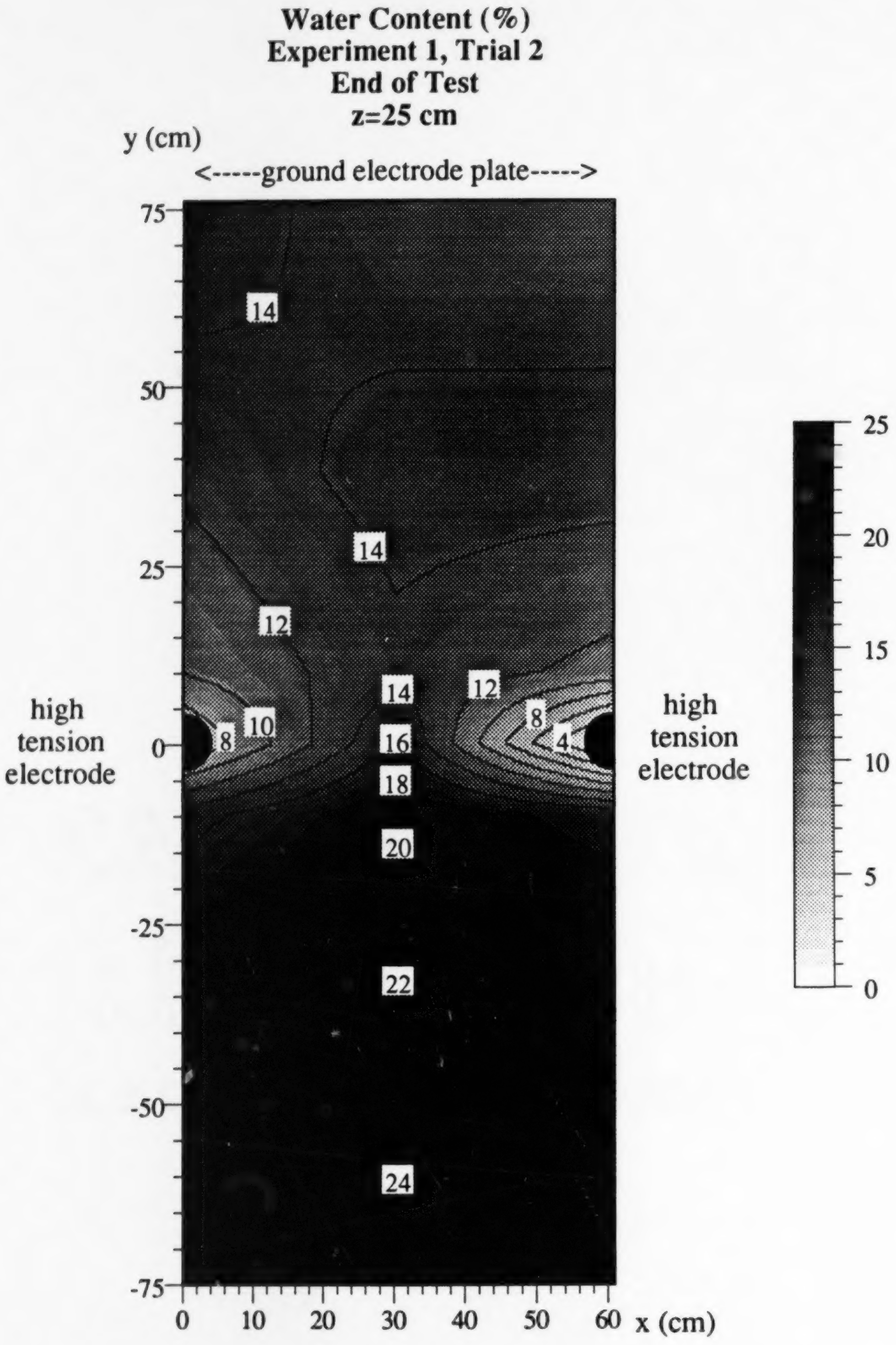

Figure 5.17: Water content in the plane z=25 cm after 8:07 hours @1500 W, experiment 1, trial 2, stage 2, day 3.

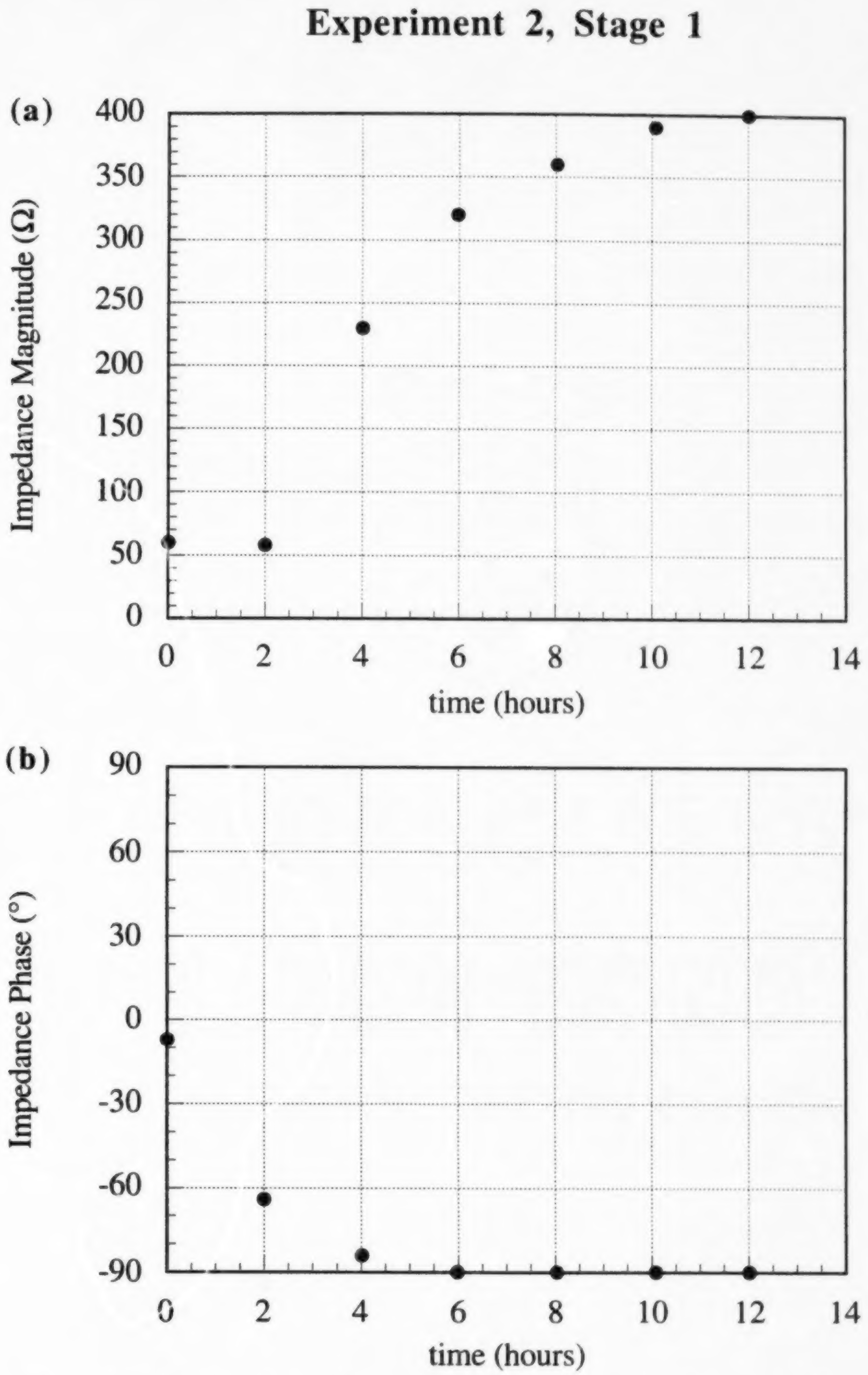

Figure 5.18: Engineering scale test, impedance, experiment 2, stage 1, (a) magnitude, (b) phase.

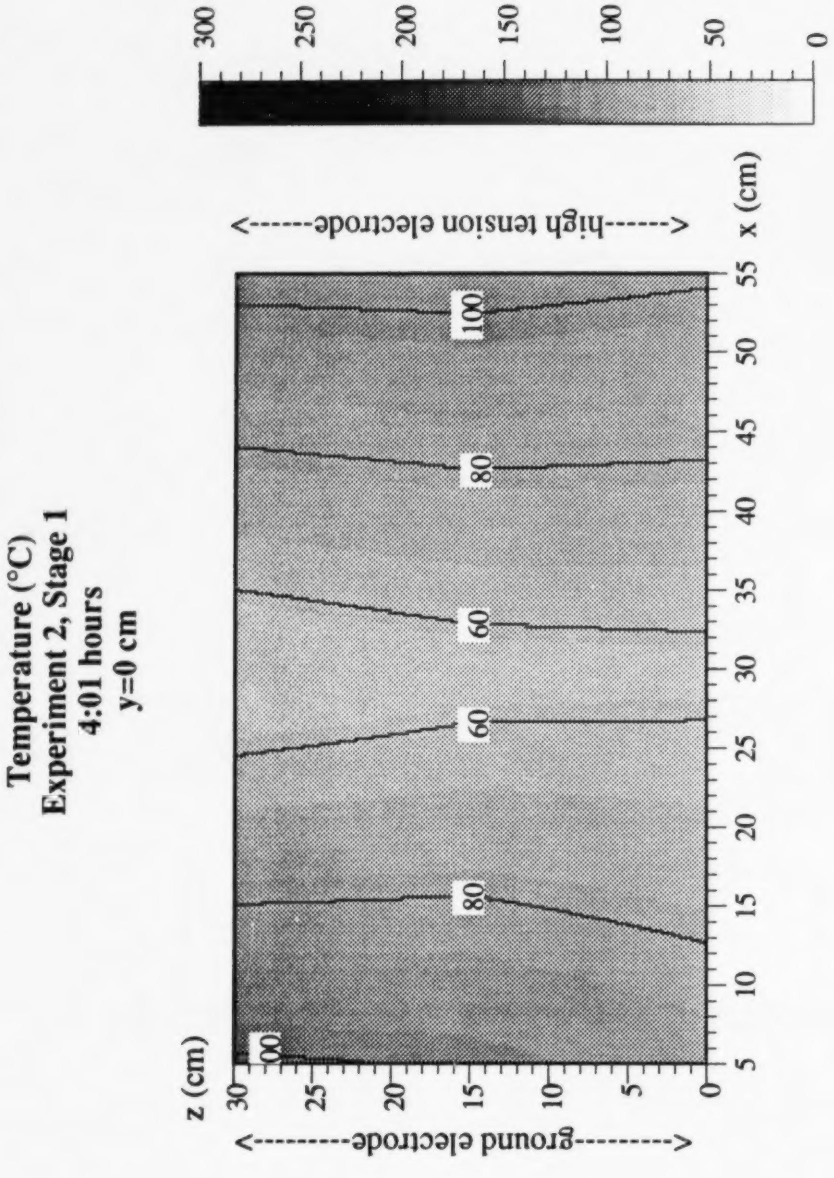

Figure 5.19: Temperature in the plane y=0 cm, 4:01 hours @1500 W, experiment 2, stage 1.

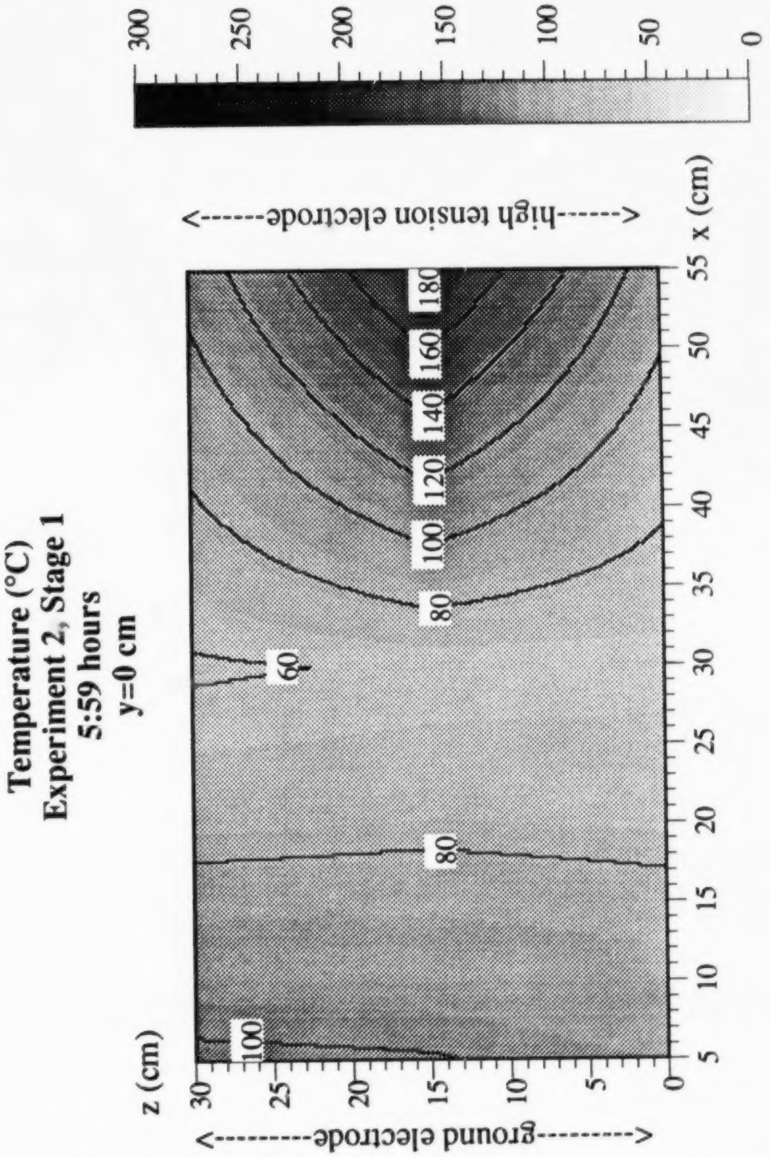

Figure 5.20: Temperature in the plane y=0 cm after 5:59 hours @1500 W, experiment 2, stage 1.

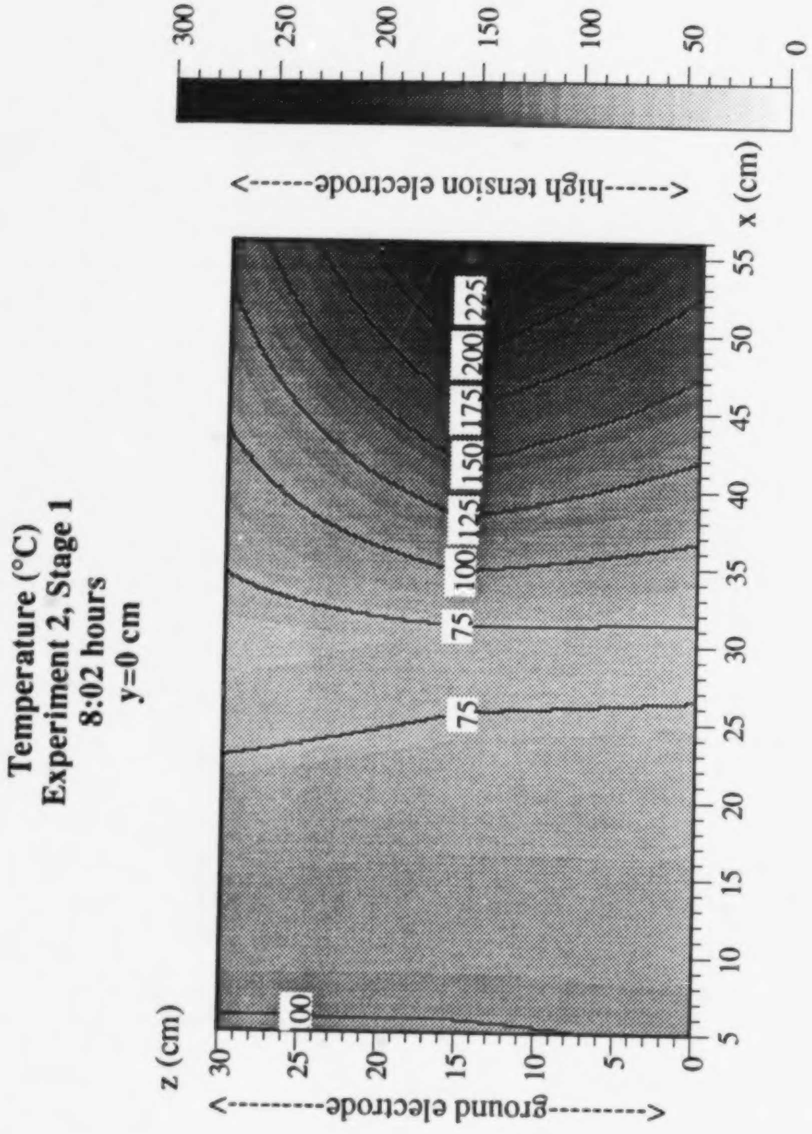

Figure 5.21: Temperature in the plane y=0 cm after 8:02 hours @1500 W, experiment 2, stage 1.

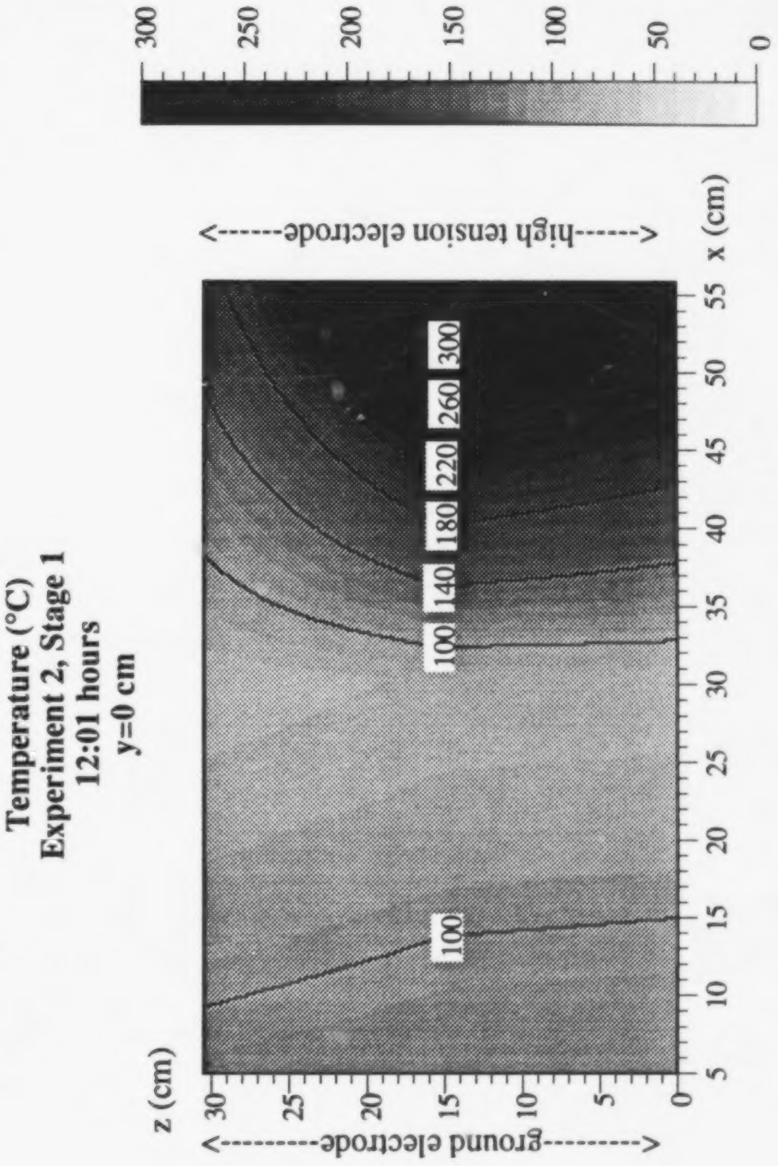

Figure 5.22: Temperature in the plane y=0 cm after 12:01 hours @1500 W, experiment 2, stage 1.

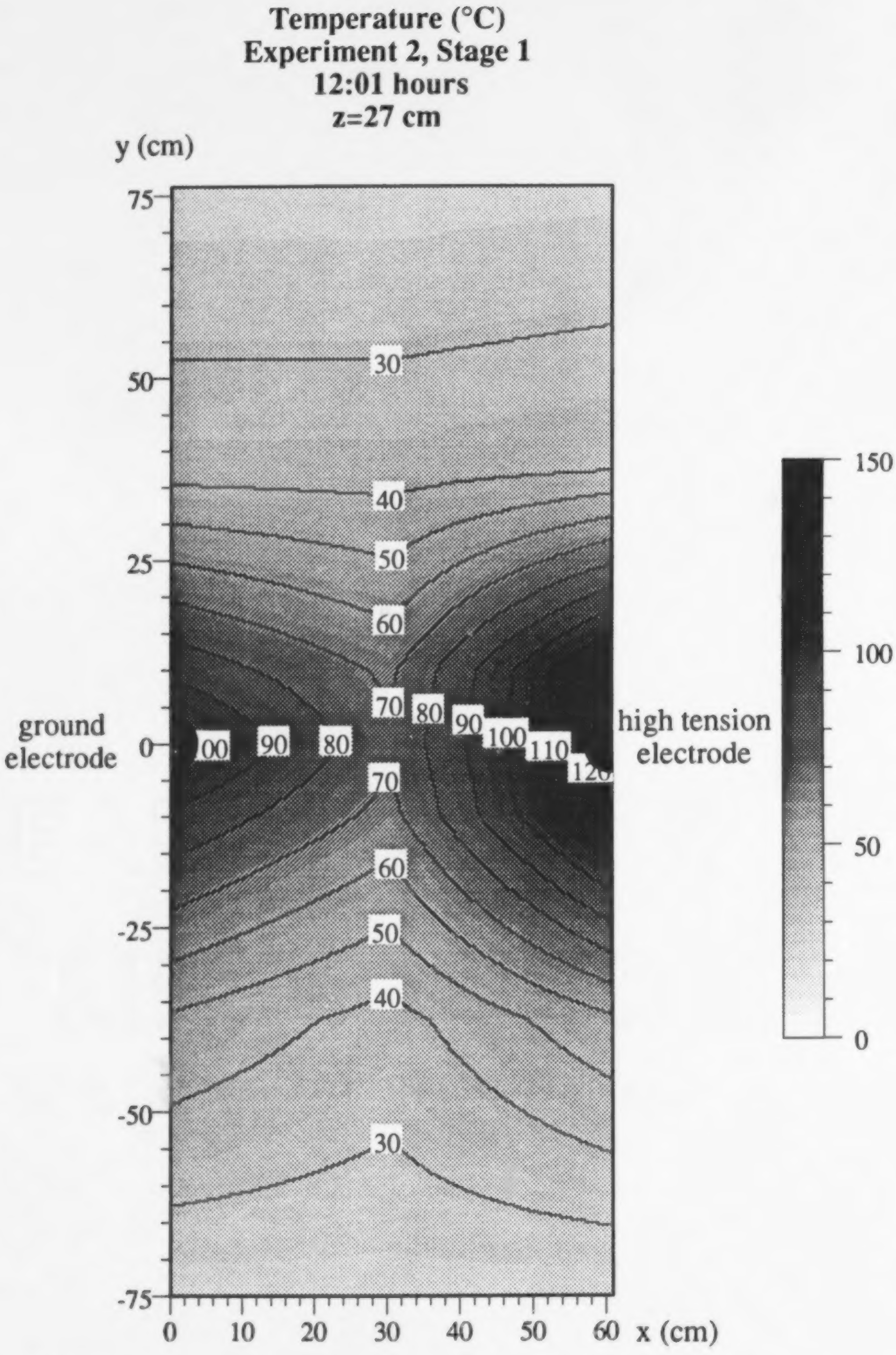

Figure 5.23: Temperature in the plane z=27 cm after 12:01 hours @1500 W, experiment 2, stage 1.

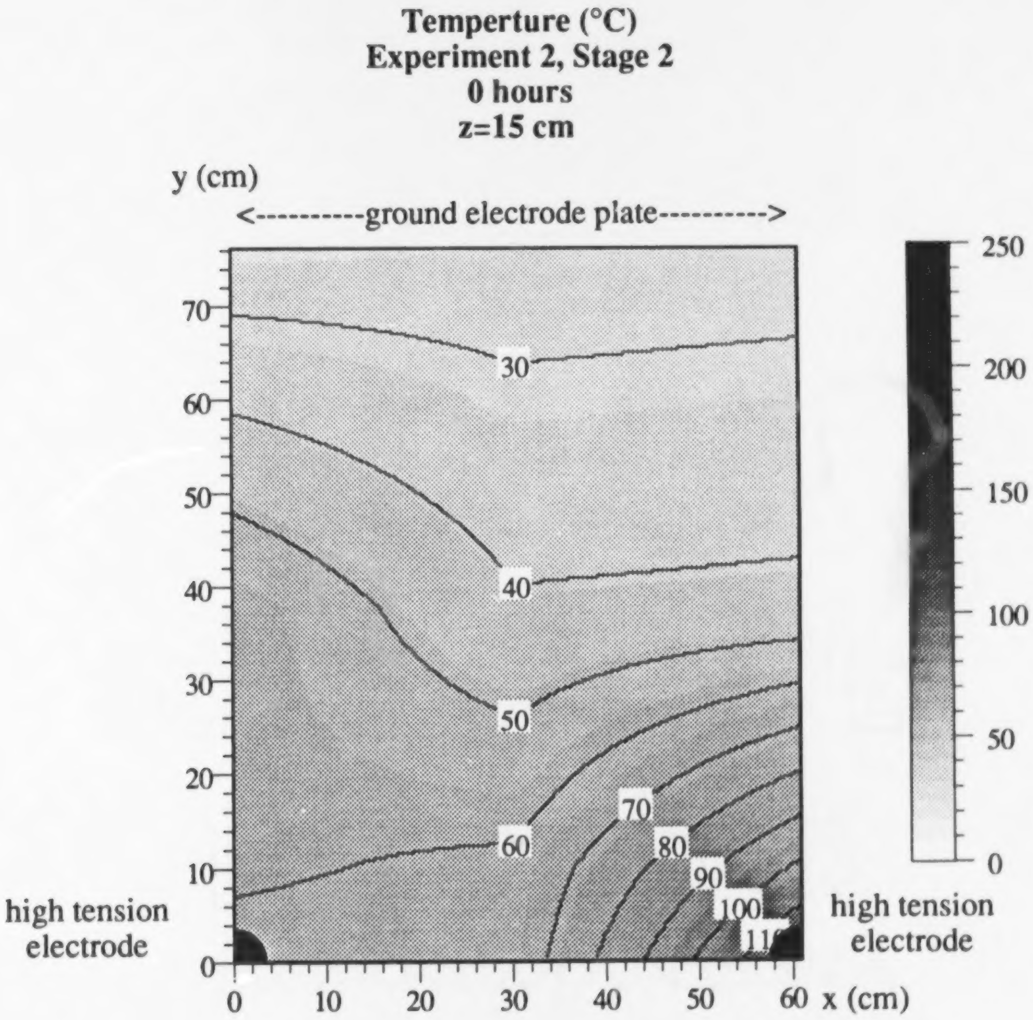

Figure 5.24: Temperature in the plane z=15 cm after 0 hours, experiment 2, stage 2.

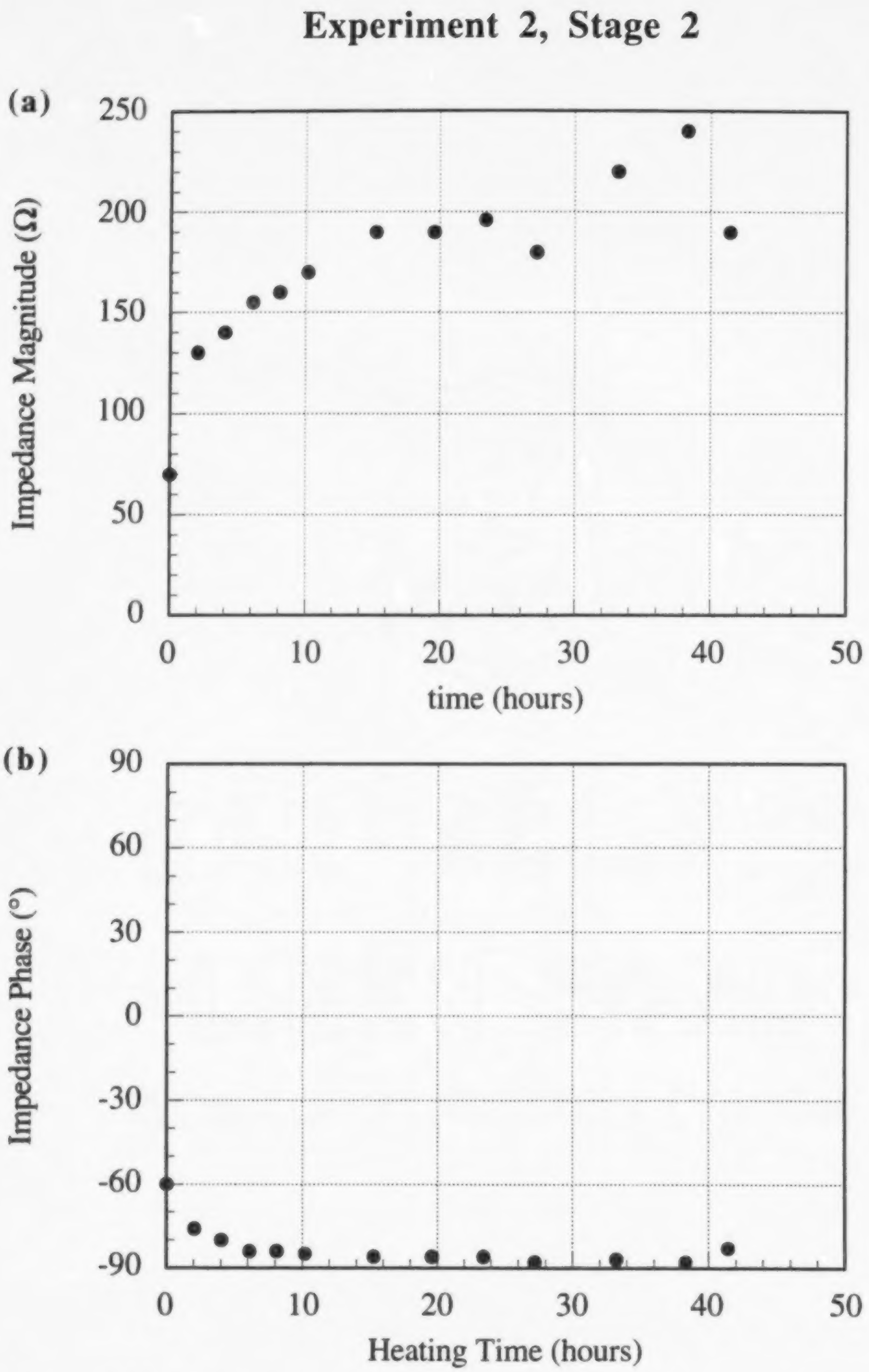

Figure 5.25: Engineering scale test, impedance, experiment 2, stage 2, (a) magnitude (b) phase.

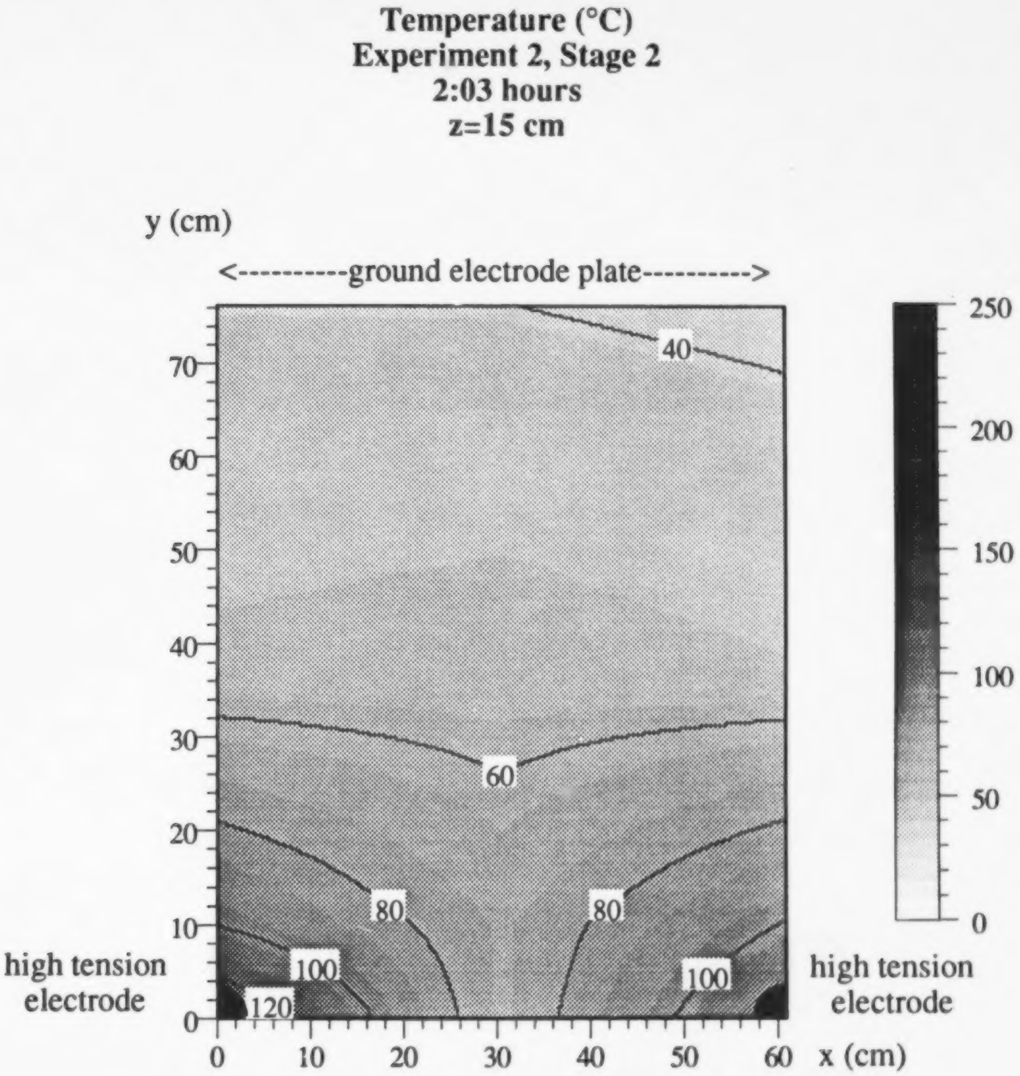

Figure 5.26: Temperature in the plane z=15 cm after 2:03 hours @1500 W, experiment 2, stage 2.

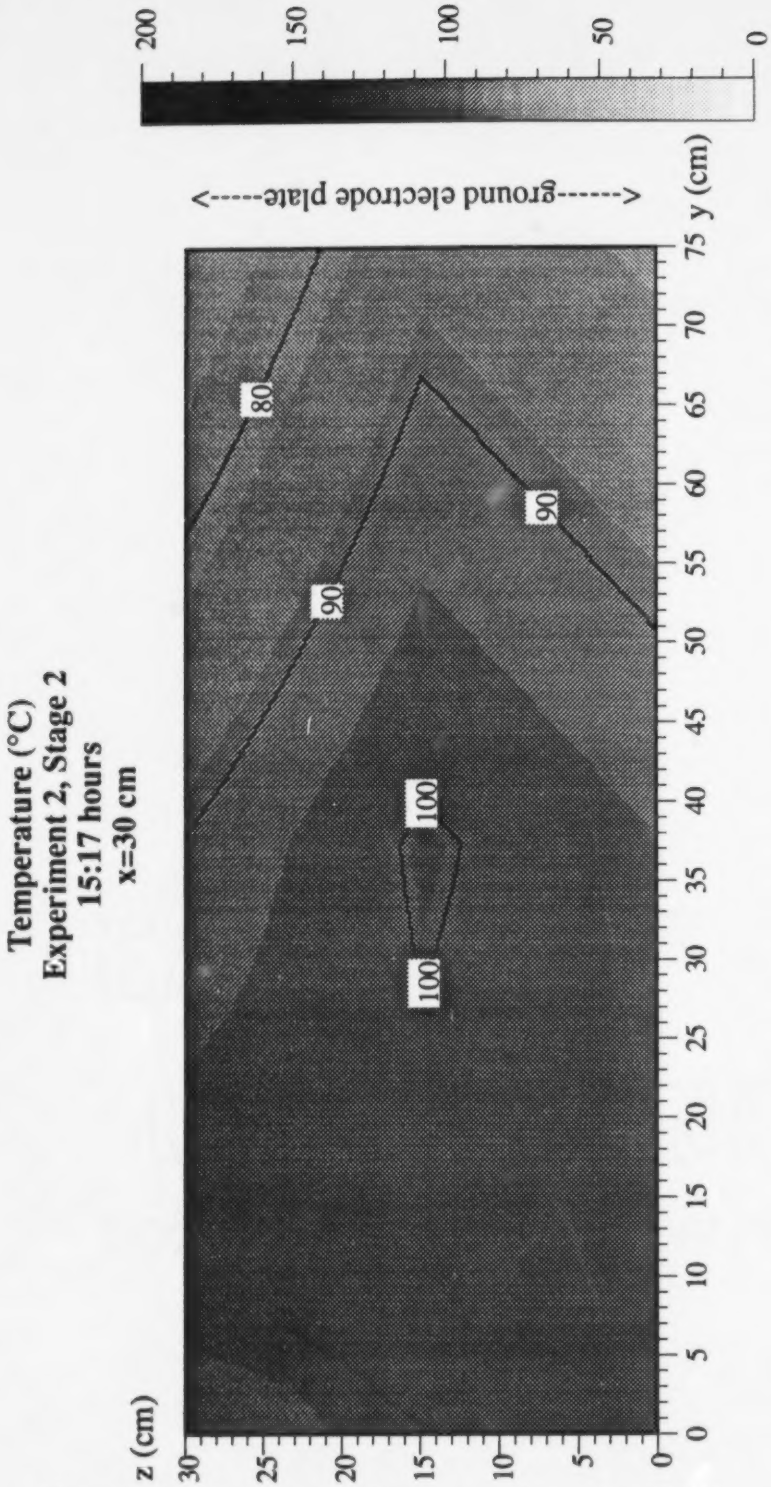

Figure 5.27: Temperature in the plane x=30 cm after 15:17 hours @1500 W, experiment 2, stage 2.

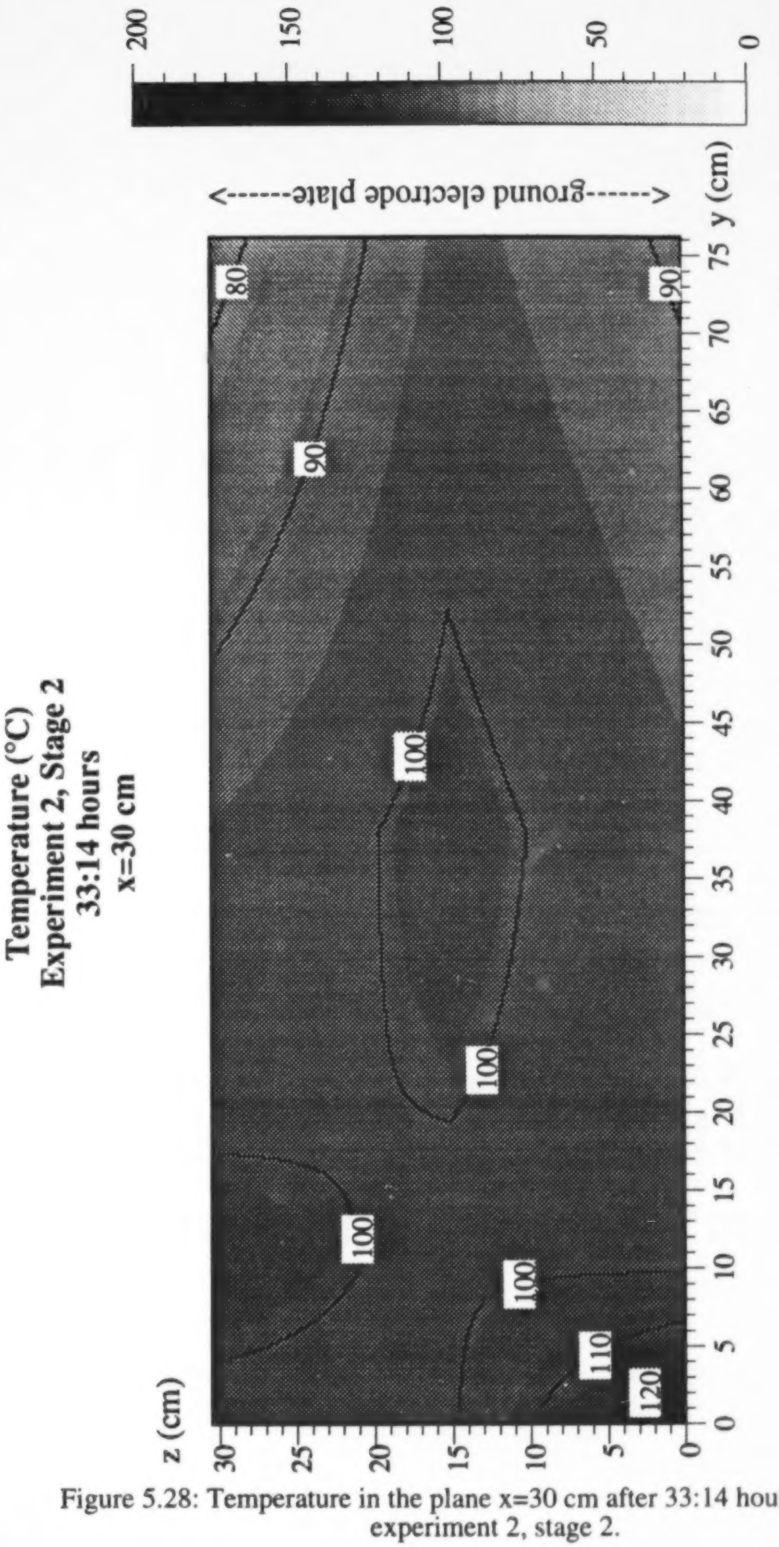

Figure 5.28: Temperature in the plane x=30 cm after 33:14 hours @1500 W, experiment 2, stage 2.

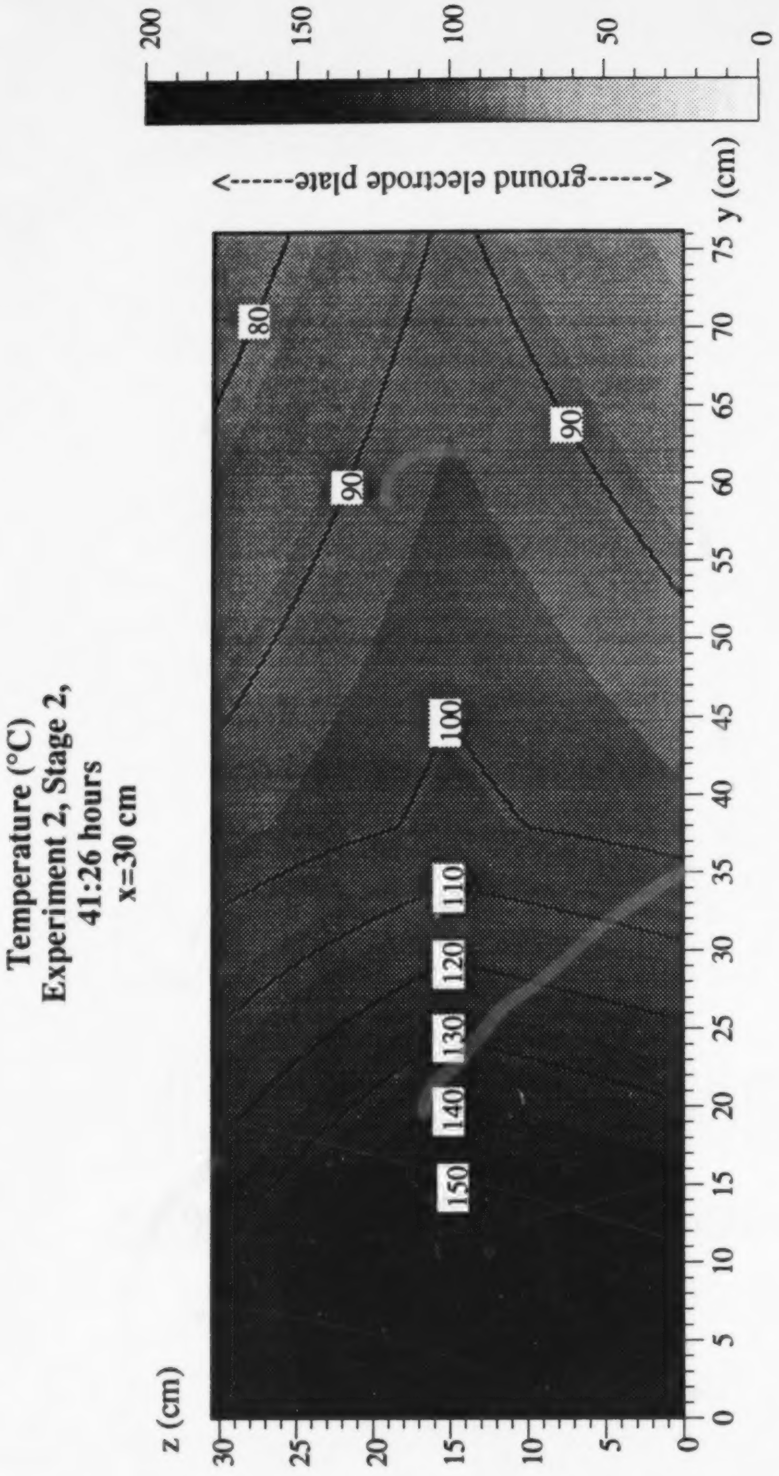

Figure 5.29: Temperature in the plane x=30 cm after 41:26 hours @1500 W, experiment 2, stage 2.

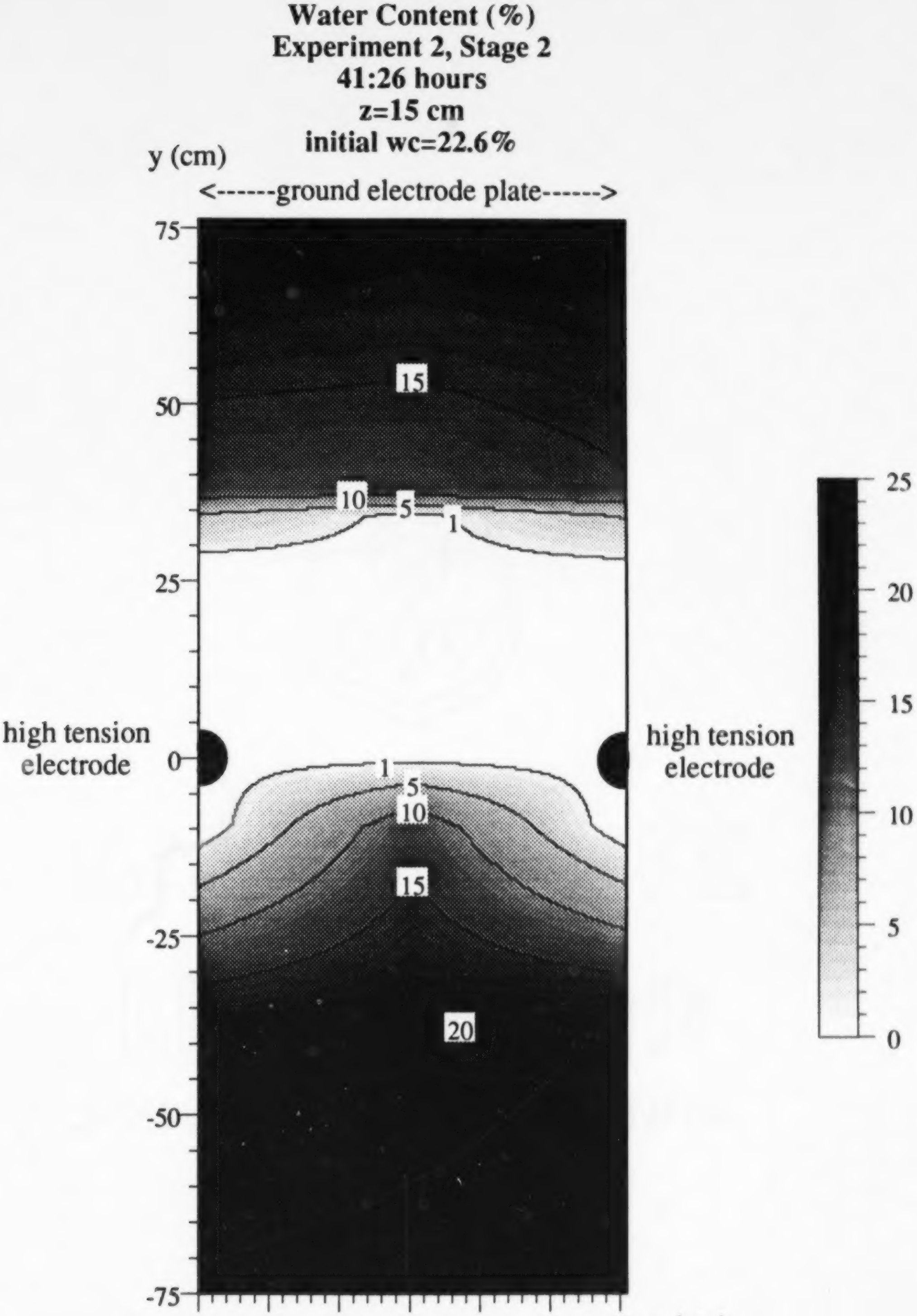

Figure 5:30: Water content in the plane z=15 cm after 41:26 hours @1500 W, experiment 2, stage 2.

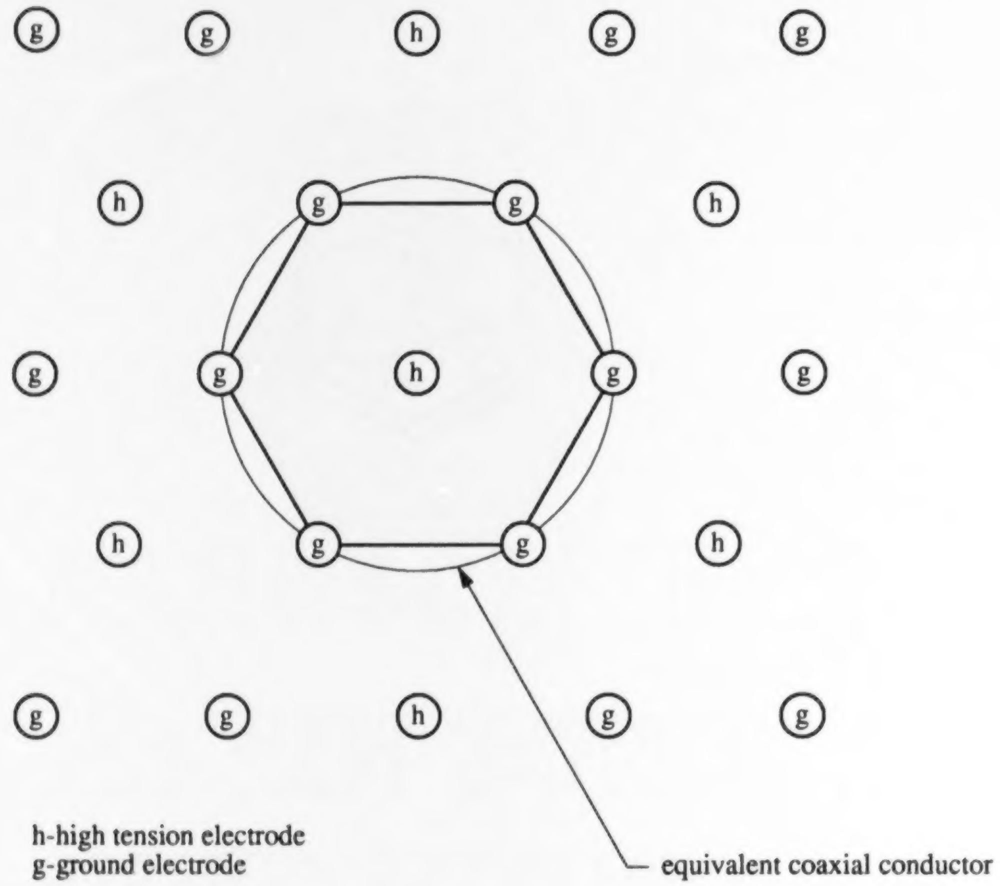
g
g
h
g
g
h
g
g
h
g
h
g
g
g
g
h
g
g
h
g
g
h
g
g
h
g
g
h-high tension electrode
g-ground electrode
equivalent coaxial conductor

Figure 6.1: Plan view of staggered single phase electrode array and computational cell (adapted from Nachai *et al* 1992).

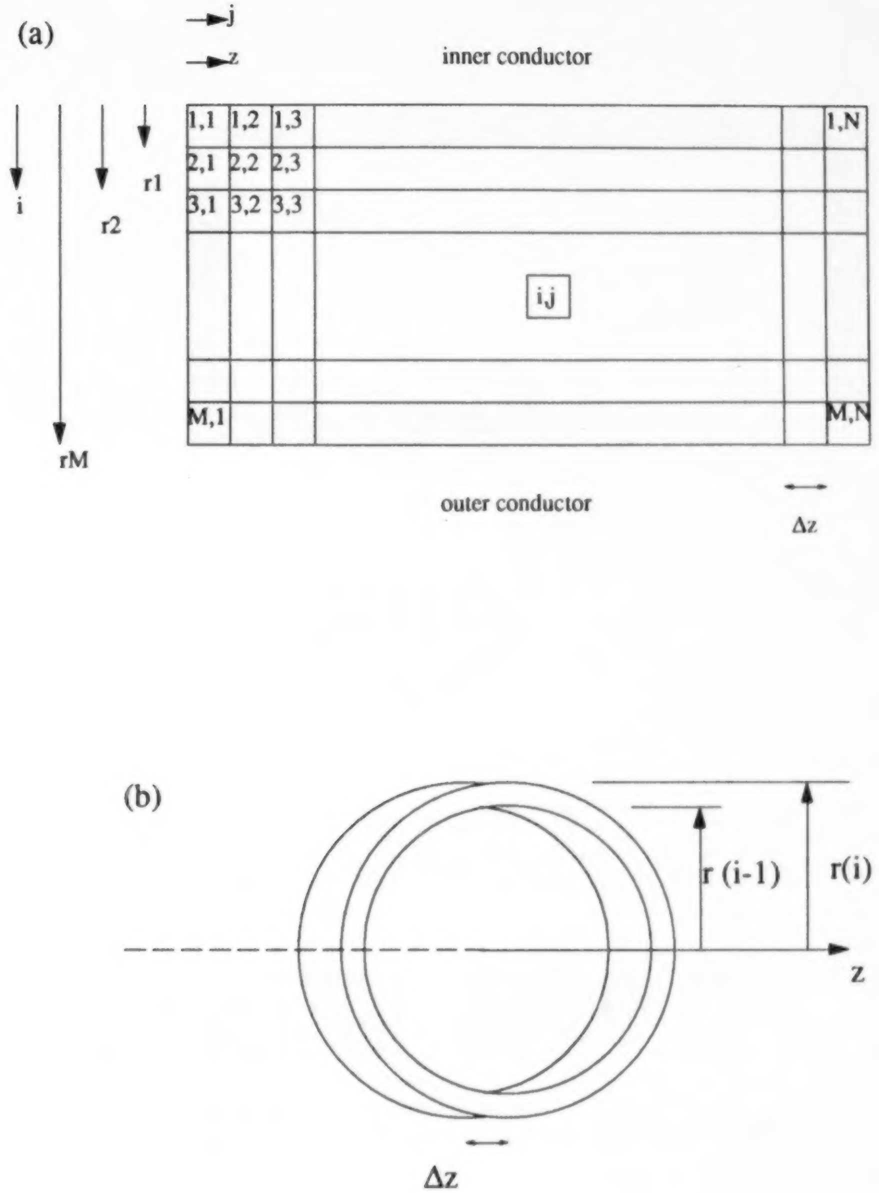
(a)
j
z
inner conductor
i
r2
r1
rM
1,1
1,2
1,3
1,N
2,1
2,2
2,3
3,1
3,2
3,3
i,j
M,1
M,N
outer conductor
Δz
(b)
r (i-1)
r(i)
z
Δz

Figure 6.2: (a) Cross-sectional view of the grid block structure in r-z space (b) three dimensional view of toroidal grid block i,j (adapted from Nachai *et al* 1992).

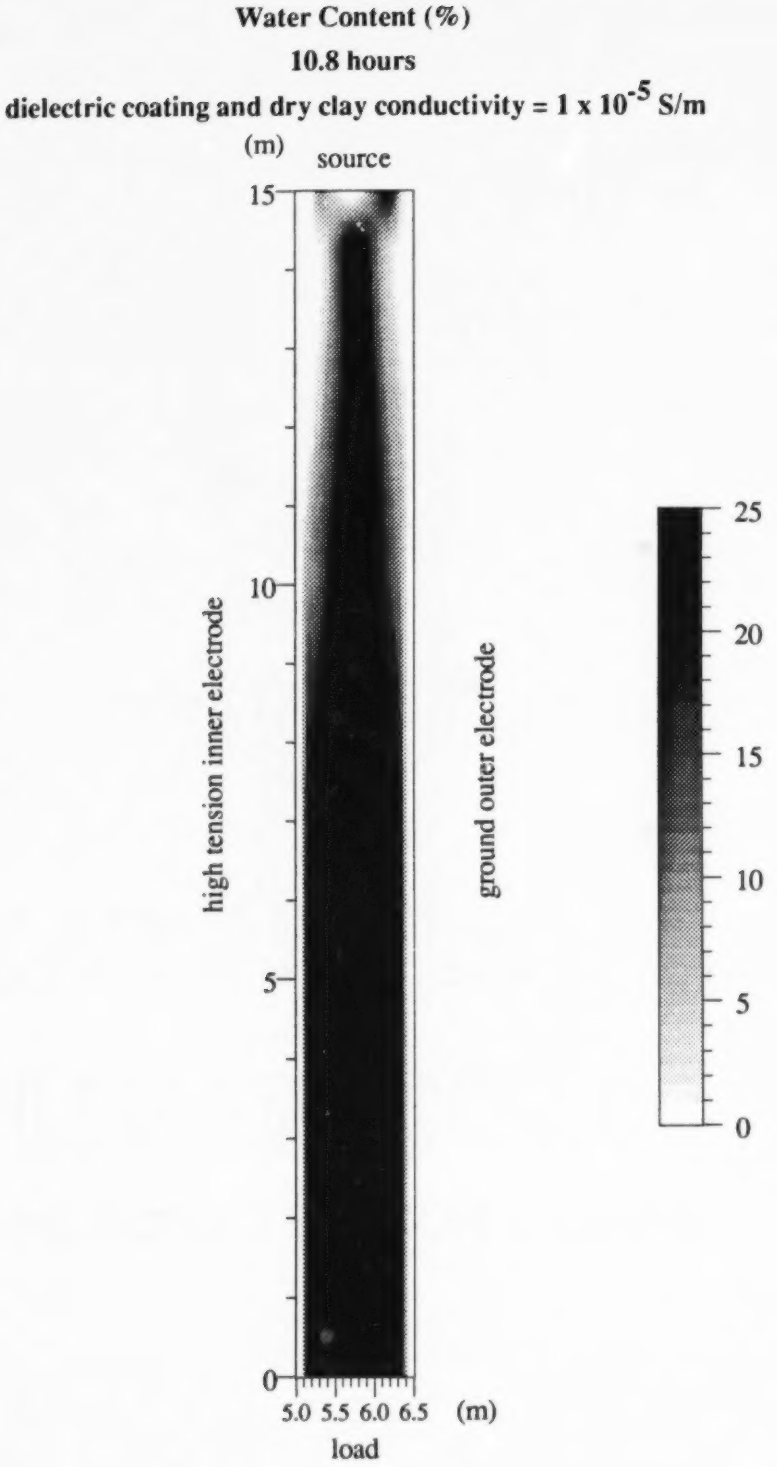

Water Content (%)

10.8 hours

dielectric coating and dry clay conductivity = 1 x 10^{-5} S/m

Figure 6.3: Water content at 10.8 hours, case with dielectric coating, residual electrical conductivity=1 x 10^{-5} S/m.

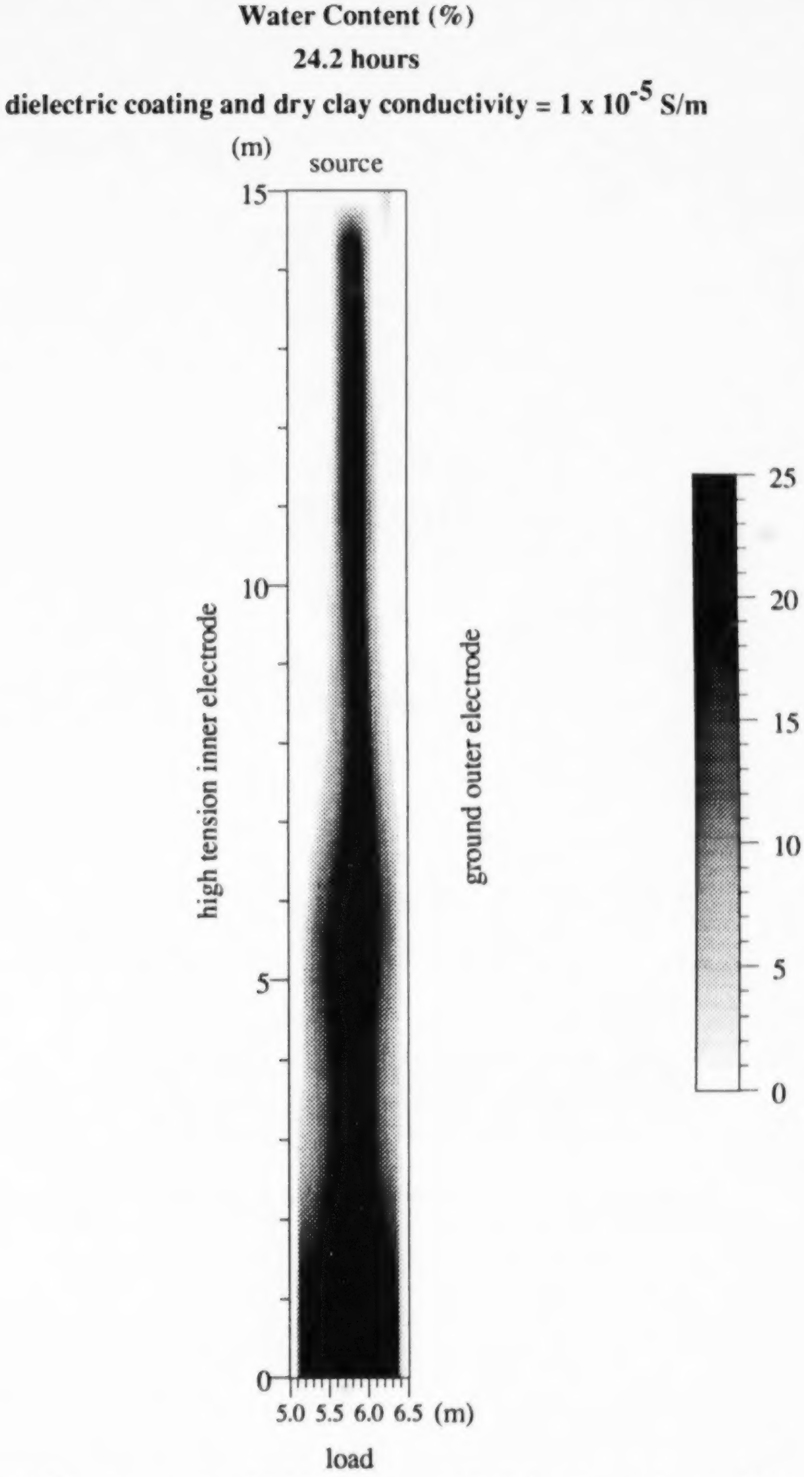

Figure 6.4: Water content at 24.2 hours, case with dielectric coating, residual electrical conductivity=1 x 10^{-5} S/m.

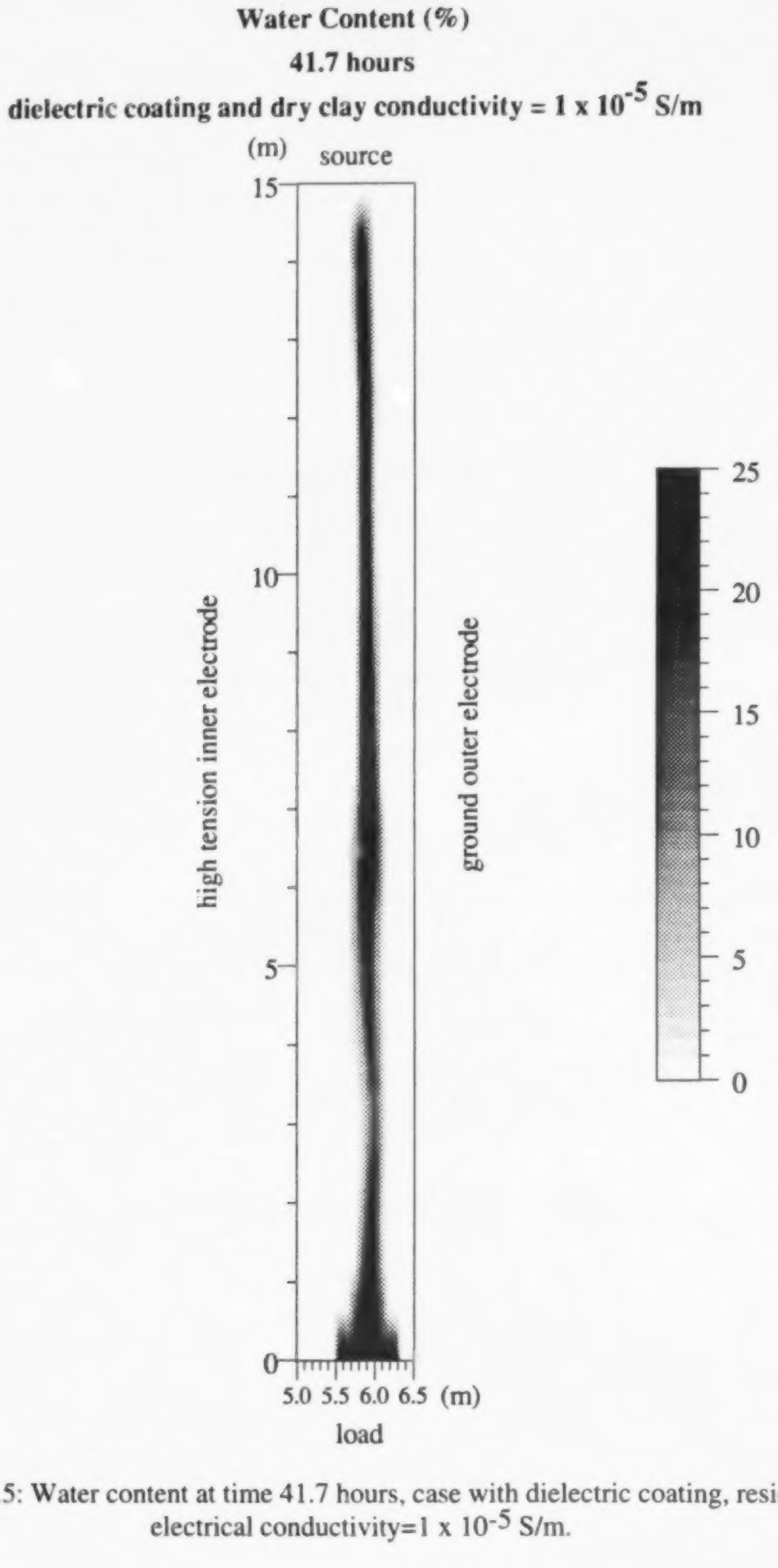

Figure 6.5: Water content at time 41.7 hours, case with dielectric coating, residual electrical conductivity=1 x 10^{-5} S/m.

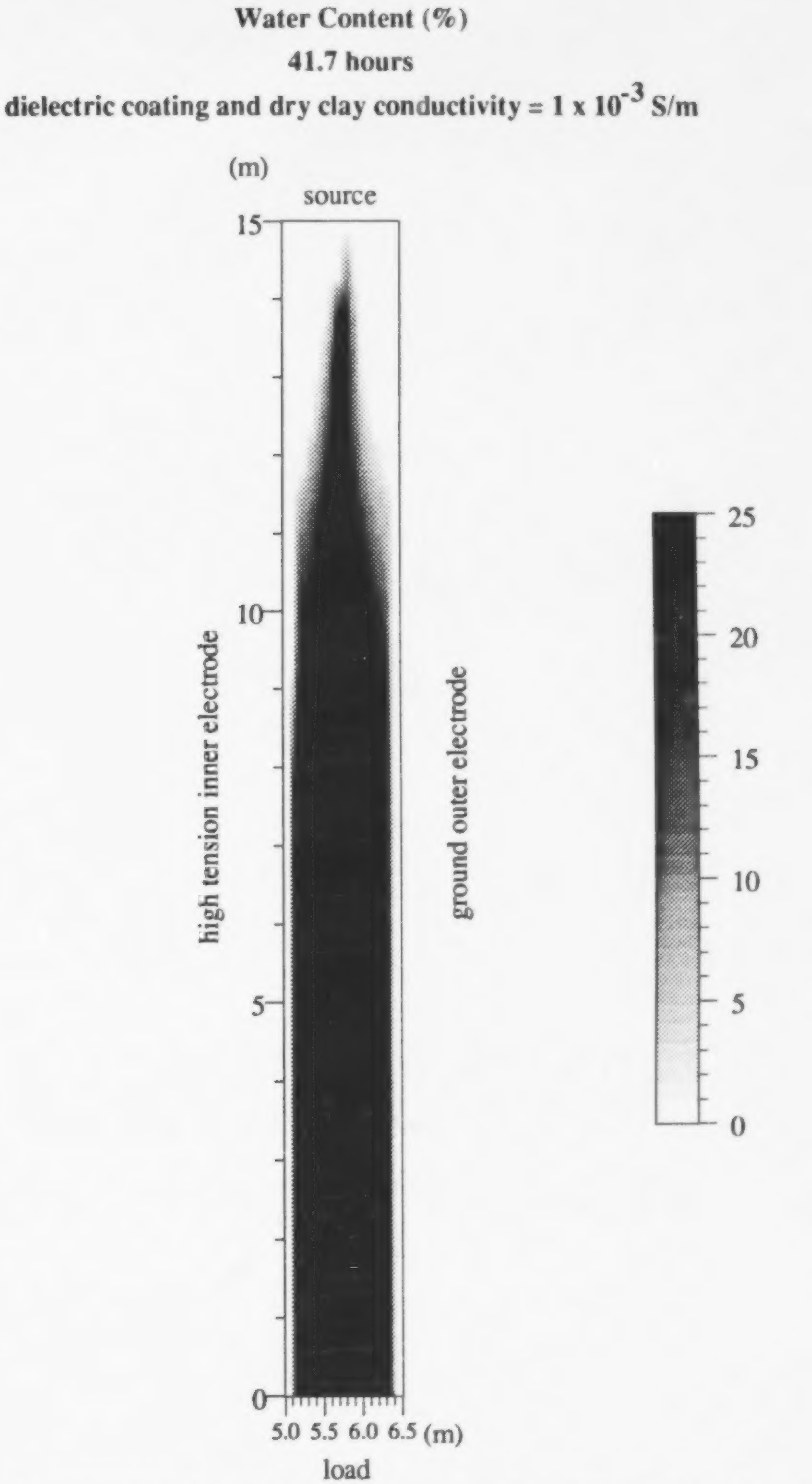

Figure 6.6: Water content at time 41.7 hours, case with dielectric coating, residual electrical conductivity=1 x 10^{-3} S/m.

PLATES

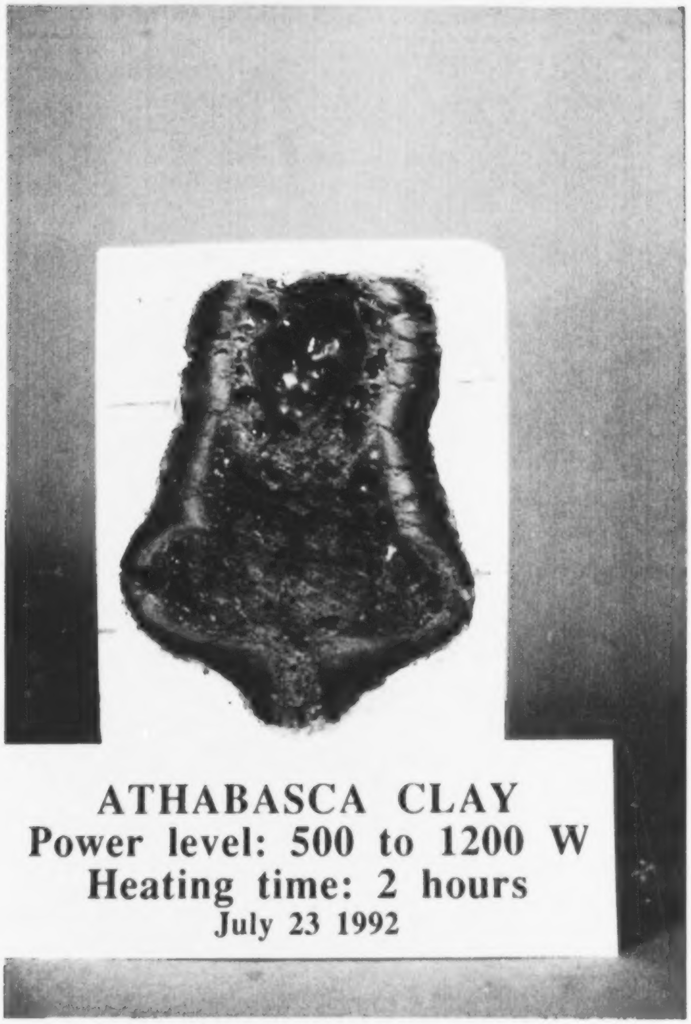
ATHABASCA CLAY
Power level: 500 to 1200 W
Heating time: 2 hours
July 23 1992

Plate 4.1: Athabasca clay (AC/Cuϕ7) vitrification experiment, cut section. The sample is 10 cm long by 7 cm wide.

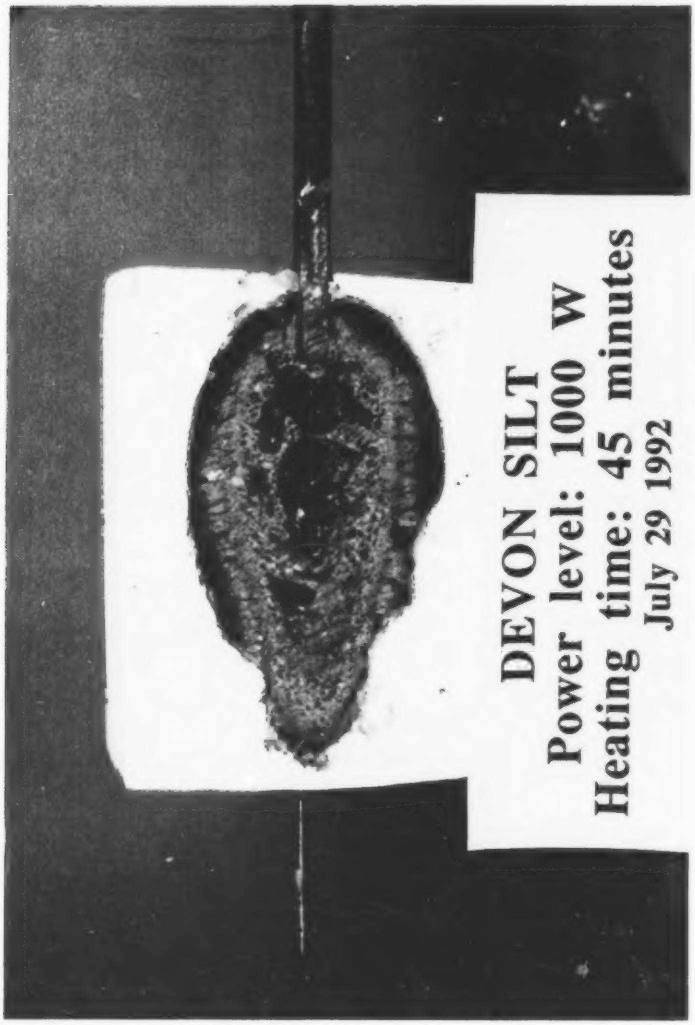
DEVON SILT
Power level: 1000 W
Heating time: 45 minutes
July 29 1992

Plate 4.2: Devon silt (DS/Cuϕ7) vitrification experiment, cut section. The sample is 6 cm long by 4 cm wide. Note the copper from the electrode on the edge of the solidified material.

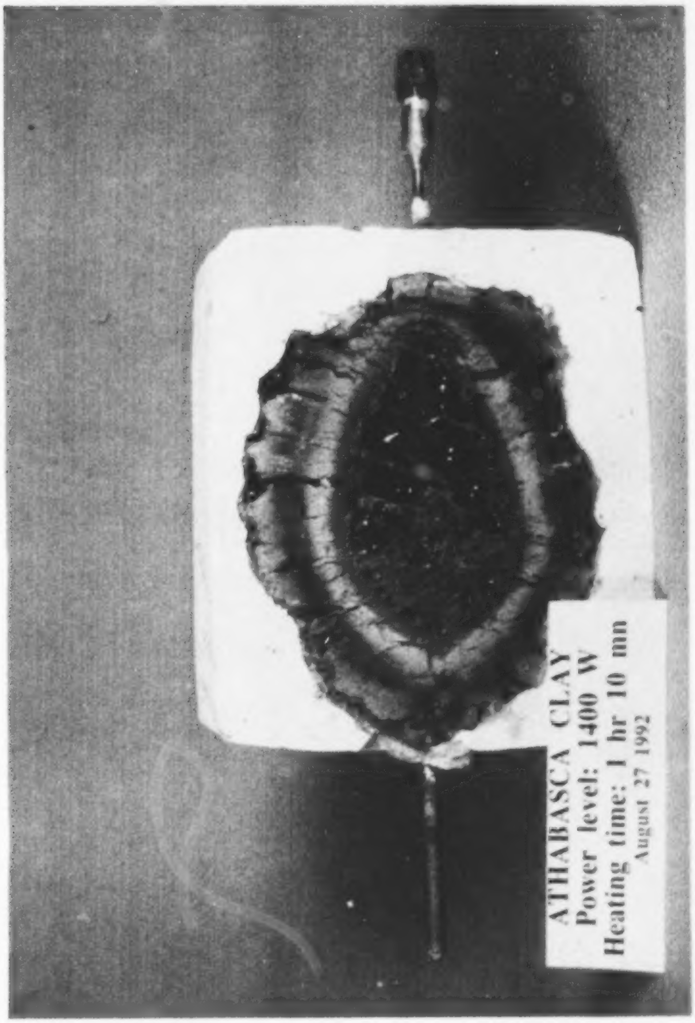
ATHABASCA CLAY
Power level: 1400 W
Heating time: 1 hr 10 mn
August 27 1992

Plate 4.3: Athabasca clay (AC/weld) vitrification experiment, cut section. The sample is 13 cm long by 10 cm wide.

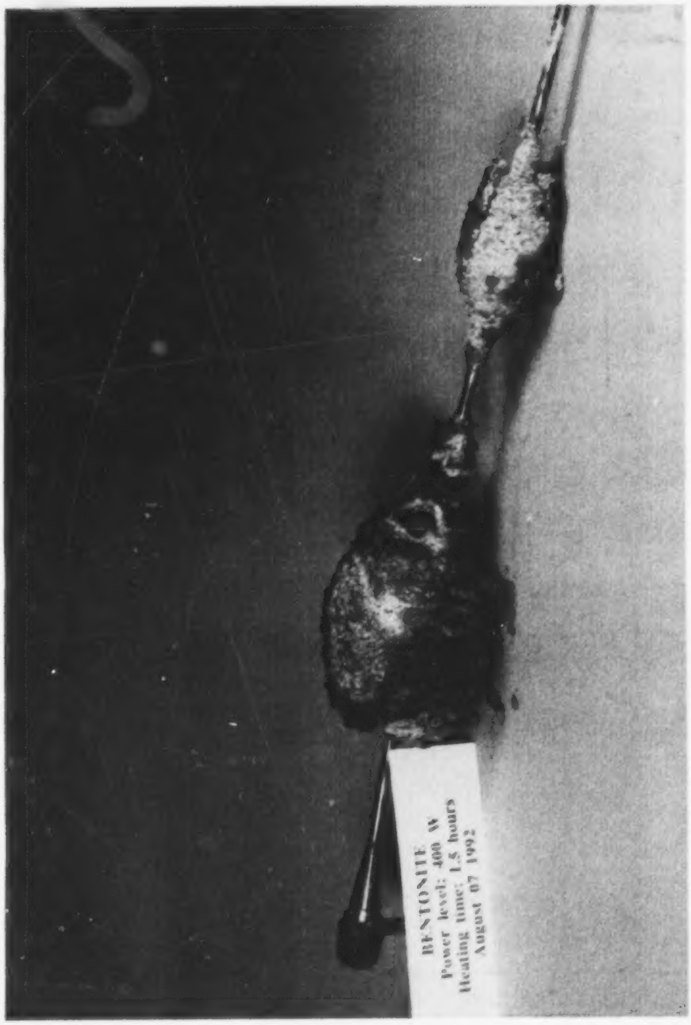
BENTONITE
Power level: 400 W
Heating time: 1.5 hours
August 07 1992

Plate 4.4: Bentonite (B/steelϕ3) vitrification experiment. The product of vitrification is a fragile shell. The sample is 6 cm long by 5 cm wide.

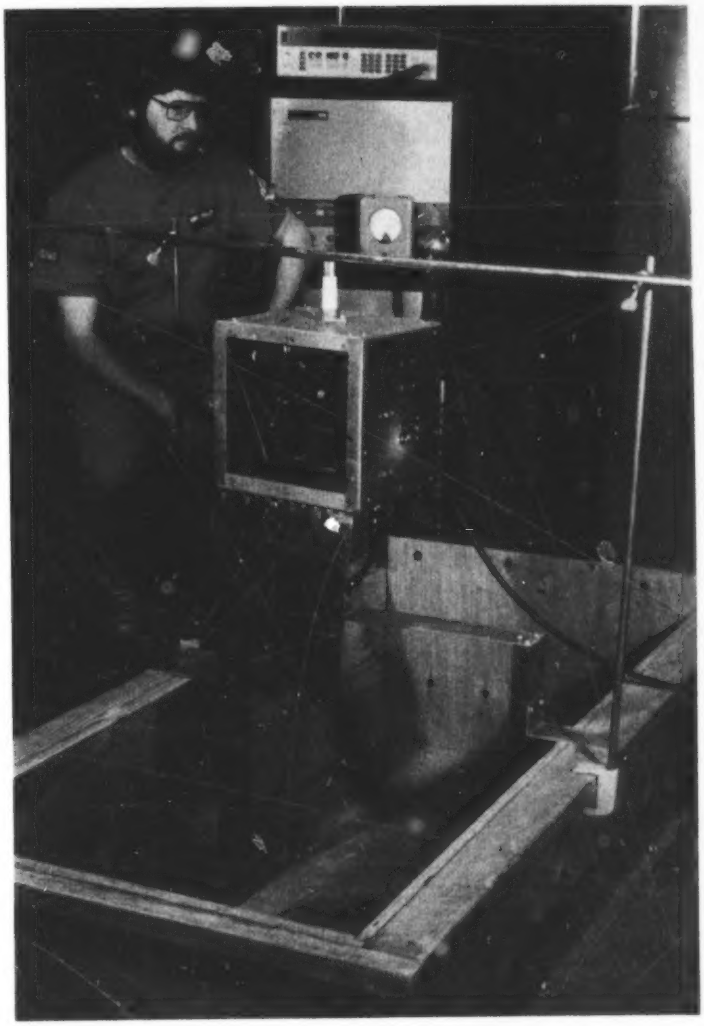

Plate 5.1: Sample holder with the matching network in place. Power amplifier and signal generator are in the background.

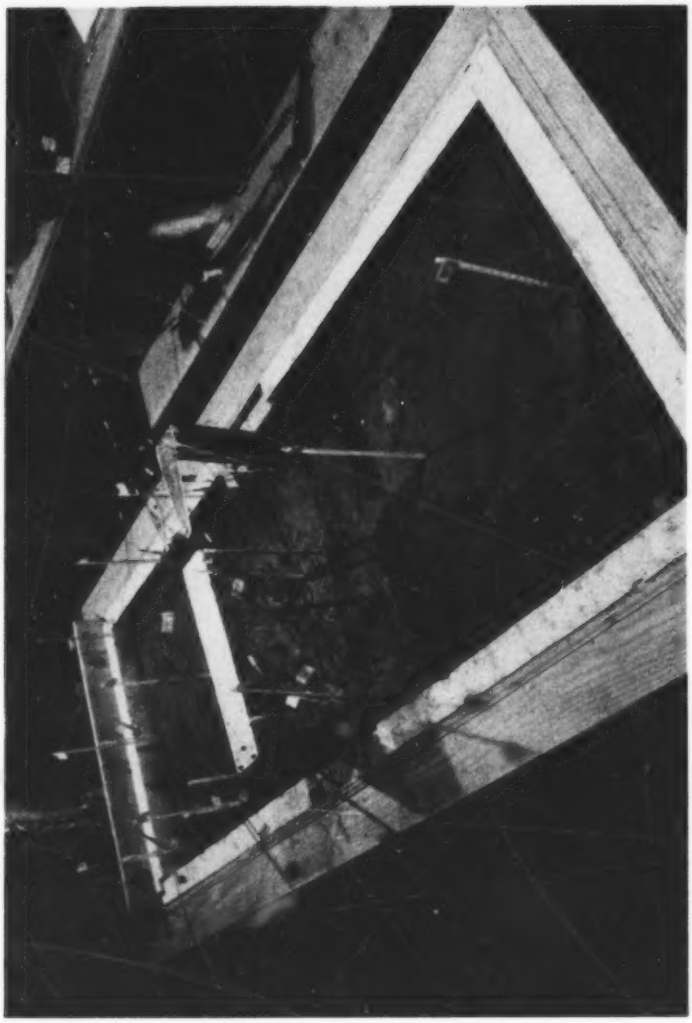

Plate 5.2: Sample prior to a test with thermocouples and thermometers in place.

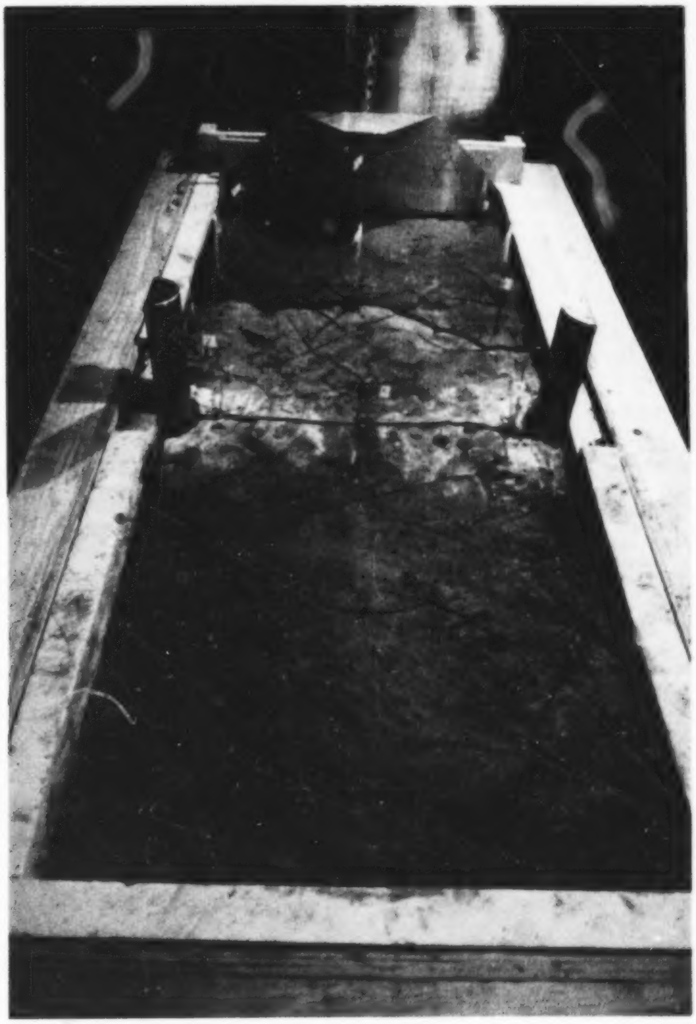

Plate 5.3: Sample after a test illustrating the shrinkage cracks.

REFERENCES

ASTM 1992a. D 4959-89. Determination of Water (Moisture) Content of Soil by Direct Heating Method. *In* Annual Book of ASTM Standards, Section 4 Construction. Volume 04.08 Soil and Rock; Dimension Stone; Geosynthetics. American Society for Testing and Materials, Philadelphia, Pa.

ASTM 1992b. D 698-91. Test Method for Laboratory Compaction Characteristics of Soil Using Standard Effort (12,400 ft-lbf/ft^3 (600 kN-m/m^3)). *In* Annual Book of ASTM Standards, Section 4 Construction. Volume 04.08 Soil and Rock; Dimension Stone; Geosynthetics. American Society for Testing and Materials, Philadelphia, Pa.

Albernathy, E.R. 1974. Production Increase of Heavy Crude Oils by Electromagnetic Heating. Proceedings, 1974 Annual Technical Meeting of the Petroleum Society of CIM, Calgary, Alberta, 1974.

Arienti, M., Wilk, L., Jasinski, M., and Prominski, N. 1988. In Situ Vitrification. *In* Dioxin-Containing Wastes, Treatment Technologies. Pollution Technology Review#160, Noyes Data Corporation. pp. 139:146.

Bridges, J., Stresty, G., Taflove, A., and Snow, R. 1979. Radio-Frequency Heating to Recover Oil from Utah Tar Sands. Chapter 44. *In* Future of Heavy Crude and Tar Sands. *Edited by* R.F. Meyer and C.T. Steele. McGraw-Hill Books Co. Inc., New York City. pp. 396:409.

Byers, M.G., FitzPatrick, V.F. and Holtz, R.D. 1991. Site Remediation by In Situ Vitrification. Transportation Research Record No. 1312: Energy and Environmental Issues 1991. pp. 162-166.

Chute, F.S., Cervenan, M.R., and Vermeulen, F.E. 1978. Simple Cell for the Measurement of the Radio Frequency Electrical Properties of Earth Materials. Review of Scientific Instruments, **49(12):** 1675-1679.

Chute, F.S., Vermeulen, F.E., Cervenan, M.R., and McVea, F.J. 1979. Electrical Properties of Athabasca Oil Sands. Canadian Journal of Earth Science, **16:** 2009-2021.

Chute, F.S., and Vermeulen, F.E. 1989. Electrical Heating of Reservoirs. *In* AOSTRA Technical Handbook on Oil Sands, Bitumens and Heavy Oils. *Edited by* L.G. Hepler and C. Hsi. pp. 338:376.

Dev, H., Condorelli, P., Bridges, J., Rodgers, C., and Downey, D. 1987. In-Situ Radio Frequency Heating Process for Decontamination of Soil. Chapter 27. *In* Solving Hazardous Waste Problems, Learning from Dioxins. *Edited by* J.H. Exner. American Chemical Society Symposium Series 338, Washington, D.C. pp. 332:339.

Dev, H., and Downey, D. 1988. Zapping Hazwastes. Civil Engineering, **58(8):** 43-45.

Dev, H., Stresty, G.C., Bridges, J.E., and Downey, D. 1988. Field Test of the Radio

Frequency Soil Decontamination Process. Proceedings, Superfund 88 National Conference, Washington, D.C., November 28-30, 1988. pp. 498-502.

Flock, D.L., and Tharin, J. 1975. Unconventional Methods of Recovery of Bitumen and Related Research Areas Particular to the Oil Sands of Alberta. Journal of Canadian Petroleum Technology , **14(3):** 17-27.

Freeze R.A. and Cherry J.A. 1979. Groundwater and Thermal Processes. *In* Groundwater. Prentice Hall. Inc., Englewood Cliffs, New Jersey. pp. 507-513.

Jacobs, G.K., Dunbar, D.W., Naney, M.T. and Williams, R.T. 1991. Petrologic and Geophysical Studies of an Artificial Magma. EOS, Transactions, American Geophysical Union, **73(38):** 401-.

Maslowski, R., Vermeulen, F.E., and Chute, F.S. 1992. Promoting Axial Uniformity in Radio Frequency Heating of a Lossy Material in a Waveguide by Introduction of an Insulating Gap. Journal of Microwave Power and Electromagnetic Energy, **27(1)**: 33-37.

Mitchell, J.K. 1993. Thermally Driven Moisture Flows. *In* Fundamentals of Soil Behavior (2nd. edition). John Wiley & Sons. Inc., New York. pp. 261-265.

Nachai, M. 1991a. Radio Frequency Heating of Porous, Moisture Bearing Materials in a Coaxial Guiding Structure. M.Sc. thesis, University of Alberta, Edmonton, Alberta.

Nachai, M. 1991b. TMCOPTER: A Two Dimensional Simulation Routine for the Electromagnetic Heating of Low Moisture, Porous, Lossy Materials Within a Coaxial Guiding Structure, Department of Electrical Engineering, University of Alberta, Edmonton, Alberta.

Nachai, M., Chute, F.E., and Vermeulen, F.E. 1992. On the Radio-Frequency Heating of Moist, Porous Earth-Type Materials by Guided Wave Propagation Along Embedded Parallel Conductors. Journal of Microwave Power and Electromagnetic Energy. 27(3): 143-159.

Oma, K.H., and Buelt, J.L. 1988. In-Situ Heating to Detoxify Organic-Contaminated Soils. Proceedings, 5th National Conference on Hazardous Wastes and Hazardous Materials, Las Vegas, Nevada, 1988. Vol. 1. pp. 154-157.

Santamarina, J.C., and Wakim, Y.N., 1992. Principles of Ground Modification with Electromagnetic Waves. *In* Grouting, Soil Improvement and Geosynthetics, A.S.C.E. Geotechnical Special Publication No. 30, Vol. 2, *Edited by* R.H. Borden, R.D. Holtz, and I. Juran. New Orleans, La. pp. 1380:1392.

Smith, L.A. and Hinchee, R.E. 1993. Radio Frequency In Situ Soil Heating. *In* In Situ Thermal Technologies for Site Remediation. Lewis Publishers, Boca Raton. pp. 93-126.

Stresty, G. S., Dev, H., Snow, R.H., and Bridges, J. E. 1986. Recovery of Bitumen from Tar Sand Deposits with the Radio Frequency Process. Society of Petroleum Engineers, Reservoir Engineering, **1(1):** 85-94.

Timmons, D.M., Fitzpatrick, V., and Liikala, S. 1990. Vitrification Tested on Hazardous Wastes. Pollution Engineering, **22(6):** 76-81.